Ph.D. Program in Civil, Chemical and Environmental Engineering

Department of Civil, Chemical and Environmental Engineering

Polytechnic School, University of Genoa

Ph.D. Program in Construction Engineering

Department of Civil and Environmental Engineering

Technical University of Catalonia

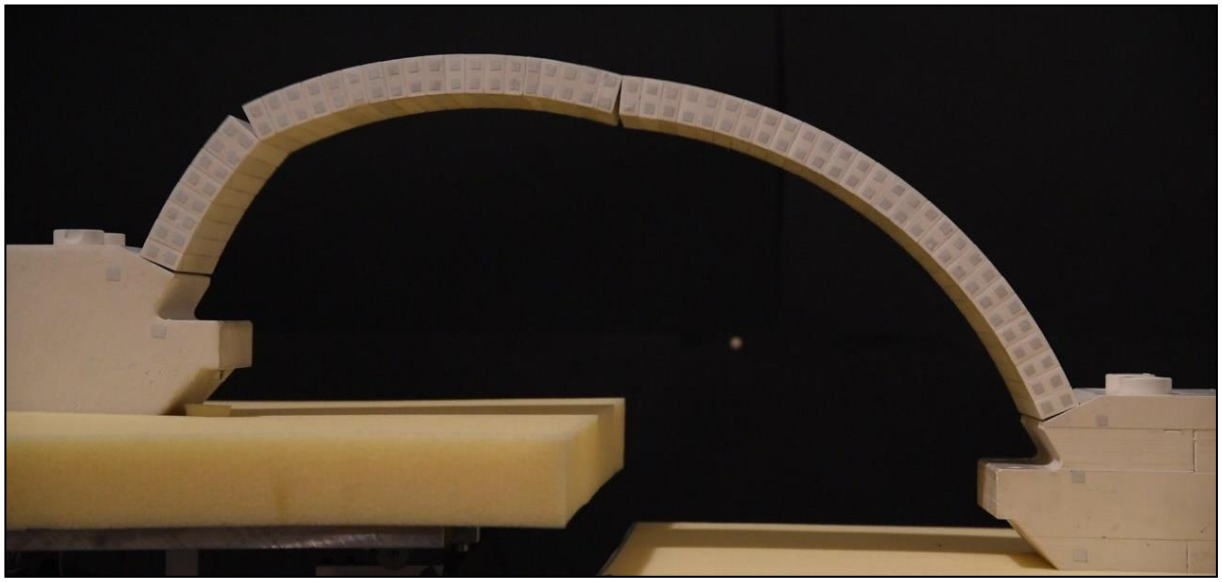

Structural Behaviour of Masonry Arches on Moving Supports: from On-site Observation to Experimental and Numerical Analysis

Chiara Ferrero

STRUCTURAL BEHAVIOUR OF MASONRY ARCHES ON MOVING SUPPORTS: FROM ON-SITE OBSERVATION TO EXPERIMENTAL AND NUMERICAL ANALYSIS

BY

CHIARA FERRERO

Dissertation discussed in partial fulfilment of
the requirements for the Degree of

DOCTOR OF PHILOSOPHY

Civil, Chemical and Environmental Engineering
University of Genoa, Genoa, Italy

Construction Engineering
Technical University of Catalonia, Barcelona, Spain

June, 2021

Thesis Supervisors

Prof. Chiara Calderini – University of Genoa, Italy
Prof. Pere Roca – Technical University of Catalonia, Spain

External Reviewers:

Prof. Vasilis Sarhosis – University of Leeds, United Kingdom
Prof. Els Verstrynge – KU Leuven, Belgium

Examination Committee:

Prof. Katalin Bagi – Budapest University of Technology and Economics, Hungary
Prof. Katrin Beyer – École Polytechnique Fédérale de Lausanne, Switzerland
Prof. Matthew J. DeJong – University of California, Berkeley, USA

Cotutelle agreement:

University of Genoa
Ph.D. program in Civil, Chemical and Environmental Engineering (Doctor Europaeus Mention)
Structural and Geotechnical Engineering, Mechanics and Materials
Cycle XXXIII

Technical University of Catalonia
Ph.D. program in Construction Engineering (International Ph.D. Mention)

ACKNOWLEDGMENTS

First of all, I want to thank my supervisors for guiding my research. I would like to express my gratitude to Prof. Chiara Calderini for involving me in such an interesting research and trusting me since the first moment. I am indebted to Prof. Roca for welcoming me in his research group in Barcelona and for sharing with me his knowledge on masonry structures. Furthermore, I want to thank him for his encouragement and valuable meetings not only during the last three and a half years, but especially during last months. Without his support, I would not have completed my thesis on time.

I would like to acknowledge the Italian Ministry of Education, University and Research (MIUR) for financing the Ph.D. grant at the University of Genoa. This work has also benefited from additional financial support from the Italian Ministry of Education, University and Research (MIUR) through the PRIN 2015 Program "Protecting the Cultural Heritage from water-soil interaction related threats" (Prot. No. 2015EAM9S5).

I gratefully acknowledge Prof. Francesco Portioli (University of Naples *Federico II*) for giving me the opportunity to use the results from his numerical model for enriching my thesis and for the fruitful discussions about numerical modelling.

I want to thank Giuseppe Tarantino, Davide Burlando and the personnel of Structural Engineering Laboratory of the University of Genoa for all the help that they have given me with the preparation of the experimental campaign. Prof. Luigi Carassale and Prof. Enrico Lertora are also gratefully acknowledged for their help with the data acquisition and preparation of the physical model, respectively.

I am grateful to all my friends and colleagues in Genova and Barcelona for their interest in my work and the nice time we had together. A special thanks goes to Ludovica for her support and all the laughs we shared, Antonetta for always being available and happy to help, and Larisa and Nirvan for their encouragement during the last weeks of work. I also want to thank my Canadians friends, Kristen and Krista, for their help with the English writing.

I want to express my deepest gratitude to Jorge for being my reference point in Barcelona, for his friendship, valuable advice, and continuous support from the very beginning to the end of this adventure. Thank you for all the time you devoted to helping me in the post-processing of the experimental data, to revising many times the same sentences and to listening to all my complaints.

I owe my deepest gratitude to my family. I am grateful for their unconditional love, patience and for supporting every choice I made in my life, even if it took me away from home.

Finally, a special thanks goes to Edoardo. I am indebted to him for his support and love, for driving me to Genova during the weekends to finish the experimental tests in the middle of a pandemic, for helping me in preparing the annexes, for reading my work, for accepting to be so many months apart. Without you, this thesis would have never been completed. Grazie.

This page is intentionally left blank.

ABSTRACT

Since ancient times, master builders have used arches to cover large spans in masonry structures. As a consequence, nowadays the safety assessment of these structural elements plays a fundamental role in the conservation of built cultural heritage.

Due to their frequent occurrence, support displacements are one of the primary sources of damage for masonry arches. Among the potential causes of support displacements, slow-moving landslides have received very little attention from the scientific community. The present thesis is motivated by the observation of extensive and severe damage in the arches of historic masonry churches exposed to slow-moving landslides. These phenomena produce a combination of vertical and horizontal supports displacements, whose effect on the arch structural behaviour has never been thoroughly investigated in the literature, especially in the framework of large displacements.

In view of the above, this thesis aims at providing a full understanding of the mechanics of masonry arches subjected to large support displacements, with special attention to inclined displacements. The methodology used to accomplish this goal included both experimental tests and numerical analyses on a segmental scaled dry-joint masonry arch subjected to different combinations of horizontal and vertical displacements at one support.

The numerical simulations were carried out in the framework of large displacements using two different numerical approaches based on finite element (FE) and rigid block (RB) modelling. A micro-modelling strategy was adopted, where the arch was modelled as an assemblage of voussoirs, very stiff and infinitely resistant in compression in the FE model and rigid in the RB model, interacting at no-tension friction interfaces. Preliminary numerical simulations, aimed at designing the experimental set-up and gaining a first insight in the arch response, were carried out considering the arch as a rigid-no tension structure. To this aim, a very large value of interface normal stiffness was adopted in the FE model.

A large experimental campaign was performed on a 1:10 small-scale model built as a dry-joint assemblage of voussoirs made of a bicomponent composite material. The results of the tests allowed, for the first time in the literature, to accurately assess the effect of the direction of the imposed support displacements on the arch response in the framework of large displacements. The comparison between numerical and experimental results showed that the numerical models were not able to accurately predict the experimental response, especially in terms of ultimate displacement capacity. To investigate this discrepancy, a sensitivity analysis on the effect of the interface normal stiffness on the FE predictions was performed. The results demonstrated that the difference between numerical and experimental results could be attributed due to the imperfections, and resulting deformability, of the joints of the physical model. A strategy to include imperfections in the numerical modelling, consisting in calibrating the interface normal stiffness based on the experimental results, was thus proposed and validated by performing further FE simulations, whose results were in very good agreement with the experimental evidence.

Finally, to investigate the effect of geometrical imperfections on the arch response, a further experimental test was performed on a physical model made of bicomponent composite voussoirs exhibiting more imperfections. The test was simulated using a FE calibrated model to further validate the strategy proposed

to model imperfections. The comparison between the experimental results for the two tested physical models showed that imperfections play a fundamental role in the response of small-scale arches to large support displacements. Furthermore, reducing the interface normal stiffness with respect to the large value adopted to model rigid interfaces proved to be an effective strategy to simulate the amount of imperfections of the experimental models.

Keywords: dry-joint masonry arches; inclined support displacements; finite element modelling; rigid block modelling; experimental testing; geometrical imperfections.

SOMMARIO

Fin dall’antichità, i maestri costruttori hanno utilizzato gli archi per coprire grandi luci nelle strutture in muratura. Di conseguenza, ad oggi la valutazione della sicurezza di questi elementi strutturali gioca un ruolo fondamentale nella conservazione del patrimonio architettonico.

A causa del loro frequente verificarsi, gli spostamenti degli appoggi sono una delle principali fonti di danno per gli archi in muratura. Tra le potenziali cause di questi spostamenti, le frane a cinematica lenta hanno ricevuto pochissima attenzione da parte della comunità scientifica. La presente tesi è motivata dall'osservazione di danni ingenti negli archi di chiese storiche in muratura interessate da frane a cinematica lenta. Questi fenomeni producono una combinazione di spostamenti verticali e orizzontali agli appoggi, il cui effetto sul comportamento strutturale dell'arco non è mai stato studiato a fondo in letteratura, soprattutto nell’ambito di grandi spostamenti.

Alla luce di queste osservazioni, questa tesi si propone di fornire una piena comprensione della meccanica degli archi in muratura soggetti a grandi spostamenti degli appoggi, con particolare attenzione agli spostamenti inclinati. La metodologia utilizzata per raggiungere questo obiettivo ha incluso sia prove sperimentali che analisi numeriche su un arco ribassato in muratura di giunti a secco in piccola scala, in cui sono state applicate diverse combinazioni di spostamenti orizzontali e verticali in corrispondenza di un appoggio.

Le simulazioni numeriche sono state eseguite nell’ambito dei gradi spostamenti utilizzando due diversi approcci numerici basati su una modellazione ad elementi finiti (FE) ed una modellazione a blocchi rigidi (RB). È stata adottata una strategia di micro-modellazione, in cui l'arco è stato modellato come un assemblaggio di blocchi, molto rigidi e infinitamente resistenti a compressione nel modello FE e infinitamente rigidi nel modello RB. In entrambi i modelli i blocchi erano collegati da interfacce senza resistenza a trazione. Simulazioni numeriche preliminari, finalizzate a progettare il set-up sperimentale e ad acquisire una prima conoscenza della risposta dell'arco, sono state eseguite considerando l'arco come una struttura rigida non resistente a trazione. A tal fine, nel modello FE è stato adottato un valore molto elevato di rigidezza normale delle interfacce.

Un’ampia campagna sperimentale è stata eseguita su un modello in scala 1:10 costruito come un assemblaggio a secco di blocchi realizzati con un materiale composito bicomponente. I risultati delle prove sperimentali hanno permesso, per la prima volta in letteratura, di valutare con precisione l'effetto della direzione degli spostamenti imposti sulla risposta dell'arco nell’ambito dei grandi spostamenti. Il confronto tra i risultati numerici e sperimentali ha mostrato che i modelli numerici non erano in grado di cogliere in maniera accurata la risposta sperimentale, specialmente in termini di spostamento ultimo al collasso. Al fine di indagare le ragioni di questa discrepanza, è stata quindi eseguita un'analisi di sensitività relativa all’effetto della rigidezza normale delle interfacce sulle previsioni del modello FE. I risultati hanno dimostrato che la differenza tra risultati numerici e sperimentali poteva essere attribuita alle imperfezioni, e conseguente deformabilità, delle interfacce del modello fisico. Una strategia per includere le imperfezioni nella modellazione numerica, consistente nel calibrare la rigidezza normale delle interfacce sulla base dei

risultati sperimentali, è stata quindi proposta e validata attraverso ulteriori simulazioni FE, i cui risultati si sono rivelati in ottimo accordo con le evidenze sperimentali.

Infine, per indagare l'effetto delle imperfezioni geometriche sulla risposta dell'arco, è stata eseguita un’ulteriore prova sperimentale su un modello fisico costituito da blocchi dello stesso materiale composito bicomponente che presentavano però più imperfezioni. Al fine di validare ulteriormente la strategia proposta per modellare le imperfezioni, la prova sperimentale è stata simulata utilizzando un modello FE calibrato. Il confronto tra i risultati sperimentali per i due modelli fisici ha mostrato che le imperfezioni giocano un ruolo fondamentale nella risposta di archi in piccola scala a grandi spostamenti degli appoggi. Inoltre, ridurre la normale rigidezza dell'interfaccia rispetto al valore molto alto adottato per modellare interfacce rigide si è rivelata una strategia efficace per simulare la quantità di imperfezioni dei modelli sperimentali.

RESUMEN

Desde la antigüedad, los maestros constructores han utilizado el arco como elemento estructural para salvar grandes luces en estructuras de mampostería. En consecuencia, para la conservación del patrimonio arquitectónico es hoy en día de fundamental importancia la correcta verificación estructural de este tipo de elementos.

Se ha observado frecuentemente que el desplazamiento de los apoyos es una de las principales causas de daño en arcos de mampostería. De entre las distintas causas que pueden provocar dicho desplazamiento, el deslizamiento de tierras ha recibido poca atención por parte de la comunidad científica. La presente tesis encuentra su motivación en el daño extenso y severo observado en los arcos de las iglesias de mampostería ubicadas en zonas expuestas a deslizamiento de tierras. Este fenómeno produce una combinación de desplazamientos verticales y horizontales, cuyo efecto en el comportamiento estructural de los arcos no ha sido investigado en profundidad, especialmente en lo relativo a grandes desplazamientos.

Esta tesis aspira a contribuir al conocimiento del comportamiento mecánico de los arcos de mampostería sometidos a grandes desplazamientos de apoyos, con especial atención a los desplazamientos inclinados. La metodología utilizada para dicho fin incluye ensayos experimentales y análisis numéricos en un modelo a escala de un arco de mampostería a junta seca. El modelo fue ensayado bajo diferentes combinaciones de desplazamientos horizontales y verticales en uno de sus apoyos.

La simulación numérica fue desarrollada en el marco de grandes desplazamientos usando dos métodos numéricos diferentes consistentes en un modelo de elementos finitos (FE) y en un modelo de bloques rígidos (RB). Los modelos fueron concebidos como un conjunto de dovelas rígidas con infinita resistencia a compresión en el modelo FE y como dovelas infinitamente rígidas en el modelo RB. En ambos modelos la interfaz entre dovelas fue modelada sin resistencia a tracción y con posibilidad de deslizamiento friccional. Con el objetivo de diseñar la configuración experimental y adquirir una comprensión inicial de la respuesta del arco, se llevaron a cabo simulaciones numéricas preliminares en las cuales se consideró al arco estudiado como una estructura rígida. Para ello en el modelo FE del arco, la rigidez normal de la interfaz fue inicialmente caracterizada con un valor muy elevado.

La campaña experimental fue llevada a cabo en modelos a escala 1:10 construidos como un conjunto a junta en seco de dovelas moldeadas con un material bicomponente. Los resultados de los ensayos experimentales permitieron, por primera vez en la literatura, un análisis preciso del efecto que tiene la dirección del desplazamiento impuesto en el comportamiento del arco en marco de grandes desplazamientos. La comparación entre los resultados numéricos y experimentales mostró que los modelos numéricos no eran capaces de capturar de manera precisa la respuesta experimental, especialmente en lo relativo al desplazamiento de colapso. Para investigar esta discrepancia, se realizó un estudio de sensibilidad relativo al efecto de la rigidez normal de la interfaz sobre las predicciones del modelo FE. Los resultados demostraron que la diferencia entre los resultados numéricos y experimentales se debía a las imperfecciones de las juntas del modelo físico. Como consecuencia, se propuso la inclusión de imperfecciones en el modelo numérico. Para ello se calibró la rigidez normal de la interfaz según los

resultados experimentales y el modelo se validó con nuevas simulaciones cuyos resultados finalmente concordaron muy bien con la evidencia experimental.

Finalmente, con el fin de investigar el efecto de las imperfecciones en la respuesta del arco, se llevó a cabo otro ensayo con el mismo modelo experimental, pero añadiéndole imperfecciones. El ensayo fue simulado con el modelo calibrado FE para validar la estrategia propuesta para la modelación de imperfecciones. Al comparar los resultados experimentales de los dos modelos ensayados, se puso en evidencia que las imperfecciones juegan un rol fundamental en la respuesta de arcos a pequeña escala con grandes desplazamientos en los apoyos. Además, la reducción de la rigidez normal de la interfaz con respecto al valor muy elevado inicialmente adoptado demostró ser una estrategia efectiva para simular las imperfecciones de los modelos experimentales.

CONTENTS

This page is intentionally left blank.

LIST OF FIGURES

LIST OF TABLES

This page is intentionally left blank.

NOTATION AND ABBREVIATIONS

Notation

Symbol	Name
L	Net span length of the arch
α	Direction of the imposed support displacement (measured from the vertical)
δ	Imposed support displacement
δ_x	Horizontal component of the imposed support displacement δ
δ_z	Vertical component of the imposed support displacement δ
δ_x/L	Span increase
δ_z/L	Deflection ratio
f_{Di}	Vertical dead loads
ρ	Unit weight
i	Arch block identifier
V_i	Volume of the arch block
k	Contact points identifier
j	Frictional contact interfaces identifier
t_k	Shear force components at contact points
n_k	Normal force components at contact points
$\boldsymbol{x_i}$	Positions at block centroid
$\boldsymbol{\Delta x_i}$	Displacements at block centroids
$\boldsymbol{\Delta u_k}$	Displacement rates at contact points
s	Movable block identifier
f_s	Inclined load applied at the movable block s
f_{Ds}	Constant dead load of the movable block s
f_{Ls}	Live load
b	Number of arch blocks
λ	Collapse load multiplier
$\boldsymbol{c}$	Vector of the unknown internal forces at interfaces
c	Number of contact points
$\boldsymbol{g_0}$	Vector collecting the gaps between contact point k and related surfaces
$\boldsymbol{f_D}$	Vector of dead loads applied at the centroid of the blocks
$\boldsymbol{f_{Di}}$	Subvectors collected in the vector f_D

$\boldsymbol{f_L}$	Vector of live loads
$\boldsymbol{A_0}$	Equilibrium matrix
$\boldsymbol{Y^T}$	Matrix of failure conditions corresponding to sliding and opening failure at contact points
$\boldsymbol{x_0}$	Given configuration
k_n	Interface normal stiffness adopted in the FE model
k_s	Interface tangential stiffness adopted in the FE model
$\delta_{x,u}/L$	Span increase at collapse
$\delta_{z,u}/L$	Deflection ratio at collapse
R_x	Horizontal support reaction
R_z	Vertical support reaction
$R_{x,u}$	Horizontal support reaction at collapse
$R_{z,u}$	Vertical support reaction at collapse
$R_{x,min}$	Minimum thrust
β	Radial position of hinge A
β_t	Radial position of hinge A in the theoretical continuous arch
Φ	Friction angle
$\Delta_{z,v}$	Vertical displacement of the arch voussoir net of the imposed vertical displacement δ_z
Δd_v	Change in the distance between the markers of adjacent voussoirs
$\Delta d_{v,0}$	Initial value of the distance between the markers of adjacent voussoirs (prior to the application of support displacements)

Abbreviations

CH	Church
2D	Two-dimensional
3D	Three-dimensional
FE	Finite element
FEM	Finite element model(ling)
RB	Rigid block
RBM	Rigid block model(ling)
DE	Discrete element
DEM	Discrete element model(ling)
E	Extrados
I	Intrados

CHAPTER 1

INTRODUCTION

1.1. BACKGROUND AND MOTIVATION

“The cultural heritage of each is the cultural heritage of all”. This simple but fundamental principle of UNESCO, reported in the Nara document of authenticity (ICOMOS, 1994), clearly indicates that the modern society has a moral responsibility to preserve built cultural heritage and leave it as a legacy for future generations. The protection of heritage buildings against natural (i.e. earthquakes, floods, landslides, etc.) and anthropic (i.e. subsidence) hazards is relevant from the two perspectives of safety and conservation. Heritage assets are still used and inhabited all over the world. Consequently, their structural safety must be assessed and guaranteed to protect human life and avoid fatalities. Moreover, built heritage has a cultural intangible value that has to be preserved over time.

Among heritage buildings, churches are of particular importance since they represent a place of social aggregation and cultural identity where people may gather in large numbers, and, furthermore, they are often rich in movable and immovable cultural assets.

Among the hazards threatening historic churches, earthquakes have so far drawn the greatest attention from academics and institutions. In the last decades, several research works were devoted to the damage and vulnerability assessment of historic masonry churches subjected to horizontal actions. These studies, which led to the identification of the collapse mechanisms of churches under seismic loading, were motivated by the extensive and severe damage produced to churches by past and recent earthquakes in Italy (e.g. Canuti et al. 2019; da Porto et al. 2012; De Matteis et al. 2016; Doglioni et al. 1994; Lagomarsino 2012; Lagomarsino and Podestà 2004a, 2004b, 2004c; Penna et al. 2019; Podestà et al. 2010) and other European regions (e.g. Guerreiro et al. 2000; Romão et al. 2013).

Although earthquakes pose a major threat to the conservation of historical masonry churches, a number of different phenomena can be considered as a potential source of risk. Among them, landslides are an important hazard in the Italian territory. According to the 2018 Summary report of the Institute for Environmental Protection and Research (ISPRA, Trigila et al. 2018), Italy is one of the European countries most affected by landslides. Between 1116 and 2017, 620808 landslides, affecting an area of 23700 km^2, equal to 7.9% of the national territory, were recorded. The cultural heritage buildings exposed to landslide risk are 37847, corresponding to 18.6% of the total. Although the 2018 Summary report by ISPRA does not specify the number of historic churches at risk, Italy has about 67013 churches, of which 32000 are listed (Calderini and De Matteis 2020). Consequently, the probability that a number of them are exposed to landslide risk is very high.

Differently from what was observed for earthquakes, in the case of landslides no abacus of collapse mechanisms or damage classification is available for historic masonry churches, as the effects of landslides

on the structural response of this type of buildings have never been systematically investigated. It is worth noting that this applies not only to landslides, but also, more generally, to all the phenomena involving soil movements. Subsidence and foundation settlements have been addressed only through the analysis of case studies (e.g., Ayensa et al. 2015; Calabresi 2013; Drougkas et al. 2020; Lancellotta 2013; Saloustros et al. 2015; Sánchez et al. 2016; Taliercio and Binda 2007) or single structural elements such as arches and vaults (e.g. D'Altri et al. 2020; Galassi et al. 2018; McInerney and DeJong 2015; Torres et al. 2019a, 2019b; Van Mele et al. 2012). The literature related to churches located in landslide-affected areas has mainly focused on the geotechnical and geological analysis of the slope movement (Cigna et al. 2013; Margottini et al. 2013; Soccodato et al. 2013; Spizzichino et al. 2012) rather than on soil-structure interaction.

Among the region in which Italy is divided, Liguria is one of the most affected by landslide phenomena. Liguria is a hilly region of Northern Italy confined within a narrow strip of land bounded to the North by the Alps and Apennines, and to the South by the Ligurian sea. Due to the geographical location, orography as well as morphological and geological setting of the Ligurian territory, landslides frequently occur. As reported in Guzzetti et al. (2004), 1806 landslide events damaged 1233 localities between 1800 and 2001. Furthermore, in 2017, an area of 751.9 km^2, equal to 13.9% of the regional territory, was classified as a high or very high landslide hazard zone (Trigila et al. 2018).

Within the framework of the National Research Program PRIN 2015 "PERICLES- Protecting the Cultural Heritage from water-soil interaction related threats" (grant n. 2015EAM9S5 from Ministry of Education, University and Research), on-site inspections and damage surveys were performed on a large sample of historic masonry churches located in Liguria in areas affected by slow-moving landslides. This activity was carried out by the thesis author in collaboration with the former Ph.D candidate Ludovica Cambiaggi, Prof. Rita Vecchiattini and Prof. Chiara Calderini from the Department of Civil, Chemical and Environmental Engineering and the Architecture and Design Department of the University of Genoa (Liguria).

The main aims of this activity were to describe the damage suffered by historic masonry churches in terms of crack patterns and deformation as well as to identify the damage mechanisms produced by slow-moving landslides. Attention was paid only to the landslides that can be classified as very slow or extremely slow according to the classification provided by Cruden and Varnes (1996). These types of phenomena produce soil displacements that are small in their instantaneous values, as their velocity does not exceed 1.6 m/year and 16 mm/year in the case of very slow and extremely slow landslides, respectively. Notwithstanding the very low speed, slow-moving landslides were found to cause severe damage to masonry structures over time (Antronico 2015; Nicodemo 2017).

Extensive and severe damage, congruent with the landslide direction, was detected in several churches of the sample, suggesting the need for further investigation on the effects of slow-moving landslides. In particular, widespread cracks and very large deformations were observed in the arches of the large majority of the churches inspected. Arches have a primary structural role in the skeleton of a masonry church, as they transfer the vertical loads and thrusts transmitted by vaults and roof to pillars and foundations. A full understanding of their structural behaviour is thus essential for the damage and vulnerability assessment of historic masonry churches exposed to slow-moving landslides.

Since landslides involve both downward and lateral ground movements (Cooper 2008), they are expected to produce a combination of vertical and horizontal displacements at the arch supports. The assessment of the damage induced by slow-moving landslides to masonry arches thus requires to evaluate their structural performance under inclined support displacements. However, this is a new field of research. Although a large body of recent literature was devoted to investigating purely vertical and horizontal supports displacements, there is still a lack of studies dealing with their combination. It is the motivation of this work to address this gap and provide a full understanding of the mechanics of masonry arches subjected to inclined support displacements. The identification of the damage and collapse mechanisms of these structural elements will help in the interpretation of the crack patterns produced by slow-moving landslides in historic masonry churches. Nevertheless, it is worth noting that the conclusions drawn from this study are not applicable only to the case of slow-moving landslides. Support displacements can be produced by a range of different causes, including foundation settlements, subsidence, leaning of supporting piers and buttresses, and many others. Similarly to slow-moving landslides, these phenomena evolve slowly over time, but they can affect a church over its entire life, causing support displacements to substantially increase and thus producing damage and deformations. If foundations settlements and subsidence result in vertical support displacements, the leaning of piers and buttresses, generally produced by the horizontal thrusts of arches and vaults, causes horizontal support displacements. Since these phenomena often occur simultaneously in historic masonry churches, it is unlikely that the displacements at the arch supports are purely vertical or horizontal. In view of these considerations, this work does not deal with a specific source of support displacements, but it seeks to investigate any type of support displacements that evolve slowly over time.

1.2. OBJECTIVES AND METHODOLOGY

The main aim of this thesis is to provide a full understanding of the static behaviour of masonry arches subjected to large support displacements increasing slowly over time. To accomplish this goal, a set of specific objectives was defined as follows:

- To identify the recurrent crack patterns and deformations caused by slow-moving landslides in arches of historic masonry churches.
- To gather information on the existing knowledge about the structural behaviour of masonry arches on moving supports.
- To study the response of masonry arches to inclined support displacements by means of experimental tests and numerical simulations.
- To assess the effect of the displacement direction on collapse mechanism, hinge position, support reaction-displacement curves, ultimate displacement capacity and support reactions at collapse.

- To evaluate the ability of numerical models to predict the experimental response of masonry arches on moving supports.

- To propose a strategy to calibrate the numerical models so as to accurately capture the structural behaviour observed in the experimental tests.

The methodology followed to accomplish these objectives is presented below.

On-site inspections and damage surveys were first carried out on 33 historic masonry churches located in the Liguria region (Italy) in areas affected by slow-moving landslides. The crack patterns and deformations exhibited by arches and vaults were described and critically analysed in an attempt to identify the recurrent damage mechanisms.

The existing literature on masonry arches subjected to support displacements was then comprehensively reviewed with the aim to: (i) provide insights in the arch mechanics thanks to the analysis of the results of the experimental investigations, and (ii) present all the computational methods used so far to address this topic. The literature review was also extended to the research works dealing with masonry vaults on moving supports.

To evaluate the effect of inclined support displacements on the response of masonry arches, experimental tests and numerical analyses were performed on a segmental scaled dry-joint arch subjected to different combinations of vertical and horizontal support displacements.

The experimental tests were performed on a 1:10 small-scale model built as a dry-joint assembly of voussoirs made of a bicomponent composite material. A new testing machine was designed ad hoc to impose vertical, horizontal and inclined displacements at one support of the arch.

The numerical simulations were carried out in the framework of large displacements using two different numerical approaches, namely finite element (FE) modelling and rigid block (RB) modelling. With the aim of accurately simulating the experimental tests on a dry-joint voussoir arch, a micro-modelling strategy was adopted. The arch was thus modelled as an assembly of voussoirs, very stiff and infinitely resistant in compression in the FE model and rigid in the RB model, interacting at no-tension friction interfaces. The ability of the two models to simulate the response of masonry arches to large support displacements was evaluated through comparison with experimental results from the literature.

Prior to performing the experimental tests, preliminary numerical simulations were carried out to gain a first insight in the response of the arch to different combinations of vertical and horizontal support displacements. A specific aim was to determine the maximum allowable displacement at collapse, which was needed for the design of the experimental set-up. In these preliminary numerical simulations, the arch was analysed as a rigid-no tension structure. To this aim, a very large value of interface normal stiffness, determined based on a sensitivity analysis, was adopted in the FE model.

To assess the ability of the numerical models to accurately simulate the experimental response, the numerical predictions were compared to the experimental results. Since some discrepancies were observed, a strategy to calibrate the numerical models was sought. For this purpose, a sensitivity analysis on the effect of the interface normal stiffness adopted in the FE model was performed. The results suggested that this

parameter could be used as the variable to tune to obtain a better matching between experimental and numerical results. The interface normal stiffness was thus calibrated according to the experimental evidence, and further FE simulations were carried out to verify the effectiveness of the strategy proposed.

Finally, a further experimental test was performed on a small-scale arch made of bicomponent composite voussoirs exhibiting more imperfections. A calibrated FE model was used to simulate the experimental test. The effect of geometrical imperfections on the arch response was evaluated by comparing the experimental and numerical results obtained for the two small-scale models built.

1.3. THESIS OUTLINE

This thesis consists of seven chapters.

Chapter 1 presents the motivation and background that inspired this research work and states the main aim and specific objectives.

Chapter 2 describes the on-site inspections and the damage surveys performed on a sample of historic masonry churches exposed to slow-moving landslide threats. The criteria adopted for the selection of the case studies as well the methodology used to perform on-site inspections and gather data are presented. A brief description of the sample of case studies is also provided. After describing the recurrent crack patterns and deformations observed, the main conclusions obtained from the critical assessment of the surveyed damage are presented. Lastly, the crack patterns and deformations observed in masonry arches and vaults are described and critically analysed.

Chapter 3 proposes a comprehensive review of the existing literature for masonry arches and vaults on moving supports. The first part of the chapter reviews in detail the experimental investigations. For masonry arches, the experimental results are analysed to provide a detailed description of the damage and collapse mechanisms experienced. The second and third parts of the chapter describe the computational methods used in the literature to investigate the stability of masonry arches and vaults when subjected to support displacements. A distinction is provided between the analytical and computational methods based on Limit Analysis and modern methods based on finite element, discrete element and rigid block modelling. The ability of the computational methods to predict the experimental results is also discussed.

Chapter 4 presents the preliminary numerical analyses carried out on the segmental scaled dry-joint arch chosen as case study in this thesis. The static behaviour of the arch, which is modelled as a rigid-no tension structure, is investigated under different combinations of vertical and horizontal support displacements using FE and RB models. First, both models are validated against experimental results from the literature. A discussion on the value of interface normal stiffness to adopt in the FE model is also presented. Second, the results obtained from FE and RB simulations for the scaled dry-joint arch under study are compared and discussed in detail. Lastly, the sensitivity of the results to the number of voussoirs is investigated.

Chapter 5 presents the design, execution and results of the experimental campaign performed on a 1:10 small-scale model of the segmental dry-joint arch under investigation. The arch is subjected to different combinations of vertical and horizontal displacements at one support. Results are obtained in terms of damage evolution, ultimate displacement capacity, displacements of the voussoirs and support reactions.

Chapter 6 provides a critical interpretation of the experimental tests. The experimental results are first compared to the numerical predictions for the rigid-no tension arch. A strategy to calibrate the numerical models on the basis of the experimental is then proposed, and further numerical analyses are performed using a calibrated FE model. Lastly, the effects of geometrical imperfections on the experimental response of the small-scale arch are evaluated by performing a further experimental test as well as numerical simulations on a FE calibrated model.

Chapter 7 summarizes the results and provides suggestions for future works.

1.4. RESEARCH DISSEMINATION

The work presented in this thesis has resulted in the following scientific publications:

Papers in peer-reviewed international journals

- Ferrero, C., Calderini, C., Portioli, F., and Roca P. (2021) Large displacement analysis of dry-joint masonry arches subject to inclined support movements. *Engineering Structures*, 238, 112244. https://doi.org/10.1016/j.engstruct.2021.112244.

- Ferrero, C., Rossi, M., Roca, P. and Calderini, C. (2021) Experimental and numerical analysis of a scaled dry-joint arch on moving supports. *International Journal of Masonry Research and Innovation*, 6(4) (Special issue on Simple Mechanical Models for Unreinforced Historic Masonry Constructions, in press). https://doi.org/10.1504/IJMRI.2021.10035577.

- Ferrero, C., Cambiaggi, L., Vecchiattini, R. and Calderini, C. (2021) Damage assessment of historic masonry churches exposed to slow-moving landslides. *International Journal of Architectural Heritage* (In press). https://doi.org/10.1080/15583058.2020.1799259.

Peer-reviewed conference papers

- Ferrero, C., Cambiaggi, L., Fenialdi, A., Roca, P., Vecchiattini, R. and Calderini, C. Slow-moving landslide damage assessment of historic masonry churches: some case-studies in Italy. *12th International Conference on Structural Analysis of Historical Constructions - SAHC2021* (Accepted; oral presentation at the forthcoming conference).

- Cambiaggi, L., Ferrero, C., Berardi, R., Calderini, C. and Vecchiattini, R. Effect of slow-moving landslides on churches in the Liguria region: a geotechnical approach. *12th International Conference on Structural Analysis of Historical Constructions - SAHC2021* (Accepted).

- Ferrero C., Rossi, M., Roca P. and Calderini, C. Effect of geometrical imperfections on the response of dry-joint masonry arches to support settlements. *12th International Conference on Structural Analysis of Historical Constructions - SAHC2021* (Accepted; oral presentation at the forthcoming conference).

Presentations at international conferences

- Ferrero, C., Calderini, C., Portioli, F., and Roca P. (2021). Collapse mechanisms of masonry arches on moving supports. *14th WCCM & ECCOMAS Congress 2020*, Virtual Congress 11-15 January 2021.

REFERENCES

Antronico, L., L. Borrelli, R. Coscarelli, and G. Gullà. 2015. Time evolution of landslide damages to buildings: the case study of Lungro (Calabria, southern Italy). *Bulletin of Engineering Geology and the Environment* 74: 47-59.

Ayensa, A., B. Beltran, E. Ibarz, and L. Gracia. 2015. Application of a new methodology based on Eurocodes and finite element simulation to the assessment of a romanesque church. *Construction and Building Materials* 101(1): 287-297.

Calabresi G. 2013. The role of geotechnical engineers in saving monuments and historic sites. Kerisel Lecture. In: *Proceedings of the 18th International Conference on Soil Mechanics and Geotechnical Engineering*, ed. P. Delage, J. Desrues, R Frank, A. Puech, and F. Schlosser, 71–83, Paris, France: Presses des Ponts.

Calderini, C., and G. De Matteis. 2020. Report. Task 4.8_Modelli e curve di fragilità delle chiese. WP4_MAppe di Rischio e Scenari di danno sismico (MARS). Progetto ReLUIS-DPC 2019-2021.

Canuti, C., S. Carbonari, A. Dall'Asta, L. Dezi, F. Gara, G. Leoni, M. Morici, E. Petrucci, A. Prota, and A. Zona. 2019. Post-Earthquake Damage and Vulnerability Assessment of Churches in the Marche Region Struck by the 2016 Central Italy Seismic Sequence. *International Journal of Architectural Heritage*.

Cigna, F., V. Liguori, C. Del Ventisette, and N. Casagli. 2013. Landslide impacts on Agrigento's Cathedral imaged with radar interferometry. In: *Landslide Science and Practice*, ed. C. Margottini, P. Canuti and K. Sassa, 475-481. Springer Berlin Heidelberg.

Cooper, A. H. 2008. The classification, recording, databasing and use of information about building damage caused by subsidence and landslides. *Quarterly Journal of Engineering Geology & Hydrogeology* 41: 409-424.

Cruden, D.M. and D.J. Varnes. 1996. Landslide types and processes. In: *Landslides: investigation and mitigation*, Transportation Research Board, Special Report 247, 36-75. Washington, D.C.: National Academy of Sciences.

D'Altri, A.M., S. De Miranda, G. Castellazzi, V. Sarhosis, J. Hudson, and D. Theodossopoulos. 2020. Historic barrel vaults undergoing differential settlements. *International Journal of Architectural Heritage* 14(8): 1196-1209. https://doi.org/10.1080/15583058.2019.1596332.

da Porto, F., B. Silva, C. Costa, and C. Modena. 2012. Macro-scale analysis of damage to churches after earthquake in Abruzzo (Italy) on April 6, 2009. *Journal of Earthquake Engineering* 16(6): 739–758.

De Matteis, G., E. Criber, and G. Brando. 2016. Damage probability matrices for three-nave masonry churches in Abruzzi after the 2009 L'Aquila earthquake. International Journal of Architectural Heritage 10(2–3): 120–145.

Doglioni, F., A. Moretti, and V. Petrini. 1994. *Le chiese e il terremoto*. National Research Council, Trieste, IT: Lint Press (in Italian).

Drougkas, A., E. Verstrynge, P. Szekér, G. Heirman, L.E. Bejarano-Urrego, G. Giardina, and K. Van Balen. 2020. Numerical Modeling of a Church Nave Wall Subjected to Differential Settlements: Soil-Structure Interaction, Time-Dependence and Sensitivity Analysis. *International Journal of Architectural Heritage* 14(8): 1221-38. https://doi.org/10.1080/15583058.2019.1602682

Galassi, S., G. Misseri, L. Rovero, and G. Tempesta. 2018. Failure modes prediction of masonry voussoir arches on moving supports. *Engineering Structures* 173: 706–17. https://doi:10.1016/j.engstruct.2018.07.015.

Guerreiro, L., J. Azevedo, J. Proenca, R. Bento, and M. Lopes. 2000. Damage in ancient churches during the 9th of July 1998 Azores earthquake. *Proceedings of the 12th World Conference on Earthquake Engineering*, Auckland, New Zealand, paper no. 780.

Guzzetti, F., M. Cardinali, P. Reichenbach, F. Cipolla, C. Sebastiani, M. Galli, and P. Salvati. 2004. Landslides triggered by the 23 November 2000 rainfall event in the Imperia Province, Western Liguria, Italy. *Engineering Geology* 73(2): 229–245.

ICOMOS 1994. *Nara document on authenticity*. In: Conference on Authenticity in Relation to the World Heritage Convention. Nara, Japan.

Lagomarsino, S. 2012. Damage assessment of churches after L'Aquila earthquake (2009). *Bulletin of Earthquake Engineering* 10(1): 73–92.

Lagomarsino, S. and S. Podestà. 2004a. Seismic vulnerability of ancient churches. Part 1: damage assessment and emergency planning. *Earthquake Spectra* 20(2): 377–394.

Lagomarsino, S. and S. Podestà. 2004b. Seismic vulnerability of ancient churches. Part 2: statistical analysis of surveyed data and methods for risk analysis. *Earthquake Spectra* 20(2): 395–412.

Lagomarsino, S. and S. Podestà. 2004c. Damage and vulnerability assessment of churches after the 2002 Molise, Italy, earthquake. *Earthquake Spectra* 20(S1): S271–S283.

Lancellotta, R. 2013. La torre Ghirlandina: Una storia di interazione struttura-terreno. In: XI Croce Lecture. *Rivista Italiana di Geotecnica* 47(2): 7–37 (in Italian).

Margottini, C., D. Spizzichino, and A. Sonnessa. 2013. Landslide risk and monitoring system for conservation of Vardzia monastery, Georgia. In: *Geotechnical Engineering for the Preservation of Monuments and Historic Sites*, ed. E. Bilotta, A. Flora, S. Lirer, and C. Viggiani, 549-558. London, UK: CRC Press (Taylor & Francis Group).

McInerney, J., and M. J. DeJong. 2015. Discrete element modeling of groin vault displacement capacity. *International Journal of Architectural Heritage* 9(8): 1037-49. http://dx.doi.org/10.1080/15583058.2014.923953

Nicodemo, G. 2017. Vulnerability analysis of buildings in areas affected by slow-moving landslides and subsidence phenomena. PhD diss., University of Salerno.

Penna, A., C. Calderini, L. Sorrentino, C. F. Carocci, E. Cescatti, R. Sisti, A. Borri, C. Modena, and A. Prota. 2019. Damage to churches in the 2016 central Italy earthquakes. *Bulletin of Earthquake Engineering* 17(10): 5763-5790.

Podestà, S, A. Brignola, E. Curti, S. Parodi, and A. Lemme. 2010. Damage assessment and seismic vulnerability of churches: the Abruzzo earthquake. Ingegneria Sismica 2(1): 21–35 (in Italian).

Romão, X., A.A. Costa, E. Paupério, H. Rodrigues, R. Vicente, H. Varum, and A. Costa. 2013. Field observations and interpretation of the structural performance of constructions after the 11 May 2011 Lorca earthquake. Engineering Failure Analysis 34: 670–692.

Saloustros S., L. Pelà, P. Roca, and J. Portal. 2015. Numerical analysis of structural damage in the church of the Poblet Monastery, *Engineering Failure Analysis* 48: 41–61.

Sánchez A. R., R. Meli, and M. M. Chávez. 2016. Structural monitoring of the Mexico City cathedral (1990-2014), *International Journal of Architectural Heritage* 10(2-3): 254-68.

Soccodato, F.M, E. Martini, L. Tortoioli and A.M. Mazzi. 2013. The preservation of historical, archaeological and artistic heritage of Orvieto: an interdisciplinary project. In: *Geotechnical Engineering for the Preservation of Monuments and Historic Sites*, ed. E. Bilotta, A. Flora, S. Lirer, and C. Viggiani, 683-96. London, UK: CRC Press (Taylor & Francis Group).

Spizzichino, D., C. Margottini and L.M. Puzzilli. 2012. Landslide risk assessment and management in the archaeological site of Machu Picchu (Peru). In: *Geotechnical Engineering for the Preservation of Monuments and Historic Sites*, ed. E. Bilotta, A. Flora, S. Lirer, and C. Viggiani, 697-707. London, UK: CRC Press (Taylor & Francis Group).

Taliercio, A. and L. Binda. 2007. The Basilica of San Vitale in Ravenna: Investigation on the current structural faults and their mid-term evolution. *Journal of Cultural Heritage* 8: 99–118.

Torres, B., E. Bertolesi, P. A. Calderón, J. J. Moragues, and J. M. Adam. 2019. Experimental investigation of a full-scale timbrel masonry cross vault subjected to vertical settlement. *Construction and Building Materials* 221: 421–32. https://doi.org/10.1016/j.conbuildmat.2019.06.015.

Torres, B., E. Bertolesi, P. A. Calderón, J. J. Moragues, and J. M. Adam. 2019. A full-scale timbrel cross vault subjected to vertical cyclical displacements in one of its supports. *Engineering Structures* 183: 791-804. https://doi.org/10.1016/j.engstruct.2019.01.054.

Trigila, A., C. Iadanza, M. Bussettini, and B. Lastoria. 2018. Dissesto idrogeologico in Italia: pericolosità e indicatori di rischio. Rapporti 287/2018. Istituto Superiore per la Protezione e la Ricerca Ambientale – ISPRA (in Italian).

Van Mele, T., J. McInerney, M. J. DeJong, and P. Block. 2012. Physical and computational discrete modelling of masonry vault collapse. In *SAHC2012: Proceedings of 8th International Conference on Structural Analysis of Historical Constructions*, ed. J. Jasienko, 2552–2560. Dolnośląskie Wydawnictwo Edukacyjne.

CHAPTER 2

DAMAGE SURVEY OF HISTORIC MASONRY CHURCHES EXPOSED TO SLOW-MOVING LANDSLIDES

2.1. INTRODUCTION

This chapter presents the results of the damage survey performed on 33 historic masonry churches located in the Liguria region (Italy) in areas affected by slow-moving landslides. The criteria adopted to select the sample of case studies are described in Section 2.2. The methodology followed to perform on-site inspections and gather data about both churches and landslide movements is presented in Section 2.3. To better characterize the assets investigated, a brief description of the sample, providing information about construction date, layout, dimensions, and past interventions for each church, is also included. Section 2.4 describes the damage observed in the churches and presents the results of a critical damage assessment. The main conclusions regarding the structural response of historic masonry churches to slow-moving landslides are reported in terms of recurrent types of damage, damage levels and overall damage mechanisms. After dealing with the church in its entirety, attention is paid to arches and vaults. Although this thesis is focused on masonry arches only, the structural behaviour of masonry vaults is also analysed, since there is structural continuity between the two structural elements. Furthermore, slow-moving landslides produce the same displacements at the abutments of arches and vaults. In Section 2.5, the cracks patterns and deformations observed in arches and vaults are described in detail and critically analysed in an attempt to identify recurrent damage mechanism.

It should be noted that the damage assessment performed in this thesis was mainly based on visual inspections and was aimed to provide the first conclusions about the response of historic masonry churches as well as arches and vaults to slow-moving landslides. Nevertheless, a more accurate interpretation of the damage would require a deep knowledge of history, past alterations, materials, construction details and morphology (i.e. internal composition of structural members and connections) for each building investigated.

2.2. IDENTIFICATION OF THE SAMPLE OF CHURCHES

2.2.1. Churches located on active landslides

To select the sample of assets to be investigated, the landslide classification of the Liguria region and the list of heritage buildings protected by the Ministry of Cultural Heritage and Activities were taken into account.

According to the Italian regulations, the identification and classification of the areas exposed to slow-moving landslide threats are closely related to environmental planning. With the Law no. 183/1989 (G.U. no. 120, 1989), Italy was divided in a series of hydrographic basins. For each basin, a basin authority was established, with the main task of developing the basin management plan. The latter had to include maps containing geological, morphological and hydrographic information regarding the area of interest as well as data concerning landslide, hydraulic and geological risk. Since the Law no. 183/1989 (G.U. no. 120, 1989) provided only an indication of the contents of the basin plan, each basin authority adopted different criteria to develop its maps, with the result that they are not currently standardized at national level. This applies also to the maps providing information about zoning, classification, typology and state of activity of landslides, with the result that these maps differ from one hydrographic basin to the other.

This work focuses in the Liguria region, which is divided in three different basins: Tyrrhenian basins for the portion of the Tyrrhenian drainage basins located in the Ligurian territory (the other portion belongs to the Tuscany region), Magra River basin and Po River basin. Different types of maps identify landslides areas in the three basins: the *Carte della Suscettività al Dissesto* (Regione Liguria 2017) for the Tyrrenian and Magra River basins and the maps of the *Atlante dei Rischi Idraulici e Idrogeologici* (Autorità di bacino distrettuale del fiume Po 2017) for the Po River basin. Note that, hereafter, the maps of the three Ligurian basins will be generically named landslide maps.

The different criteria adopted for each basin in order to zone and identify landslides are presented next:

- The entire territory of the Tyrrhenian basin is divided in five classes of landslide susceptibility on a scale from Pg0 to Pg4. Pg4 class is characterized by the presence of active landslide, thus corresponding to the highest level of landslide susceptibility. Pg3 class is divided in two subclasses, Pg3a and Pg3b, respectively denoting areas with dormant landslide and territories with indirect indicators of movements (i.e. bent trees, damage in retaining wall, etc.) or stabilized landslides. The other three classes, Pg2, Pg1 and Pg0, only indicate the existence of geomorphological indicators, such as springs or cracks in the ground, but they are not actually characterized by landslides.

- The same criteria adopted for the Tyrrhenian basin are used to define the classes of landslide susceptibility in the Magra river basin. However, for the latter, only the areas classified as Pg2, Pg3 and Pg4 are indicated in the Carte della Suscettività al Dissesto (Regione Liguria 2017).

- The territory of the Po River basin is not classified according to landslide susceptibility levels. The areas affected by active, dormant or stabilized landslides are the ones reported in the Atlante dei Rischi Idraulici e Idrogeologici (Autorità di bacino distrettuale del fiume Po 2017). Landslides are represented either with their actual extension or with a dot when their perimeter is unknown.

Regarding heritage buildings, due to the large number of assets spread throughout the Ligurian territory, attention was paid only the churches and other religious buildings (i.e. sanctuaries, oratories and chapels) that are explicitly listed according to the Legislative Decree no. 42/2004 (G.U. no. 45, 2004). This choice

was driven by the need to limit the number of case studies in order to make it possible to collect detailed information about all of them.

The sample of buildings to analyse was then identified by superimposing the landslide maps of the Ligurian river basins, updated as of 2017/2018, on the regional map of the listed architectural assets, named *vincoli architettonici puntuali* in Italian (Regione Liguria e Segretariato Regionale del MiBACT per la Liguria 2017), which reports the position of all the listed buildings located in Liguria, including churches and other religious buildings. This superimposition was performed by means of the QGIS software, which allows one to manage a large amount of data spread throughout a territory (QGIS 2017). An example of superimposition of the two different maps is presented in Figure 2-1 for Sant'Olcese church in Sant'Olcese (CH_13).

Since different classification systems were adopted to map landslide areas in the three basins of the Liguria region, different criteria were used to select the case studies: (i) for the Magra River basin and Tyrrhenian basins, the churches located in the areas characterized by the highest landslide susceptibility, identified as Pg4, were considered; (ii) for the Po River basin, the churches situated in areas affected by active landslides were selected.

Extended to the entire Liguria region, this approach led to the detection of 28 listed churches located on active landslides (Table 1). The position of each church within the Ligurian territory is illustrated in Figure 2-2.

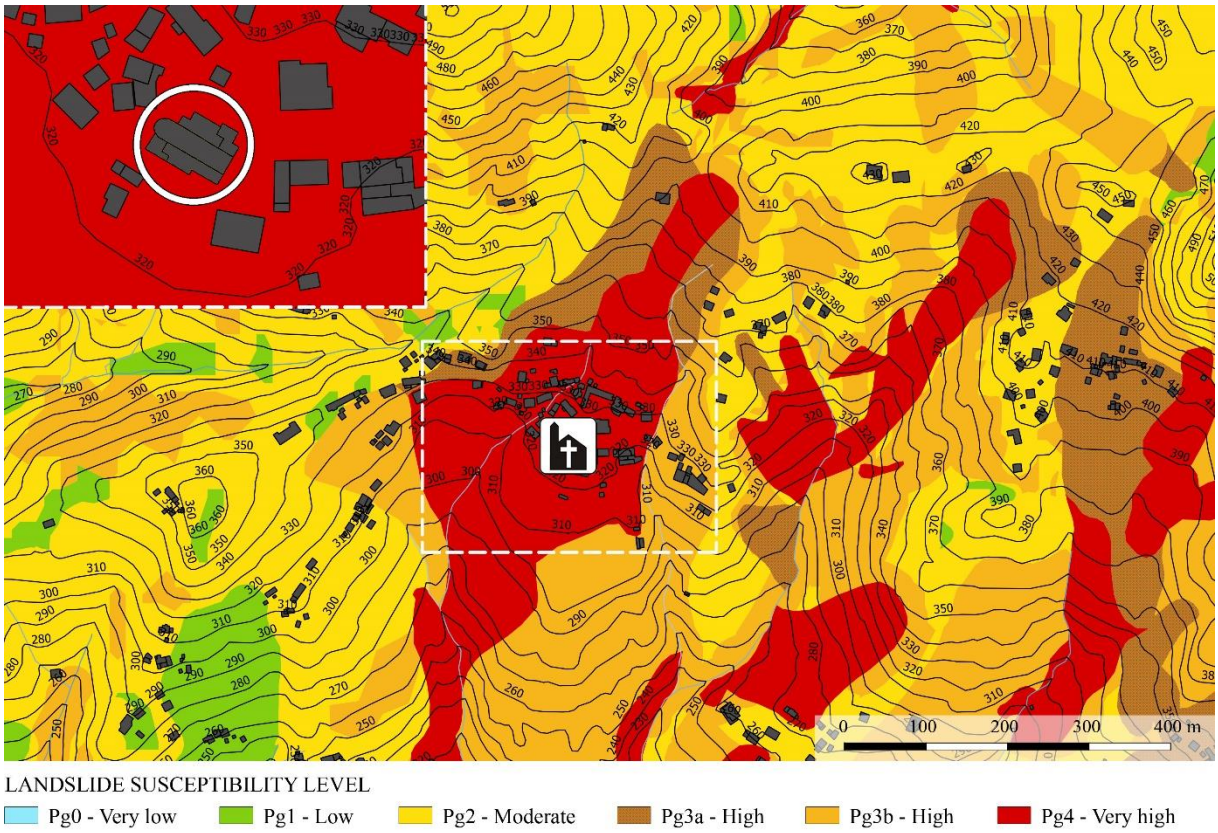

Figure 2-1 - Identification of churches located on active landslides: the case of Sant'Olcese church in Sant'Olcese (CH_13) (Regione Liguria 2017).

Table 1 Set of churches located on active landslides.

Id	Church name	Municipality, locality, province
CH_1	San Pietro Apostolo di Pino	Genova (Loc. Pino Soprano) (GE)
CH_2	Santo Stefano	Lumarzo (Loc. Pannesi) (GE)
CH_3	San Rocco	Neirone (Loc. Ognio) (GE)
CH_4	San Pietro in Vincoli	Borgomaro (Loc. Ville San Pietro) (IM)
CH_5	Santa Caterina	Mendatica (IM)
CH_6	Santa Maria Assunta	Moneglia (Loc. Lemeglio) (GE)
CH_7	Sant'Anna	Deiva Marina (Loc. Piazza) (SP)
CH_8	San Rocco oratory	Rezzoaglio (Loc. Alpepiana) (GE)
CH_9	San Bernardo da Mentone	Santo Stefano d'Aveto (Loc. Ascona) (GE)
CH_10	Santa Maria Assunta	Borzonasca (Loc. Prato Sopralacroce) (GE)
CH_11	San Giacomo oratory	Borzonasca (Loc. Prato Sopralacroce) (GE)
CH_12	San Martino	Ceranesi (Loc. San Martino di Paravanico) (GE)
CH_13	Sant'Olcese	Sant'Olcese (GE)
CH_14	San Giovanni Battista oratory	Sant'Olcese (GE)
CH_15	San Martino di Struppa	Genova (Loc. Struppa) (GE)
CH_16	San Pasquale Baylon	Maissana (Loc. Disconesi) (SP)
CH_17	San Pietro Apostolo	Savignone (GE)
CH_18	Santa Maria del Soviore sanctuary	Monterosso al Mare (Loc. Soviore) (SP)
CH_19	San Pietro	Portovenere (SP)
CH_20	Madonna della Neve	Erli (SV)
CH_21	San Bernardo chapel	Calice Ligure (Loc. Eze) (SV)
CH_22	Santa Margherita	Diano Arentino (IM)
CH_23	Santi Nazario e Celso	Mendatica (IM)
CH_24	Nostra Signora di Roverano chapel	Borghetto di Vara (Loc. Termine di Roverano) (SP)
CH_25	San Tommaso di Boasi	Lumarzo (Loc. Boasi) (GE)
CH_26	Santi Cosma e Damiano	Vobbia (Loc. Arezzo) (GE)
CH_27	Nostra Signora Addolorata chapel	Noli (SV)
CH_28	San Carlo	Fascia (Loc. Cassingheno) (GE)

Loc. = locality; (GE) = Genova; (IM) = Imperia, (SP) = La Spezia; (SV) = Savona

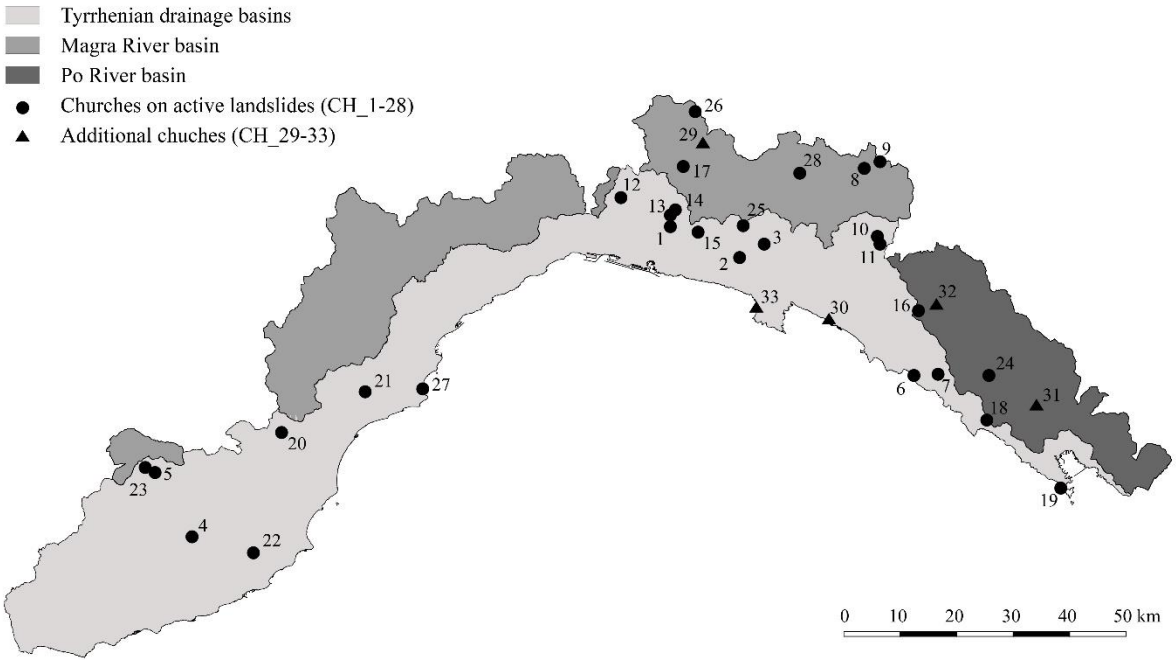

Figure 2-2 Location of the churches analysed in the Ligurian territory.

2.2.2. Additional churches considered in the survey

During the development of this research, some cases of listed churches that experienced damage potentially due to ground movements were reported to the author. Checking the position of these churches on landslide maps (see Figure 2-3 as reference), it was observed that two churches were located very close to active landslides, one was situated on a Pg3 area and two were located near Pg3 areas. The distance of each church from the nearest active or dormant landslide is reported in Table 2. For the purpose of this work, these five additional churches were included among the case studies in order to compare their damage with the crack pattern exhibited by churches located on active landslides. This brought the number of churches investigated in this study to 33 (Figure 2-2).

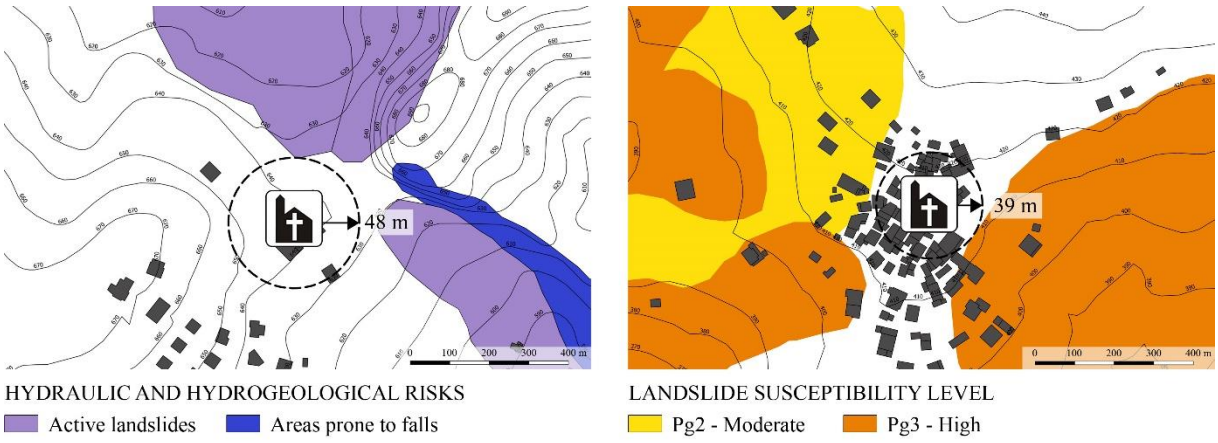

Figure 2-3 Position of the additional churches on landslide maps: a) Nostra Signora della Bastia Sanctuary in Bastia (CH_29), located close to active landslides (Autorità di bacino distrettuale del fiume Po 2017), b) San Martino church in Cembrano (CH_32), located close to a Pg3 area (Regione Liguria 2017).

Table 2 Additional churches: identification and position with respect to landslide-affected areas.

Id	Church name	Municipality, locality, province	Position on landslide maps
CH_29	Nostra Signora della Bastia sanctuary	Busalla (Loc. Bastia) (GE)	48 m from active landslide*
CH_30	Nostra Signora delle Grazie sanctuary	Chiavari (GE)	Pg3 (34 m from Pg4)
CH_31	San Lorenzo	Follo (Loc. Sorbolo) (SP)	Pg3
CH_32	San Martino di Cembrano	Maissana (Loc. Cembrano) (SP)	Pg0 (39 m from Pg3)
CH_33	San Nicolò di Capodimonte	Camogli (Loc. San Rocco) (GE)	Pg2 (70 m from Pg4)

Loc. = locality; (GE) = Genova; (IM) = Imperia, (SP) = La Spezia; (SV) = Savona; * = Po River basin

2.3. METHODOLOGY AND SAMPLE DESCRIPTION

2.3.1. Information gathering

Once the churches to investigate were identified, further information about landslides and geotechnical soil characterization in the surrounding areas was collected and analysed. Geotechnical data derived from geological surveys, in situ tests, inclinometers or piezometers installed in the landslide area, when available, were downloaded from the *Geoportale* (Geo-portal) of the Liguria region (Geoportale Regione Liguria 2020). The availability of data obtained by means of advanced satellite techniques, such as the differential SAR interferometry (Cascini et al. 2009), was also verified. However, as described by Cambiaggi (2020), the geotechnical data were really poor or completely missing for the large majority of the churches. Although the state of activity, type and estimated direction of the landslide phenomena could be identified, almost no information was found about magnitude, rate and dominant component (vertical or horizontal) of the landslide movements. This type of data can be obtained by means of advanced satellite techniques (such as the differential SAR interferometry) or inclinometers, the latter providing a profile of subsurface horizontal deformation. In the case of the Liguria region, good-quality displacement data could not be derived from interferometry due the morphological setting of the territory, which consists primarily of hilly and scarcely urbanized areas characterized by low distributions of the targeted ground points used by satellites to acquire interferometric data (Arpa Piemonte 2008). Furthermore, most of the landslide-affected areas were not monitored by means of inclinometers.

Useful data about state of activity, type and estimated direction of the landslide were found in the *Atlante dei Centri Abitati Instabili della Liguria* (hereafter called Atlante) (Federici et al. 2001; Federici et al. 2004; Federici et al. 2006; Federici and Chelli 2007), which collects studies performed on villages of the Ligurian territory that were affected by phenomena of slope instability. For each centre, the Atlante provides maps, updated between 2001 and 2007, showing the geological conformation of the area as well as the state of activity and type of movement (Varnes 1978) of landslides. In order to evaluate any potential evolution of landslide areas over time, the maps of the Atlante and the ones of the basin plans (more recent since updated as of 2017/2018) were superimposed, as illustrated in Figure 2-4. Furthermore, the landslide direction was estimated on the basis of the orientation of the symbols used in the maps of the Atlante to represent landslides (Figure 2-4). When the churches were located in areas not included in the maps of the Atlante,

the landslide maps together with the contour curves of the slope were used to identify a potential direction of the landslide movement. On the basis of the above remarks and considering also that landslide phenomena may evolve over time, it should be noted that the landslide direction assumed in this work has to be considered approximate.

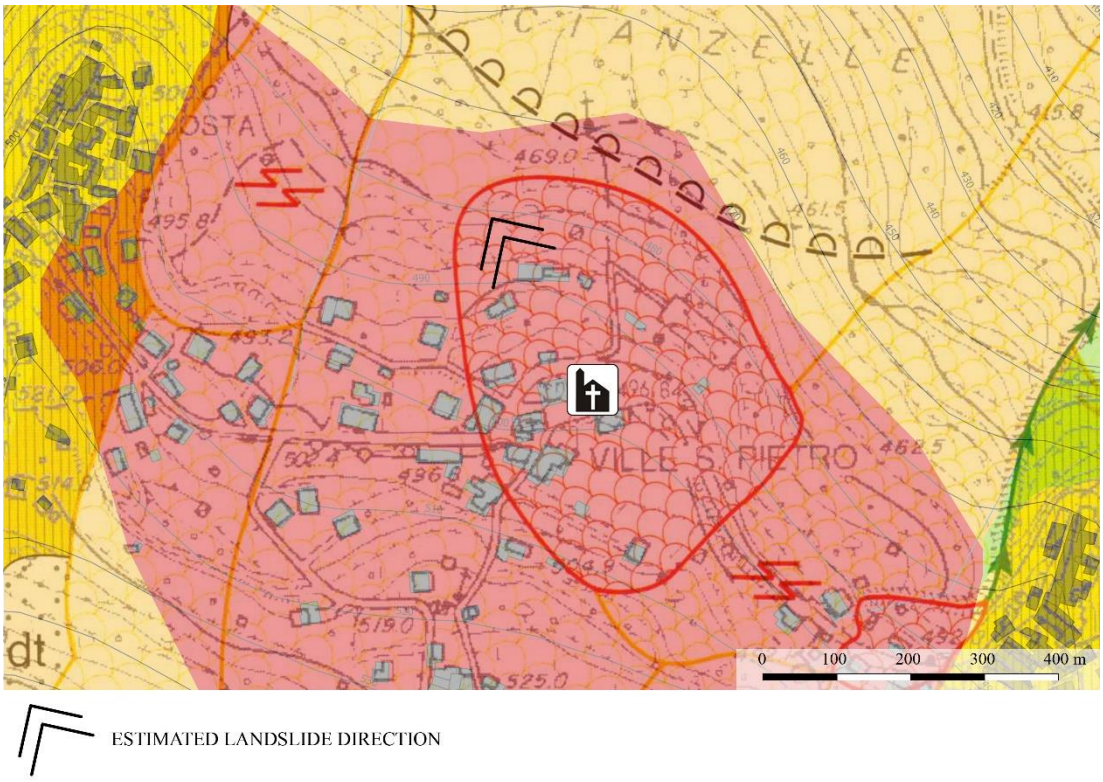

Figure 2-4 Superimposition between the maps of the *Atlante dei Centri Abitati Instabili della Liguria* (Federici and Chelli 2007) and the *Carte della Suscettività al Dissesto* (Regione Liguria 2017) for San Pietro in Vincoli church in Ville San Pietro (CH_4).

An accurate research was also carried out in the Archives of the Ligurian Office of the Italian Ministry of Cultural Heritage and Activities in order to obtain any useful material or information regarding the churches to inspect (i.e. historical information, geometry, past alterations etc). For some churches, a detailed documentation was found including, for instance, historical information, surveys, past crack surveys and description of past interventions. However, not every church had all of these documents available: in many cases, even plans and elevations were not existing or were incomplete, so this involved their elaboration or verification during the inspections. Additional information was also obtained thanks to a bibliographical research

2.3.2. On-site inspections

Inspections and damage surveys were performed in the 33 churches selected as case studies. Firstly, the damage observed in each church was surveyed and mapped in detail. It should be noted that no access was provided to the attic; therefore, the extrados of arches and vaults was not inspected. When a geometric survey was available, cracks and distortions were marked on it, otherwise simple sketches of plans and

elevations were traced on site using laser distance meters and measuring tapes. Cracks affecting walls and pillars were marked on the building plan by means of symbols identifying their orientations (vertical, horizontal and diagonal).

A classification of the cracks surveyed was also taken into consideration. Cracks were classified according to three levels of width: (i) thin for a width up to 1 mm (the latter included), (ii) medium for a width between 1 mm and 5 mm, and (iii) large for a width equal or larger than 5 mm. Crack width was accurately measured by means of crack scales and callipers (accuracy ÷ 0.05 mm) for cracks that were easily accessible, while it was only estimated for cracks located at a significant height from the ground level. When cracks were repointed and did not re-open, crack width was not reported. It is to note that construction joints were identified and distinguished from other damage signs since they are related with the construction process of the building.

In addition to the crack pattern, out-of-plumbness of walls and pillars as well as sinking of floors were surveyed and, when possible, measured by means of electric bubble levels or out-of-plumb wires.

Lastly, as shown in Figure 2-5, for each church an inspection of the surroundings was performed in order to detect any potential evidence of ground movements: (i) cracks and distortions in neighbouring buildings (Figure 2-5a), (ii) cracks in the retaining wall of the embankment on which the church parvis is resting (Figure 2-5b), (iii) cracks in road surfaces (Figure 2-5c), (iv) inclined street lights or trees (Figure 2-5d).

Figure 2-5 Evidence of ground movements in the surroundings of the churches inspected: a) cracks in neighbouring buildings, b) cracks in the retaining wall of the embankment on which the church parvis is resting, c) cracks in road surfaces, d) inclined trees.

2.3.3. Church sample description

The selected sample of assets includes 24 churches, 3 sanctuaries, 3 oratories and 3 chapels (all generically named churches). For each building, Table 3 reports construction date, layout, dimensions, and past interventions. Regarding the construction date, 19 out of the 33 selected buildings date back from the 16th to the beginning of the 19th century, whereas 7 of them were built between the 11th and 15th century. For 7 out of the 33 buildings inspected, the exact construction date is unknown.

Table 3 Features of the considered sample of churches.

Id	Construction date	Layout	Dimensions in plan[a]	Structural interventions	Architectural restorations	Floor refurbishment
CH_1	17th	single nave	27 x 11	x	x	x
CH_2	17th	single nave	28 x 10			
CH_3	16th-17th	single nave	26 x 13	x	x	
CH_4	18th	central plan	27 x 17	x		x
CH_5	17th	single nave	28 x 8	x	x	
CH_6	13th	3 naves	21 x 13		x	
CH_7	18th	single nave	22 x 9	x	x	
CH_8	17th	single nave	16 x 10			
CH_9	19th	central plan	19 x 15		x	
CH_10	18th	single nave	28 x 14	x		
CH_11		single nave	17 x 9	x		
CH_12	16th	3 naves	26 x 13	x	x	
CH_13	17th	3 naves	31 x 18	x		
CH_14		single nave	29 x 7		x	
CH_15	17th	single nave	24 x 13		x	
CH_16		single nave	14 x 10	x	x	
CH_17	17th	single nave	28 x 18		x	
CH_18	14th	single nave	39 x 13	x	x	x
CH_19	12th	3 naves	19 x 13	x		
CH_20		single nave	9 x 6		x	
CH_21		single nave	11 x 6			
CH_22	15th	3 naves	31 x 17			x
CH_23	18th	central plan	29 x 22			
CH_24	18th	single nave	5 x 9		x	
CH_25		single nave	17 x 8			
CH_26	18th	single nave	23 x 12	x		
CH_27		single nave	6 x 2			
CH_28	16th	single nave	21 x 8			
CH_29	17th-18th	3 naves	22 x 13			
CH_30	14th-15th	single nave	34 x 10	x		x
CH_31	17th	single nave	25 x 9	x	x	x
CH_32	13th	3 naves	24 x 14	x		
CH_33	11th	single nave	19 x 10	x	x	

[a] Length (including presbytery and apse) and width in meters

The large majority of the assets have a longitudinal plan with a single nave (23 assets) or three naves (7 assets), whereas only 3 buildings have a central plan. Churches and sanctuaries have areas ranging from approximately 50 m^2 to 560 m^2, whereas oratories, which are all characterized by a single nave, have areas ranging approximately from 150 m^2 to 210 m^2. All the chapels have a single nave and are small in size, with areas ranging approximately from 10 m^2 to 70 m^2.

Table 3 also reports the interventions that, to the author's knowledge, were performed in each church in the last 50 years. Reference is made to structural interventions (strengthening and/or geotechnical interventions), architectural restorations and floor refurbishment. It is interesting to observe that structural interventions and/or architectural restorations were performed in about half of the churches. Furthermore, floors were refurbished in 6 out of the 33 buildings inspected.

The 33 churches under consideration are located in hilly and scarcely urbanized areas (Figure 2-6a). For each church, Figure 2-6b reports the slope section in the direction of the maximum gradient as obtained from DTM (Digital Terrain Model) data (Geoportale Regione Liguria 2020). For an easier comparison among the different slope sections, a zero-reference height equal to the minimum height above sea level in the considered section was assumed for each slope. It is observed that most of the churches are situated on slowly to moderately inclined slopes (average slope gradients smaller than 30°), whereas only three churches are located on steep slopes (average slope gradients equal or larger than 30°). From Figure 2-6b, it is also observed that one church is located at the top of a hill, whereas one is situated in a valley.

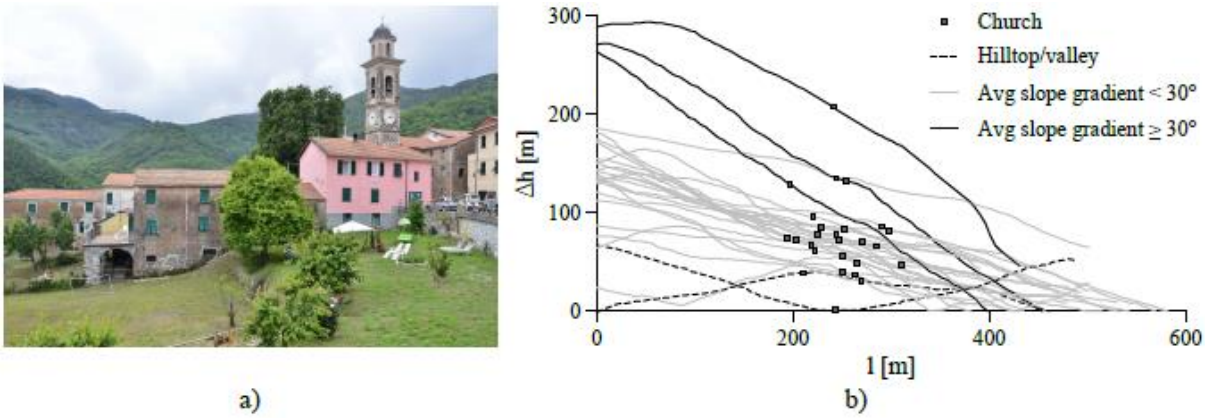

Figure 2-6 Morphology of the Ligurian territory: a) hilly and scarcely urbanized areas, b) sections of the slopes where the churches under consideration are located (where $\Delta h = h - h_{min}$, being h_{min} the minimum height above sea level in the length (l) of the slope section considered for each church).

2.4. DAMAGE OF CHURCHES

In this section, the damage observed in the 33 churches inspected is presented and critically analysed. As described by Ferrero et al. (2020), the additional churches experienced the same types of damage as the churches located on active landslides. For this reason, no distinction between them will be considered in the following paragraphs.

2.4.1. Damage survey

The damage surveyed in the sample of churches is described below for the different structural elements composing the church: floors, walls and pillars, and arches and vaults.

Damage in the floor appears in the form of cracking of tiles, gaps among tiles or sinking (Figure 2-7). Cracks are usually localized in few tiles and are especially observed on step treads and balustrades bases (Figure 2-7a). Conversely, gaps, which are separations that develop at the joints among tiles, are usually widespread in the floor (Figure 2-7b). In particular, several churches present a series of parallel gaps crossing the entire floor from one side to the other (Figure 2-7b). As shown in Figure 2-7c, in some cases cracks and gaps originate from the floor and propagate upwards into the walls. In addition to cracks and gaps, several churches exhibit sinking of floor, which is often accompanied by gaps among tiles or lifting of some of them, as shown in Figure 2-7d.

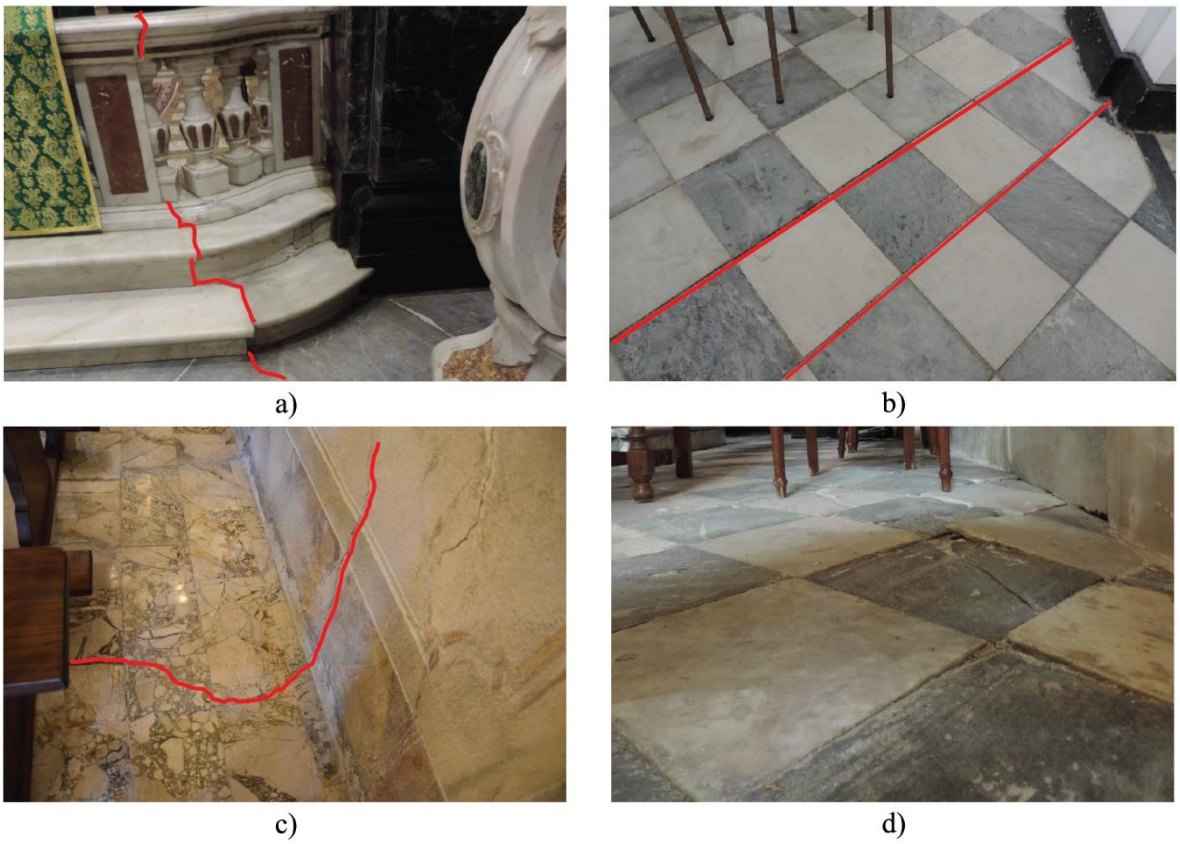

Figure 2-7 Damage of floors: a) cracks on step treads and balustrades bases (CH_17), b) parallel gaps among tiles (CH_29), c) cracks propagating from floor to wall (CH_28), d) sinking of floors (CH_15).

The majority of the churches present cracks in load-bearing masonry walls (Figure 2-8). Cracks are observed in the façade and apse walls as well as in lateral longitudinal and transverse walls. The cracks detected in the façade walls are mainly located next to openings and inside alcoves (Figure 2-8a). Lateral longitudinal walls usually exhibit cracks extending upwards from the base of the structure. Cracks are generally vertical and propagate along the entire height of the structure, in some cases continuing up into the vaults (Figure 2-8d). Significant diagonal cracks extending from the ground level are less frequently

observed (Figure 2-8b). Some churches also exhibit vertical cracks that do not propagate from the floor. These cracks, which are generally repeated in each bay, progress over the entire height of the wall, increasing in width with height (Figure 2-8c), and continue up into arches and vaults, cutting them transversally.

Finally, some churches present significant out-of-plumbness in lateral walls and pillars. In some cases, the entire building exhibits a rigid rotation, with both longitudinal walls leaning in the same direction (Figure 2-8e). Loss of horizontality of the metallic tie-rods is often observed in the case of rigid rotations (Figure 2-8e).

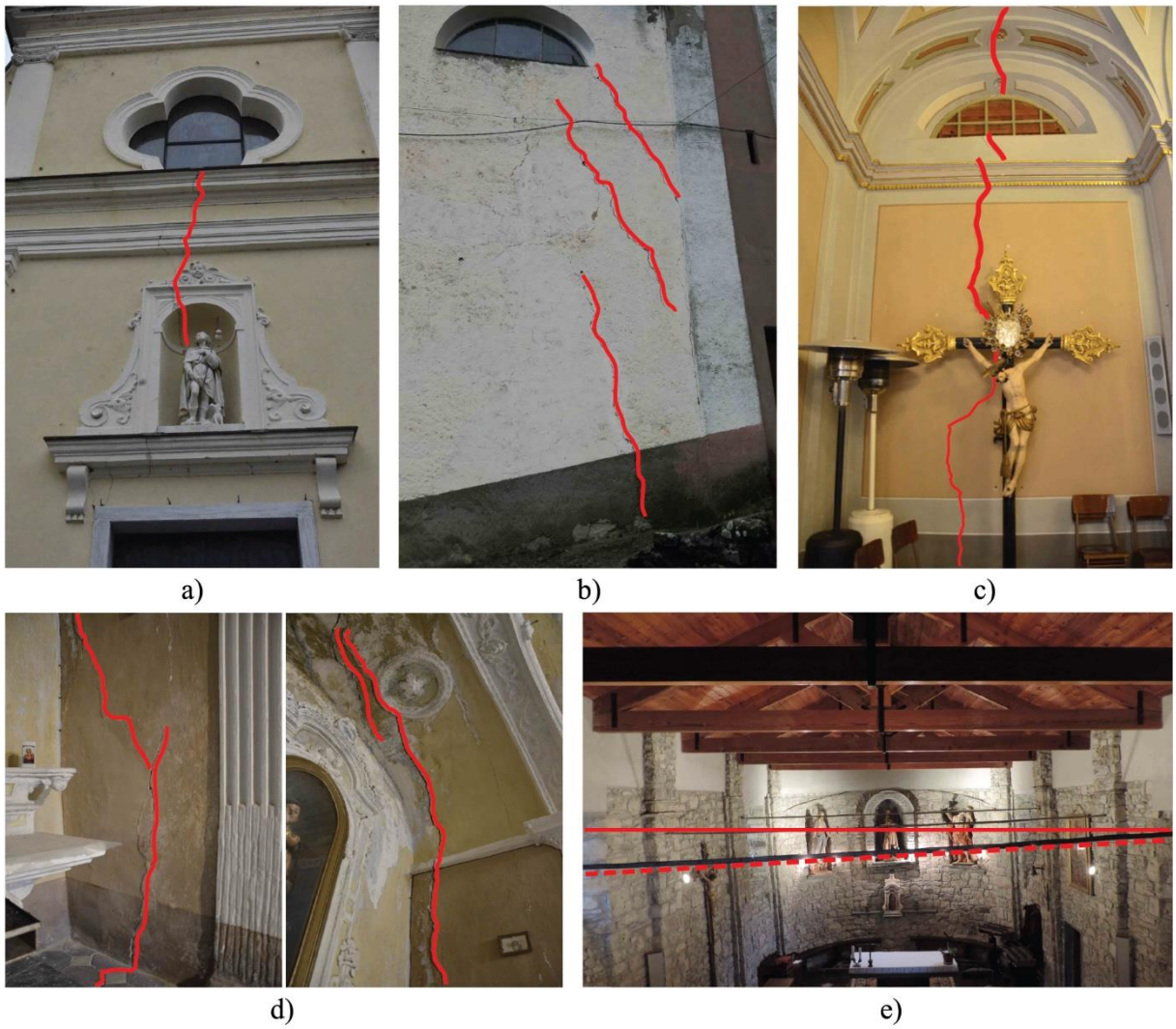

Figure 2-8 Damage of walls: a) cracks in the façade wall next to openings (CH_3), b) diagonal cracks in longitudinal walls propagating from the level of the ground (CH_9), c) vertical cracks increasing in width with height at the middle span of the wall (CH_32), d) vertical cracks in lateral walls extending from the level of the ground and continuing up into vaults, e) rigid rotation producing out-of-plumbness of longitudinal walls and loss of horizontality of metallic tie-rods (CH_8).

In most of the churches of the sample, widespread cracking and large deformations were surveyed in arches and vaults (Figure 2-9). A detailed description of this damage is provided in Section 2.5. As discussed

in further detail in Sections 2.4.2 and 2.5.2, it is interesting to observe that the vaults of several churches exhibit multiple parallel diagonal cracks, which are oriented in the same direction as the gaps of the floors.

Figure 2-9 Damage in arches and vaults: a) widespread cracking (CH_32), b) large deformations (CH_13).

2.4.2. Critical damage assessment

A critical damage assessment was performed based on the systematic observation of the damage experienced by the 33 churches under consideration. The main conclusions are reported below. For a full description of the results of the critical damage assessment, the reader is referred to Ferrero et al. (2020).

- The damage level was found to vary significantly across the 33 churches of the sample. In order to quantify its distribution, the churches were classified by the following five levels of increasing damage, which were defined using as a reference the European Macroseismic scale (EMS-98) for masonry buildings subjected to seismic actions (Grünthal 1998): (i) negligible to slight damage (*grade 1*), (ii) moderate damage (*grade 2*), (iii) substantial to heavy damage (*grade 3*), (iv) very heavy damage (*grade 4*), and (v) destruction (*grade 5*). The large majority of the churches (72.8% of the total) presented either slight or moderate damage, while 27.3% of the total suffered substantial to very heavy damage. Among these latter buildings, some were closed to public by order of local authorities due to safety reasons. It is important to note that the damage levels were assigned according to the damage surveyed during on-site inspections. Therefore, they might not reflect the damage experienced by the churches throughout their entire history. As reported in Section 2.3.3 and Table 3, interventions were performed in at least half of the buildings of the sample, with the result that part of the past damage could have been repaired or simply hidden.

- The large majority of the churches presented damage patterns *congruent* with the landslide direction, indicating that slow-moving landslides may induce significant damage to historic masonry churches. The congruence between damage and estimated landslide direction was evaluated by comparing the latter with an approximate damage direction, defined based on engineering judgment considering the crack pattern in plan as well as global rigid rotations (for an example see Figure 2-10). The damage was considered congruent with the landslide direction if the

approximate damage direction was within the range between -45° and 45° compared to the landslide direction. Figure 2-10 shows two representative examples of crack patterns *congruent* with the landslide direction. It can be easily observed that the cracks affecting floors and vaults are characterized by a consistent orientation throughout the building. Furthermore, the cracks of the walls occur in planes oriented parallel to the direction of the cracks observed in floors and vaults. This allowed to identify a clear damage direction, which was found to be inclined by not more than ±45° with respect to the landslide direction. Congruence between damage pattern and landslide direction was also observed in the churches exhibiting a global rigid rotation. In these cases, the longitudinal walls, which were oriented almost perpendicular to the landslide, leaned in the direction of the landside, as expected.

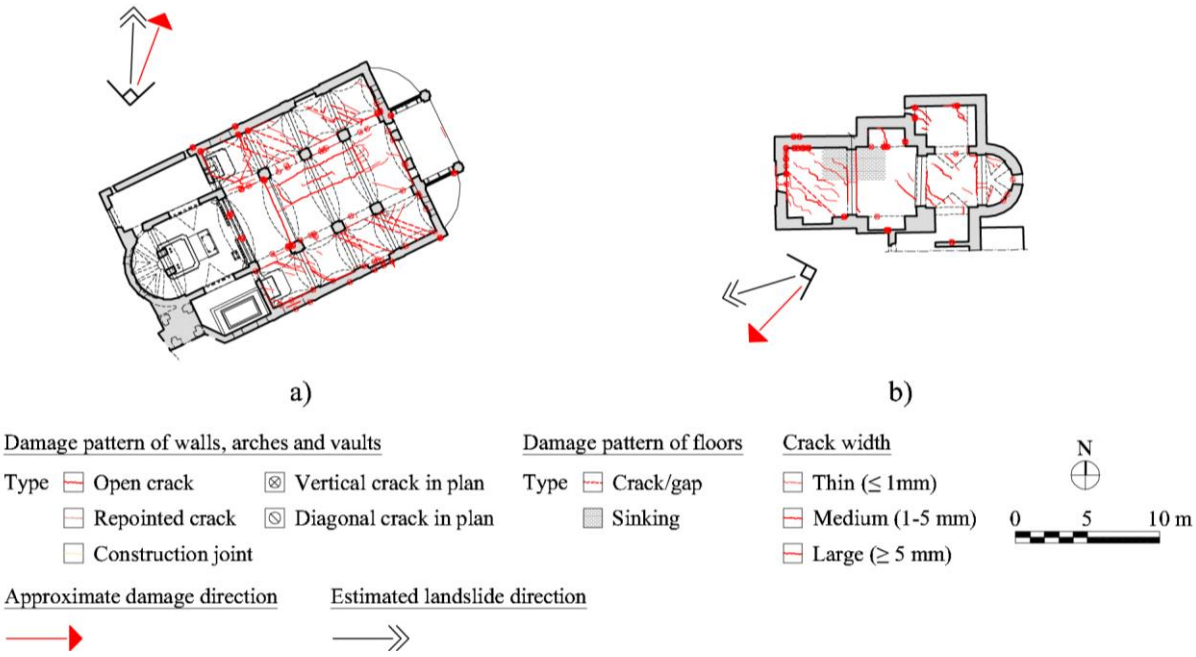

Figure 2-10 Damage patterns congruent with the estimated landslide direction: a) CH_29, b) CH_25.

- Four recurrent types of damage were identified in the churches inspected: (i) damage of floors, (ii) damage of walls, (iii) damage of arches and vaults, and (iv) rigid rotation. Figure 2-11 shows the occurrence of these types of damage, classified by damage grade, in the selected sample of churches. Note that the damage was classified according to the 5-level damage scale already adopted to estimate the global damage level. Damage of walls as well as damage of arches and vaults proved to be the most frequent types of damage. Damage of walls occurred in almost all the churches inspected (94% of the sample). Approximately 73% of the churches exhibited slight or moderate damage (*grade* 1 and 2), while 21.2% of them also presented heavy or very heavy damage (*grade* 3 and 4). Damage of arches and vaults was observed in the large majority of the churches (81.8% of the total). Damage of *grade* 1 or 2 occurred in 63.6% of the buildings, while damage of *grade* 3 or 4 was found in 18.2% of the sample. Damage of floors was also present in about half of the 33 churches inspected, whereas rigid rotations were observed only in few cases of single-nave churches of small size.

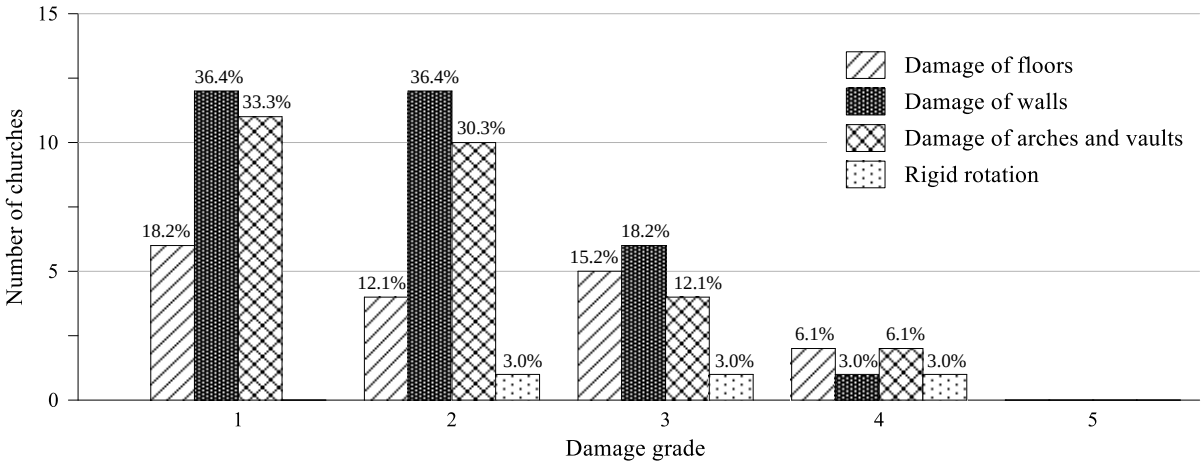

Figure 2-11 Recurrent types of damage classified by damage level.

- The damage induced to historic masonry churches by slow-moving landslides proved to be easily recognizable. Besides the identification of four recurrent types of damage, damage was not localized but widespread in the church. Cracks generally exhibited a consistent orientation throughout the building. The cracks patterns in the floors reflected the ones in the vaults. Furthermore, the cracks affecting the walls occurred in planes parallel to the orientation of the cracks observed in the floors and vaults.

- Churches were found to respond to slow-moving landslides with a global behaviour where the different structural components (i.e. walls, arches, vaults, etc.) contribute jointly to accommodate soil displacements. This behaviour is significantly different from the response by independent macroelements exhibited by churches under seismic actions. The following four global damage mechanism were identified: (i) *hogging*, (ii) *shear deformation*, (iii) *global rigid rotation*, and (iv) *extension*. As shown in Figure 2-12, each mechanism was associated to a specific soil displacement pattern produced by slow-moving landslides. The *hogging*, *shear deformation*, and *global rigid rotation* mechanisms were attributed to an incremental vertical ground movement, while the *extension* mechanism was associated to a horizontal ground movement. It is important to highlight that, since no quantitative information about the magnitude of the horizontal and vertical components of the landslide movements was generally available, the correlation between damage and soil displacements patterns was found through a critical interpretation of the surveyed crack patterns and deformation, which were used as indicators of ground movements (for further details, see Ferrero et al. 2021a). This allowed to determine if the dominant component of the landslide movements was vertical or horizontal. However, it should be recalled that landslides always involve a combination of downward and lateral ground movements (Cooper 2008); therefore, different mechanisms can occur together. Furthermore, the occurrence of a certain damage mechanism compared to the others may depend not only on the prevalent component of ground movement, but also on the direction of the landslide movement with respect to the church axes as well as on the church geometry and structural configuration.

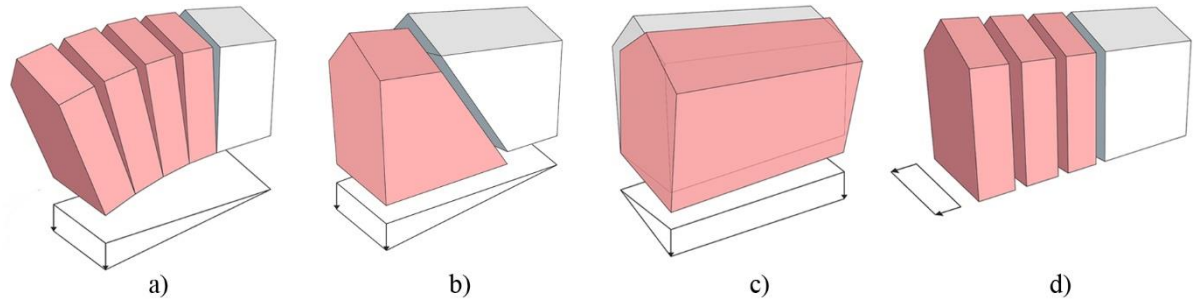

Figure 2-12 Global damage mechanism: a) *Hogging*, b) *Shear deformation*, c) *Global rigid rotation*, d) *Extension*.

2.5. DAMAGE OF ARCHES AND VAULTS

As observed in the previous section, damage in arches and vaults was observed in most of the churches of the sample. In almost one fifth of the buildings, damage was classified as heavy or very heavy, indicating that these structural elements are sensitive to slow-moving landslides.

2.5.1. Cracks and deformations of masonry arches

Damage in the arches appears in the form of cracks and deformations. Looking at Figure 2-13, which presents some examples of crack patterns, it is observed that some cracks are orthogonal to the arch external profile (Figure 2-13d-e-f-g-h), while others cut the arch diagonally and are often in continuity with the diagonal cracks observed in the vaults (Figure 2-13a-b-c). In the first case, the arch exhibits a bi-dimensional behaviour, while the second case points to the occurrence of transverse support movements. When cracks are orthogonal to the arch profile, the crack pattern can be either symmetrical or asymmetrical. In the case of symmetrical patterns, a crack occurs near the crown at the intrados (Figure 2-13d). When the crack configuration is asymmetrical, a recurrent crack pattern is more difficult to identify, as cracks appear at different locations along the arch profile in the different churches of the sample. Some examples of asymmetrical crack patterns are reported in Figure 2-13e-f-g-h. In Figure 2-13e, one cracks appears at the upper part of the arch, while some deterioration of the plaster is observed at the haunches, suggesting high levels of compressive stresses produced by the opening of two further cracks at the extrados. In Figure 2-13f, two cracks, very close one to each other, are detected at mid-span, while deterioration of the plaster is observed at one haunch only. In Figure 2-13g, two cracks appear, one located at mid-span and the other at one haunch, and deterioration of the plaster is observed in between them. In Figure 2-13h, only one crack, located at the left haunch, can be detected.

Looking at Figure 2-13, it can also be observed that cracks are often continuous between arches and vaults, indicating an adequate connection between contiguous structural elements.

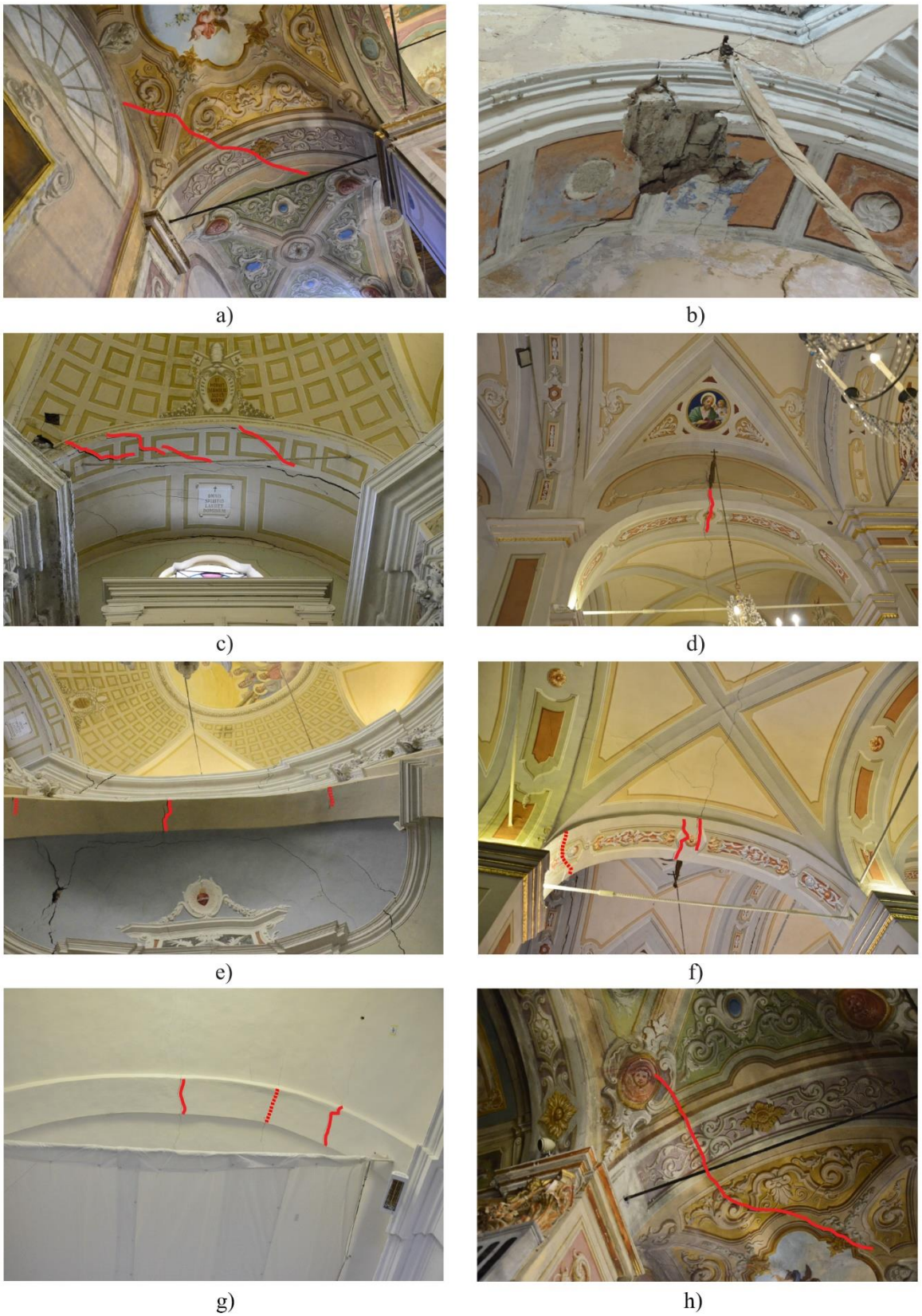

Figure 2-13 Cracks patterns observed in the arches (deterioration of the plaster indicated with a dotted line): a-b-c) diagonal cracks (CH_13, CH_22, CH_4), d) symmetrical crack pattern (CH_32), e-f-g-h) asymmetrical crack patterns (CH_4, CH_32, CH_29, CH_13).

Besides cracks, arches also exhibit large deformations, which generally involve the adjacent vaults. Figure 2-14 shows some representative examples of in-plane deformations occurring either in the arches of the lateral chapels (Figure 2-14a) or in the arches separating the different naves and bays of the church (Figure 2-14b-c-d). As expected, deformations are generally accompanied by the opening of some cracks, which are needed to accommodate such large changes in the geometry. The deformations depicted in Figure 2-14 clearly demonstrate that arches can sustain very large support displacements without the overall stability being compromised. This is particularly evident in Figure 2-14d, where a very large deformation is observed in the transverse arches and cross vaults of one lateral nave. It is easy to see, without any need for more accurate measurements, that the left part of the church (pillars and external wall) experienced a vertical settlement with respect to the pillars separating the lateral and central naves. This settlement also produced a severe crack (located closer to the settling support) in the arches involved as well as the inclination of the metallic tie-rods at the arch springings. It is interesting to observe that the tie-rods did not prevent the movement but followed the vertical displacement experienced by the left support of the arch. The analysis of the geotechnical data available for this church showed that the quality of the soil was poorer in the area where the vertical settlement occurred with respect to the rest of building. Since this type of damage and deformation was localized only in this area, it is reasonable to assume that it was produced by a foundation settlement rather than by landslide affecting the church.

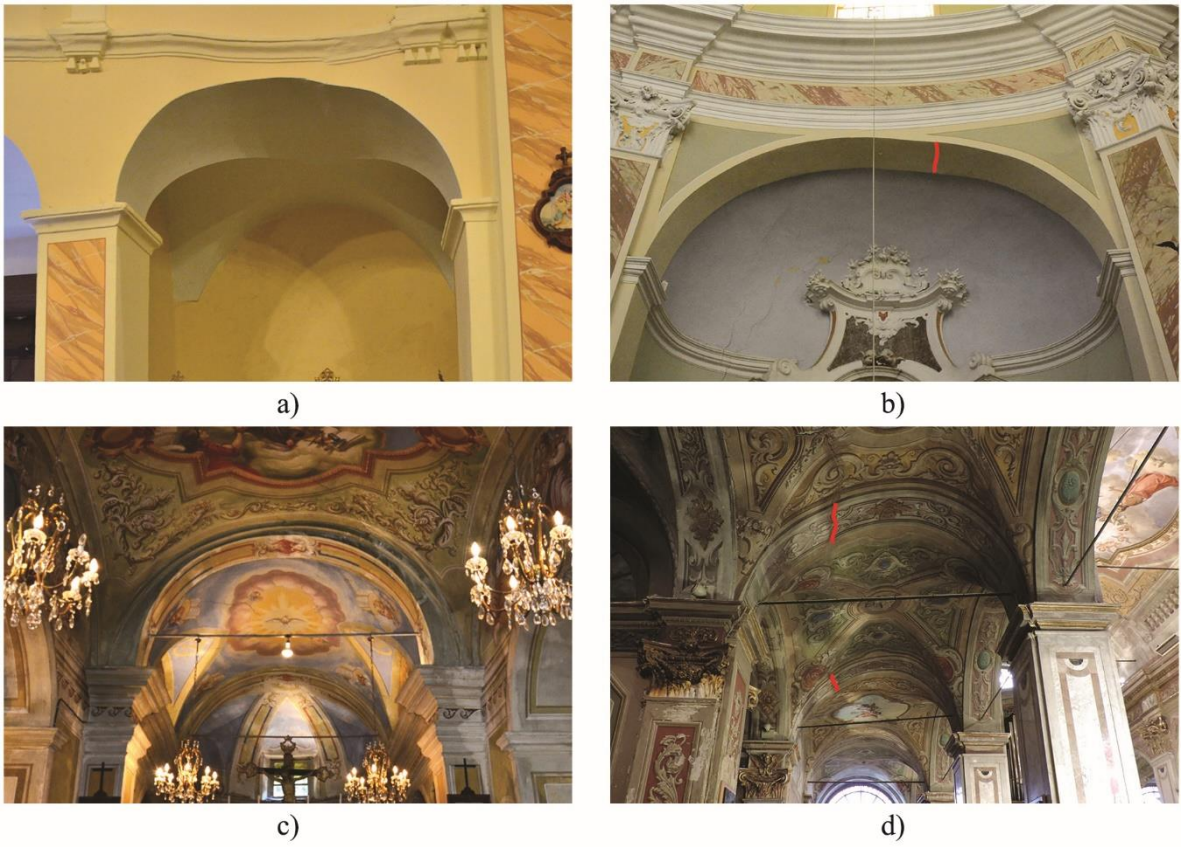

Figure 2-14 In-plane deformations in the arches: a) arches of the lateral chapels, b-c-d) arches separating the different bays of the church.

Looking at Figure 2-14c, the author has the impression that the cornice at the right side of the arch was restored or re-built to camouflage the significant deformation experienced by the arch. Although there is no historical evidence that could confirm this hypothesis, it is evident that the past interventions and restorations carried out in several churches of the sample could have hidden the actual damage experienced, preventing a correct interpretation of the crack patterns currently visible.

Two further examples of large deformations can be found in Nostra Signora della Bastia Sanctuary in Bastia (CH_29, Figure 2-15) and San Carlo Church in Cassingheno (CH_28, Figure 2-16). A laser scanner survey was performed in both churches (see Mamone 2017 and Cabella and Sacco 2021), providing valuable information about the deformations experienced by the entire building.

In Nostra Signora della Bastia Sanctuary, the arches and barrel vaults covering the central nave exhibit a very large deformation accompanied by a series of longitudinal cracks propagating over the entire length of the vault and cutting the supporting arches (Figure 2-15a). Looking at Figure 2-15b, it seems that the right part of both arches and vaults, where cracks and deformations are concentrated, experienced an upward deformation with respect to a hypothetical undeformed geometry. If the latter is assumed to be mirrored with respect to the geometry of the left part, a maximum upward deviation of about 15 cm can be measured. As shown in Figure 2-15a, the arch separating the second and third bays (numbered from the façade) exhibit two cracks, one located at mid-span and the other at the right haunch. The deterioration of the plaster observed in between them may suggest the opening of a further crack at the extrados.

To interpret the damage observed in the arches, it is important to highlight that significant sinking was surveyed in the floor (Figure 2-15c). The laser scanner survey allowed to detect sinking increasing in the direction of the landslide (indicated with an arrow in Figure 2-15c) from the left (southwest) side to the right (northwest) side of the church with a maximum value measured in the right lateral nave. Sinking of all the pillars, probably due to the deformability of the soil, was also observed. This suggests that the crack patterns and deformations observed in the arch are the consequence of differential vertical support displacements produced by both the landslide and foundation settlements. Nevertheless, the significant leaning of the pillars (see Figure 2-15b) also hints at the occurrence of horizontal displacements at the arch springings. In view of the above, it is likely that the damage of the arches is caused by a combination of vertical and horizontal support displacements.

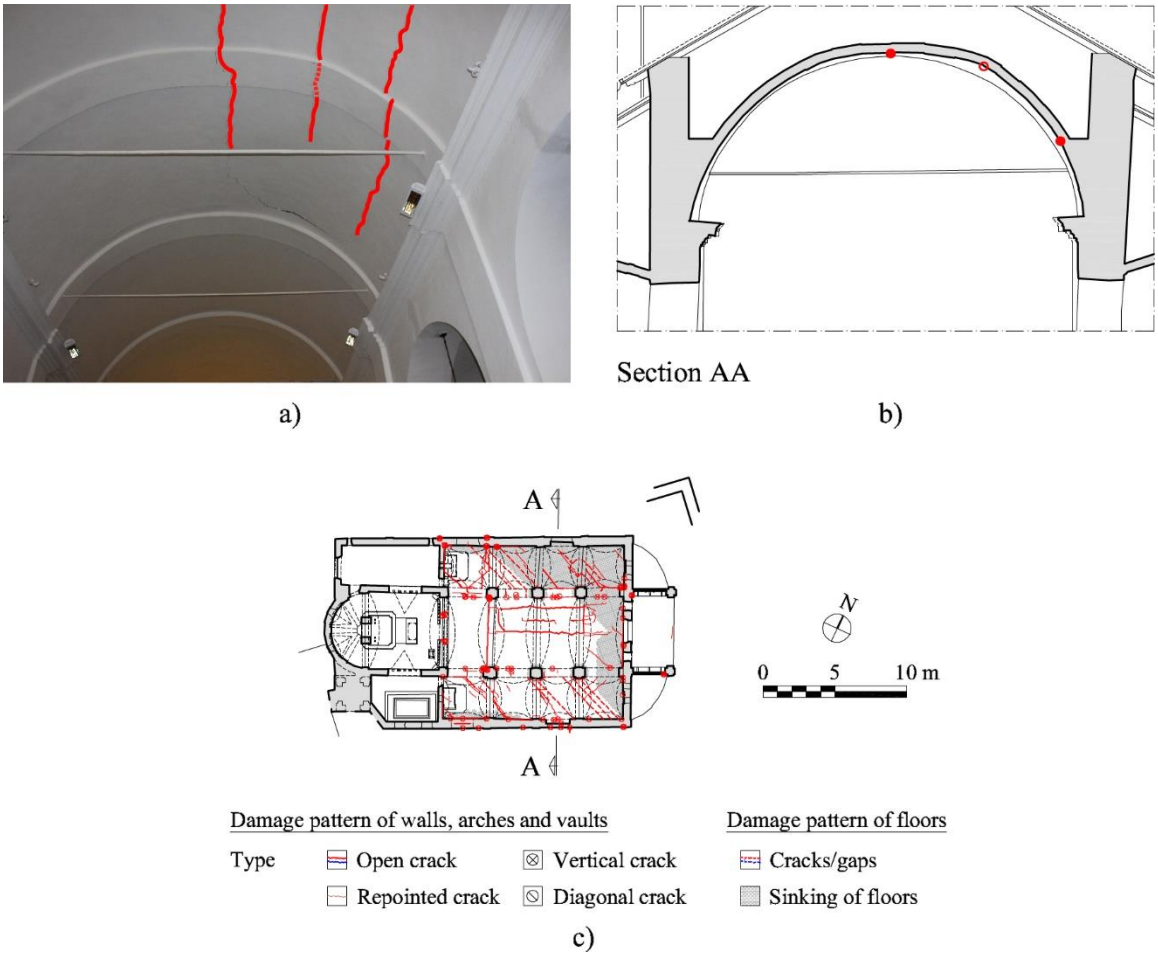

Figure 2-15 Crack pattern and deformations in Nostra Signora della Bastia Sanctuary (CH_29): a) large deformation and cracks in the transverse arches and barrel vaults of the central nave, b) deformed profile (section AA) obtained from the laser scanner survey (Mamone 2017), c) damage pattern of walls, arches and vaults (estimated landslide direction indicated with an arrow).

A very large deformation was also observed in the transverse arches of San Carlo church in Cassingheno (CH_28) (Figure 2-16). In particular, both arches 1 and 2 (indicated in the plan of the church in Figure 2-17) exhibit a loss of shape with a large lowering in the left part (see Figure 2-16e-f). In the case of arch 1, if it is assumed that the arch initial geometry was symmetrical, the maximum deviation between the hypothetical undeformed geometry and the current deformed one is about 20 cm. This value was measured from the section reported in Figure 2-16c left, which was obtained by Cabella and Sacco (2021) from the laser scanner survey. It is interesting to observe that arches 1 and 2, although exhibiting very large deformations, are not affected by extensive or severe cracking. Only a single crack was observed in both arches 1 and 2 close to mid-span (Figure 2-16b). This crack propagates longitudinally along the entire length of the vaults of the third bay and presbytery (see the damage survey reported in Figure 2-17). However, as already mentioned above, further cracks could have been repaired over time.

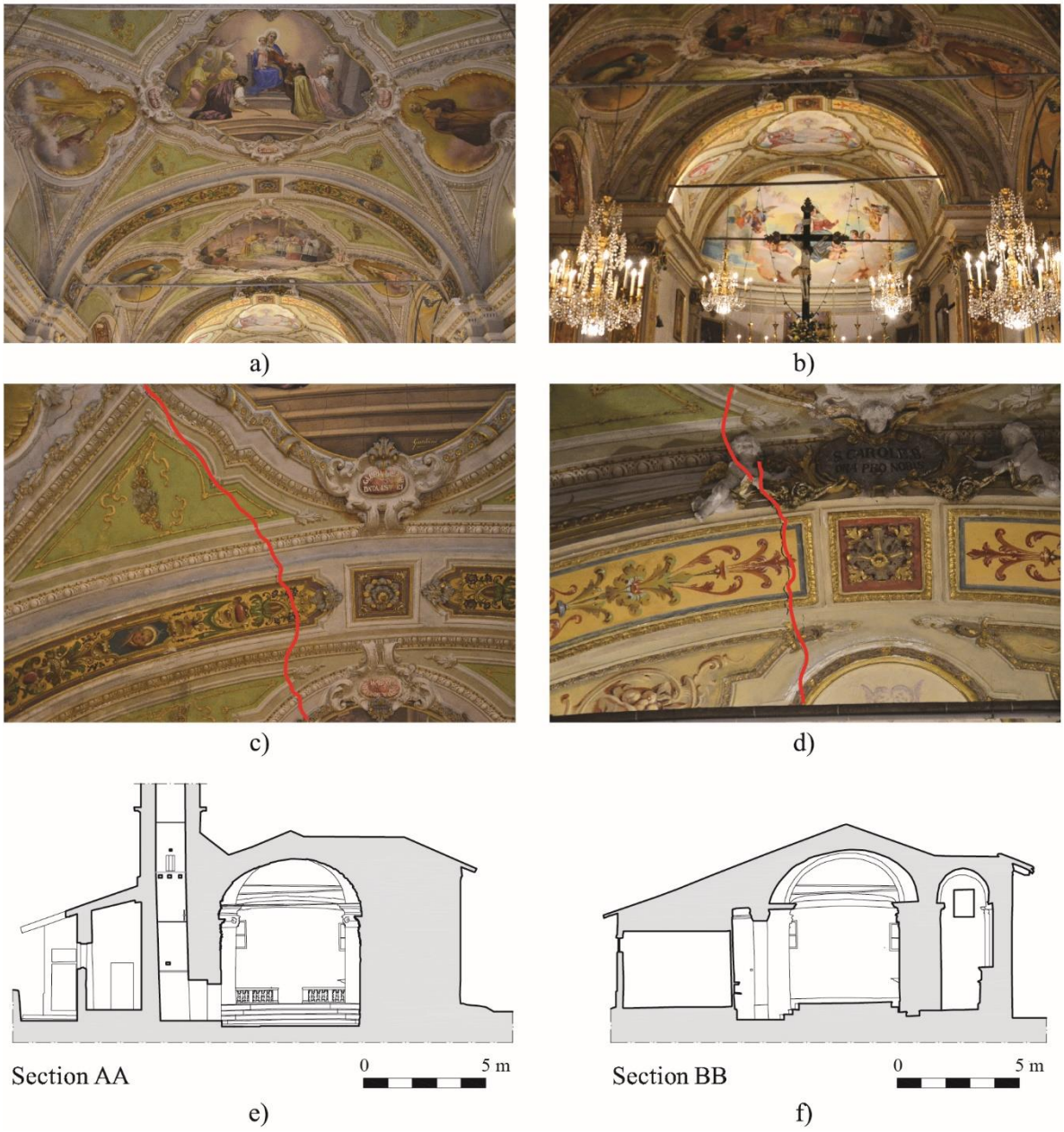

Figure 2-16 Crack patterns and deformations observed in the transverse arches 1 (left) and 2 (right) (located in the plan of the building in Figure 2-17) of San Carlo church in Cassingheno (CH_28): a) large deformations, b) crack close to mid-span, c) arch profile as obtained from the laser scanner survey (Cabella and Sacco 2021).

The analysis of the geometry obtained from the laser scanner survey highlighted that the springings of arches 1 and 2 are not at the same height. Since the left support is about 6-8 cm lower than the right one, it can be assumed that the left side of the church experienced a vertical settlement. This hypothesis is confirmed by the loss of horizontality of the metallic tie-rods present at the arch springings, which is distinctly visible on the right of Figure 2-16b-f. Thanks to the laser scanner survey (Figure 2-16b right), a difference of about 16 cm was measured between the left and right ends of the metallic tie-rod of arch 2. However, the damage and deformation observed in the arches may not result only from vertical support displacements. The laser scanner survey showed that both the lateral walls of the church lean towards the

exterior, suggesting that the arches were subjected to a mechanism of horizontal spreading supports. Furthermore, looking at the projection of the arch profiles reported in Figure 2-17, it is easy to see that arches 1, 2 and 3 experienced a distortion in plan. Such a distortion can be attributed to horizontal support displacements produced by a shear deformation of the entire church. Since the landslide direction is parallel to the longitudinal axis of the church (see the arrow in Figure 2-17), this damage mechanism can be associated to the horizontal component of the landslide movement. This is confirmed by the presence of two very large gaps (the largest one with a width of 18 mm) crossing the entire floor and propagating between longitudinal walls (see the crack pattern in Figure 2-17). Since the tiles moved apart without experiencing any vertical displacement, it is evident that these gaps are due to horizontal soil displacements.

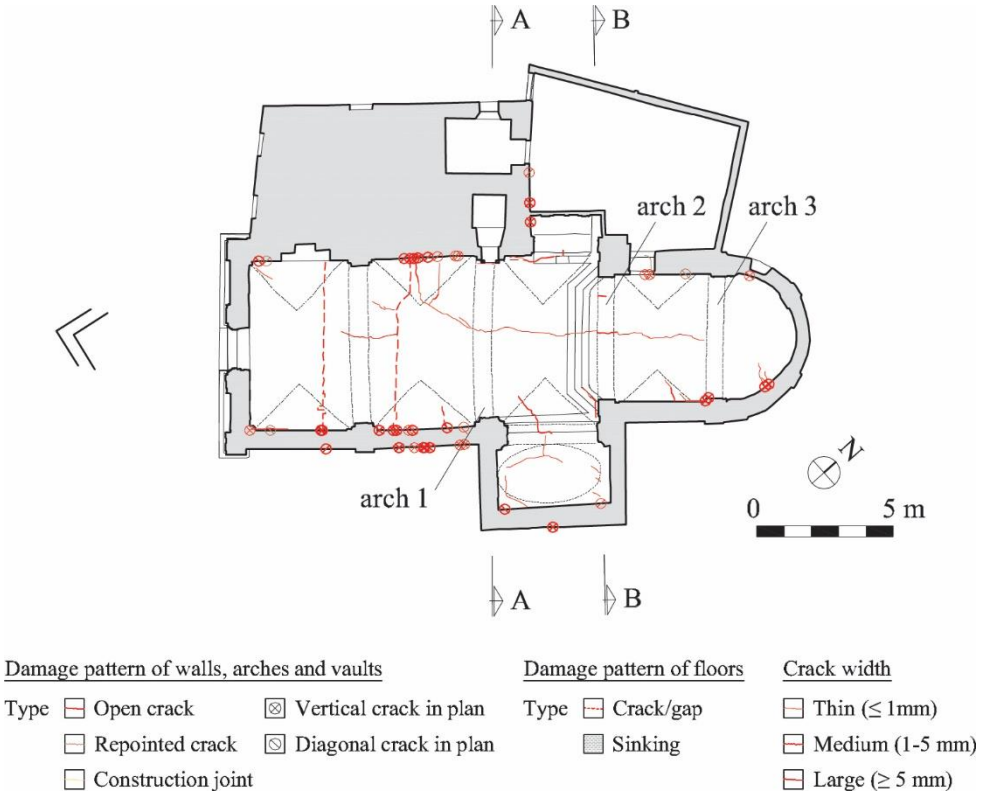

Figure 2-17 Damage survey of San Carlo church in Cassingheno (CH_28) (estimated landslide direction indicated with an arrow).

2.5.2. Cracks and deformations of masonry vaults

Several churches of the sample present extensive damage in the vaults in the form of longitudinal, transverse and diagonal cracking (Figure 2-18a-b-c). As shown in Figure 2-18d, in many cases, cracks propagate from the supporting walls into the vaults and are continuous between arches and vaults (Figure 2-18a). In other cases (Figure 2-18e-f), cracks occur at the intersection between vaults and arches or supporting walls, especially in the case of the façade, indicating an inadequate connection between contiguous structural elements.

Figure 2-18 Crack patterns of masonry vaults: a) longitudinal cracks (CH_28), b) transverse cracks (CH_17), c) diagonal cracks (CH_4), d) cracks continuous between vault and supporting wall (CH_22), e) cracks at the intersection between arches and vaults (CH_32), f) cracks at the connection between vault and supporting wall (CH_2).

In the sample of churches inspected, the most widespread types of vaults are cross and barrel vaults. Some typical cracks observed in cross and barrel vaults are presented in Figure 2-19 and Figure 2-20, respectively. Cross vaults very often exhibit a crack along one of diagonals (Figure 2-19a). In several cases, this crack is accompanied by further parallel diagonal cracks located in between the keystone and the springings (Figure 2-19b). Only in a few cases, diagonal cracks do not appear at the keystone (Figure 2-19c). Longitudinal cracks cutting the entire vault at the keystone are also observed (Figure 2-19d). Barrel vaults typically exhibit longitudinal cracks propagating for the entire length of the vault (Figure 2-20a). In

some cases, one single crack located close to mid-span is observed, while in other cases series of parallel cracks are detected. Diagonal cracks also frequently occur (Figure 2-20b).

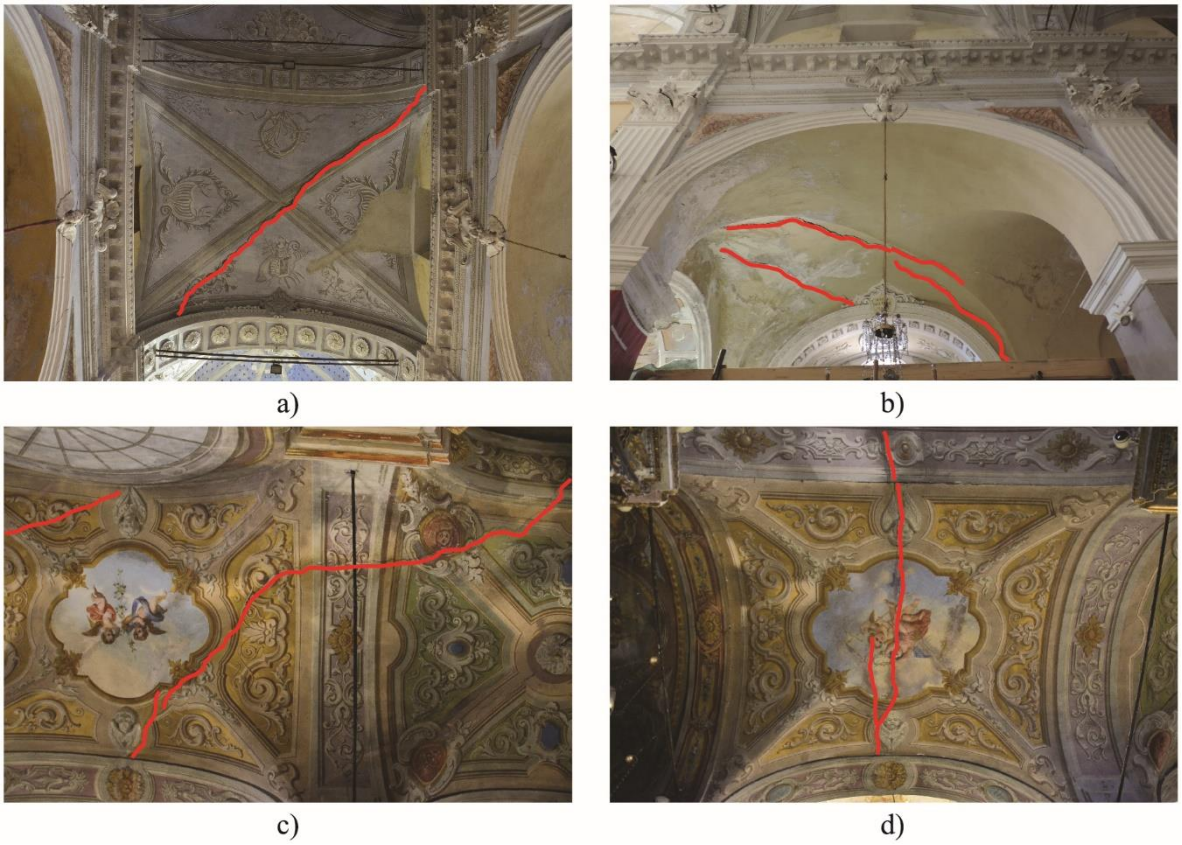

Figure 2-19 Typical cracks observed in cross vaults: a) crack along one of the diagonals (CH_22), b) parallel diagonal cracks (CH_22), c) diagonal cracks not passing through the keystone, d) longitudinal cracks.

Figure 2-20 Typical cracks observed in barrel vaults: a) longitudinal cracks, b) diagonal cracks.

As already described in Section 2.5.1, beside widespread cracking, vaults also exhibit large deformations. Representative examples for both cross and barrel vaults are presented in Figure 2-21.

Figure 2-21 Large deformations observed in cross vaults (a) and barrel vaults (b).

Some recurrent damage patterns were identified by analysing the crack distribution across all the vaults of each church investigated. Several churches present diagonal cracks that are widespread throughout the building, all oriented in the same direction and parallel to the gaps observed in the floor. In several cases, these cracks originate from the level of the ground, cut the walls for their entire height, and continue up in arches and vaults. Some representative examples are reported in Figure 2-22. Ferrero et al. (2020) associated this crack pattern to the *extension* mechanism, which is produced by the horizontal component of the landslide movement. As shown in Figure 2-22, the cracks in the vaults as well as the gaps in the floor are oriented almost perpendicular to the direction of the slope movement. Furthermore, the cracks in the walls occur in planes perpendicular to the landslide direction. This indicates that the church experienced an *extension* in the landslide direction, suggesting that the damage observed in the vaults is mainly due to horizontal support displacements.

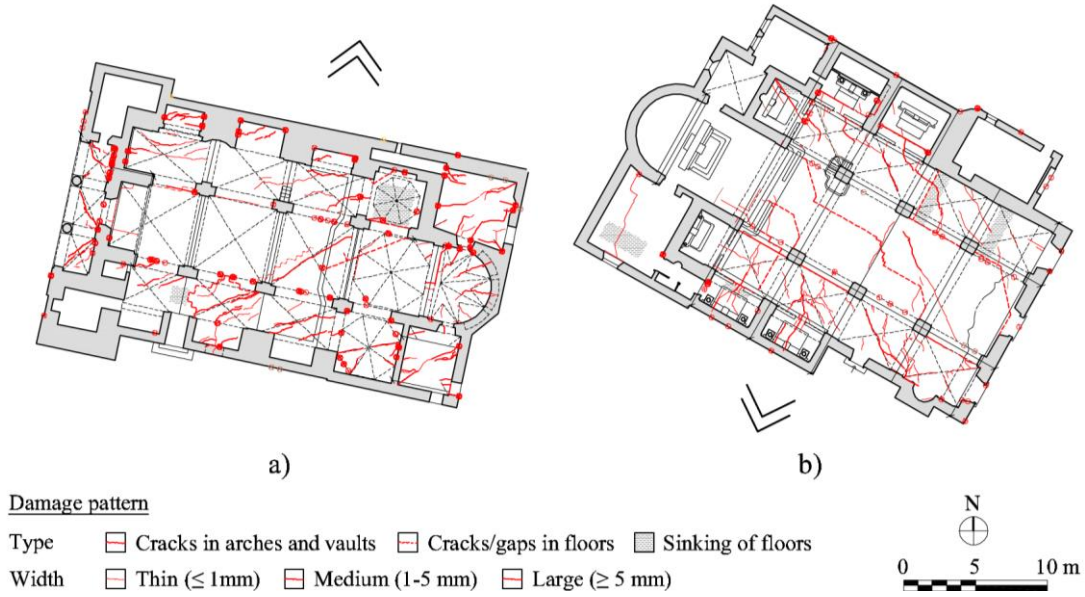

Figure 2-22 Recurrent damage pattern observed in the vaults. Multiple diagonal cracks widespread throughout the building, all oriented in the same direction and parallel to the gaps of the floor: a) CH_ 22, b) CH_13. (Estimated landslide direction indicated with an arrow.)

In some churches, the cracks of the vaults are repeated with the same pattern in almost all bays. A representative example is San Martino church in Cembrano (CH_32, Figure 2-23), where the vaults of the lateral naves are each affected by cracks that cut them transversally at the keystone (in the damage survey reported in Figure 2-23c see the cracks coloured in red). These cracks propagate from the walls and also affect the transverse arches separating the lateral and central naves (Figure 2-23a-b). Transverse cracks are also present in some vaults of the central nave. Since the cracks in the walls increase in width with height and do not propagate in the floor, this cracking pattern can be associated to a concave-upward bending (*hogging*) of the church produced by an incremental vertical ground movement in the direction of the longitudinal axis of the building (see Figure 2-12a). This indicates that arches and vaults were subjected to vertical support displacements. However, looking at the schematic representation of the *hogging* mechanism reported in Figure 2-12a, it is likely that the horizontal support displacements also occurred.

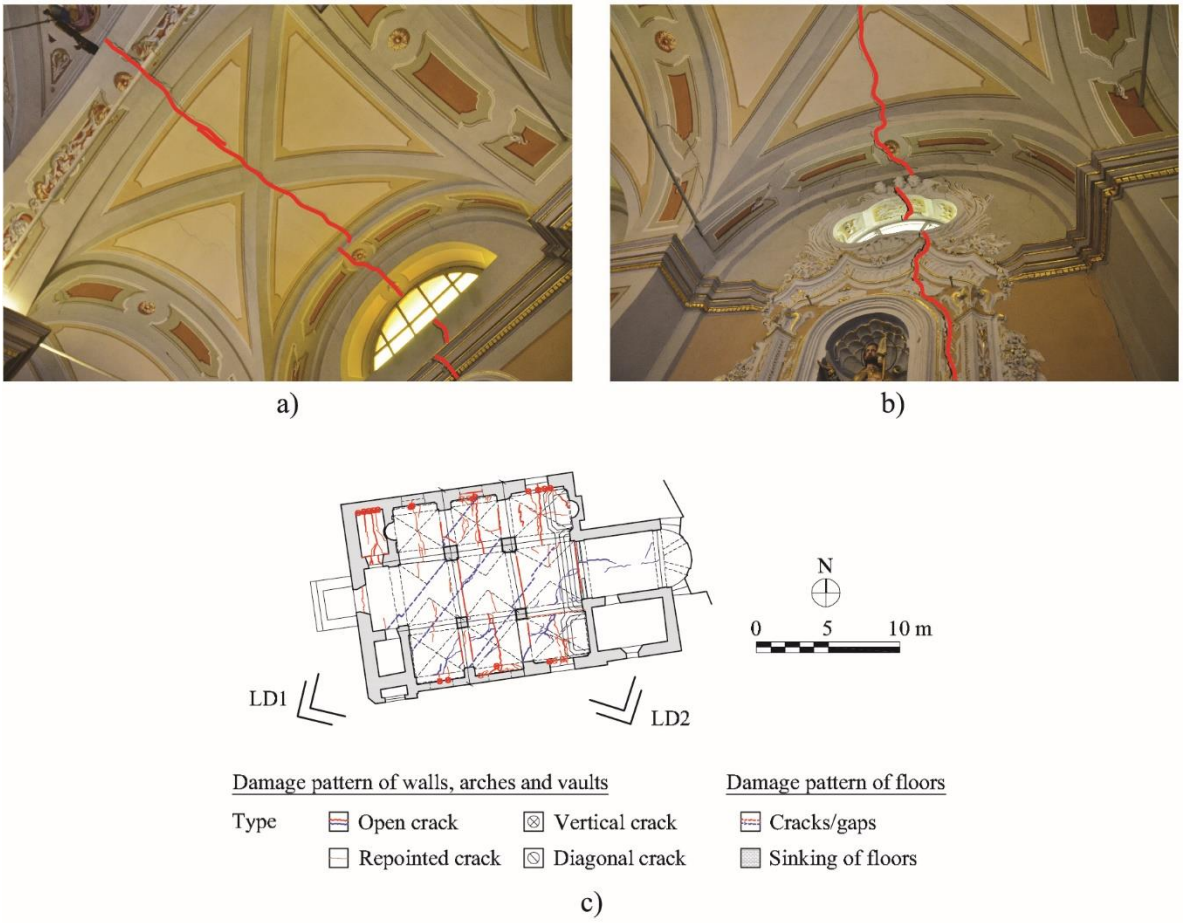

Figure 2-23 Recurrent damage patterns of masonry vaults. Crack repeated with the same pattern in each bay (CH_32): a-b) cracks propagating from the walls and continuing up into arches and vaults, b) damage survey of the entire church (estimated landslide direction indicated with an arrow).

The case of San Martino church in Cembrano is of particular interest because the church is located in an area affected by two slow-moving landslides acting in two different directions (see the arrows indicated in Figure 2-23), which produced a combination of two different global damage mechanisms. The landslide indicated as LD1 in Figure 2-23 was considered responsible of the *hogging* mechanism and corresponding

crack pattern described above (coloured in red in Figure 2-23). Conversely, the landslide named LD2 was found to produce an *extension* mechanism, which resulted in diagonal cracks in the vaults as well as parallel gaps in the floor, all oriented in the same direction (see the crack pattern coloured in blue in Figure 2-23). The occurrence of two different mechanisms, resulting from different soil displacements patterns, suggests that both vertical and horizontal displacements occurred at the supports of arches and vaults. Consequently, even if two different crack patterns were distinctly identified, it is not possible to exclude that the location at which cracks appeared was influenced by the combination of horizontal and vertical support displacements.

2.6. SUMMARY

This chapter presented the results of the systematic damage survey performed on 33 historic masonry churches exposed to slow-moving landslides. Extensive and severe damage, congruent with the landslide direction, was observed in several churches of the sample. Since some buildings were even close to public due to safety reasons, it can be concluded that that slow-moving landslides pose a threat for the conservation of historic masonry churches. Due to the lack of detailed information about landslides movements, the damage assessment was performed through a critical interpretation of the surveyed crack patterns and deformation. This allowed to identify four global damage mechanisms associated to specific soil displacements patterns.

After providing insights on the structural behaviour of the church in its entirety, attention was paid to arches and vaults. In several churches of the sample, widespread cracking and large deformations were observed, confirming that these structural elements are sensitive to slow-moving landslides. As expected, these phenomena were found to produce combinations of vertical and horizontal displacements at the abutments. However, in absence of information about the magnitude of support displacements, the damage assessment of arches and vaults was very challenging. If in the case of vaults some recurrent damage patterns were recognised, in the case of arches cracks appeared at different locations along the arch profile in the different churches of the sample. The damage interpretation was also further complicated by the impossibility of verifying the presence of cracks at the extrados, which was suggested by some deterioration of the plaster observed at the intrados.

The critical analysis of the damaged surveyed demonstrated that, even in the cases where the predominant component of support displacements could be determined, the possibility that both vertical and horizontal displacements occurred prevented from identifying univocally the damage mechanism. In this respect, the observation of various different crack patterns in the arches suggests that the location at which cracks appear is strictly dependant on the way in which vertical and horizontal support displacements are combined. This clearly indicates the need for further investigation into the effects of combined vertical and horizontal support displacements on the response of masonry arches.

REFERENCES

ARPA Piemonte (Agenzia Regionale per la Protezione Ambientale). 2008. Linee guida all'interpretazione dei dati satellitari PSInsarTM in Piemonte.

Cabella C. and G. L. Sacco. 2021. Studio degli effetti di una frana attiva su un edificio voltato: la chiesa di San Carlo Borromeo in Cassingheno (Genova). Master thesis, University of Genoa (in Italian).

Cambiaggi L. 2020. Damage assessment of churches exposed to slope displacements in sliding areas. PhD diss., University of Genoa.

Cascini L., Fornaro G. and D. Peduto. 2009. Analysis at medium scale of low-resolution DInSAR data in slow-moving landslide-affected areas. *ISPRS Journal of Photogrammetry and Remote Sensing* 64: 598-611

Federici, P.R., F. Baldacci, A. Petresi, and A. Serani. 2001. *Atlante dei Centri Abitati Instabili della Liguria. I. Provincia della Spezia* (Atlas of the Unstable Inhabited Centres of Liguria. I. La Spezia province). Regione Liguria.

Federici, P.R., M. Capitani, A. Chelli, N. Del Seppia, and A. Serani. 2004. *Atlante dei Centri Abitati Instabili della Liguria. II. Provincia di Genova* (Atlas of the Unstable Inhabited Centres of Liguria. II. Genova province). Regione Liguria.

Federici, P.R., M. Capitani, A. Serani, and S. Stano. 2006. *Atlante dei Centri Abitati Instabili della Liguria. III. Provincia di Savona* (Atlas of the Unstable Inhabited Centres of Liguria. III. Savona province). Regione Liguria.

Federici, P.R. and A. Chelli. 2007. *Atlante dei Centri Abitati Instabili della Liguria. IV. Provincia di Imperia* (Atlas of the Unstable Inhabited Centres of Liguria. IV. Imperia province). Regione Liguria.

Ferrero C., L. Cambiaggi, R. Vecchiattini, and C. Calderini. 2020. Damage assessment of historic masonry churches exposed to slow-moving. *International Journal of Architectural Heritage*.

Ferrero C., L. Cambiaggi, A. Fenialdi, P. Roca, R. Vecchiattini, and C. Calderini. 2021. Slow-moving landslide damage assessment of historic masonry churches: some case-studies in Italy. In *SAHC 2021: 12th International Conference on Structural Analysis of Historical Constructions*. Barcelona, Spain, September 2021 (Accepted).

Geoportale Regione Liguria. Visualizzatore Cartografico. Accessed January 20, 2020. https://geoportal.regione.liguria.it

Grünthal, G. 1998. European Macroseismic Scale 1998 (EMS-98), *Cahiers du Centre Europèen de Gèodynamique et de Seismologie 15*. Centre Europèen de Gèodynamique et de Seismologie, Luxembourg.

G.U. no. 120, 25/05/1989 (suppl. ord. no. 38). Law no. 183 of 18/05/1989, Norme per il riassetto organizzativo e funzionale della difesa del suolo.

G.U. no. 45, 24/02/2004 (suppl. ord. no. 28). Legislative Decree no. 42 of 22/01/2004, Codice dei beni culturali e del paesaggio, ai sensi dell'articolo 10 della legge 6 luglio 2002, n. 137.

Mamone A. 2017. Rilievo analisi e diagnosi del santuario di N.S. della Bastia in Busalla. Master thesis, University of Genoa (in Italian).

Piano di Bacino Stralcio per l'Assetto Idrogeologico, Regione Liguria, 2017. Carte della Suscettività al Dissesto (Landslide Susceptibility Maps). Accessed October 25, 2018. http://www.pianidibacino.ambienteinliguria.it/.

Piano Stralcio per l'Assetto Idrogeologico, Autorità di bacino distrettuale del fiume Po, 2017. Atlante dei Rischi Idraulici e Idrogeologici (Atlas of Hydraulic and Hydrogeological Risks). Accessed October 25, 2018. http://www.pai.adbpo.it/.

QGIS 2017. Open Source Geographic Information System. Accessed May 3, 2018. https://qgis.org/en/site/.

Regione Liguria e Segretariato Regionale del MiBACT per la Liguria. 2017. Vincoli architettonici, archeologici, paesaggistici. Accessed May 3, 2018. http://www.liguriavincoli.it/.

Varnes, D. J. 1978. Slope movements and types of processes. In *Landslides: Analysis and control*, ed. R. L. Schuster and R. J. Krizek, Transportation Research Board, Special Report 176, 11-13. Washington, DC: National Academy of Sciences.

This page is intentionally left blank.

CHAPTER 3

LITERATURE REVIEW

3.1. INTRODUCTION

This chapter presents the state-of-the-art of the research dealing with masonry arches and vaults on moving supports. The interest in the topic is rather recent, since the first systematic studies date back to the 2000s.

As well described by DeJong (2016), the study of the response of masonry structures undergoing given settlements and, more in general, support displacements can be addressed from two different perspectives. On the one hand, it is needed to assess the stability under large displacements and deformations. On the other hand, it is necessary to predict minor damage and cracking which could affect the serviceability requirements of the structure. Nevertheless, in the case of arches and vaults, the large majority of the studies available in the literature were devoted to investigating the collapse of masonry arches and vaults due to different configurations of support displacements. On the contrary, much less attention was paid to predict cracking and define damage levels associated to a given value of support displacements. Regarding this second aspect, to the author's knowledge, only Acikgoz et al. (2017) developed damage prediction maps, produced by using Limit Analysis (Heyman 1966), to correlate the damage states of a vaulted masonry structure to different scenarios of support displacements.

In Section 3.2, the experimental investigations hitherto carried out to investigate the response of masonry arches and vaults on moving supports are presented. These studies were essential to gain an understanding of the mechanics of masonry arches and vaults undergoing large support displacements. For masonry arches, which are the main subject of this work, a detailed description of the damage and collapse mechanisms observed is provided. In the case of the vaults, whose structural behaviour is not investigated in this thesis, reference is only made to the existing literature.

Sections 3.3.1 and 3.3.2 deal with the methods of structural analysis. Within the past two decades and especially in the last few years, a growing number of analytical and numerical procedures have been developed to investigate the stability of arches and vaults under support displacements. The large majority of these methods adopt the well-known assumptions on the behaviour of the masonry material that were firstly introduced by Heyman (1966, 1995) and provide the theoretical basis for the Limit Analysis theory. According to Heyman, the response of a masonry structure can be analysed considering that masonry has (i) infinite compressive strength, (ii) no tensile strength, and (iii) does not experience sliding failure. Under these hypotheses, masonry structures can be studied as assemblages of rigid blocks connected by no-tension interfaces. Since sliding cannot occur, the only way to deform is to open some cracks, which can be idealized as hinges. Stability thus becomes a matter of geometry rather than material strength (Heyman 1995).

Starting from Heyman's assumptions, some authors proposed analytical and computational methods based on a standard application of the Limit Analysis theorems (Sections 3.3.1), while others adopted modern and more complicated approaches such as finite element and discrete element modelling, among the others (Section 3.3.2). Many of these procedures were validated by comparison with the results of experimental tests performed on full-scale or small-scale models. In Sections 3.3.1 and 3.3.2, the capability of the different computational methods to predict the experimental response is evaluated.

3.2. EXPERIMENTAL INVESTIGATIONS

Experimental tests have been widely used to investigate the stability of masonry arches and vaults under large support displacements. Table 4 and Table 5 collect all the experimental studies carried out so far on masonry arches and vaults, respectively. For each test, information is provided in terms of scale, dimension and material of the mockup, geometry of the structure investigated as well as type of support displacements imposed. In all the tests, support displacements were applied at low velocities in a static or quasi-static way.

Table 4 Experimental investigations on masonry arches subjected to support displacements.

Reference	Scale	Geometry	Span length [cm]	Voussoir material	Joints	Type of support displacements
(Ochsendorf 2002, 2006)	Small-scale	Circular	39.0	Cast concrete	Dry joints	Outward horizontal
		Segmental	70.9			
(Romano 2005; Romano and Ochsendorf 2010)	Small-scale	Circular	100.0	Cast concrete	Dry joints	Outward horizontal/ inward horizontal/ vertical
		Pointed				
(Smars 2000, 2010)	Small-scale	Circular	30.0	Stainless steel	Dry joints	Vertical/horizontal
(Verstrynge et al. 2007)	Small-scale	Pointed	140	Brick	Mortar joints	Outward horizontal
		Parabolic				
(Zampieri et al. 2018a, 2018b, 2018c)	1:1	Segmental	228.1	Brick	Mortar joints (with a plexiglass plate in the middle)	Vertical/ inclined (45°)
(Galassi et al. 2018)	Small-scale	Segmental	42.4/42.4/ 53.5	PVC	Dry joints	Outward horizontal/ vertical
(Galassi et al. 2020)	Small-scale	Pointed	30.0/32.0/ 32.0/33.6/ 34.0/35.2	Autoclaved aerated concrete	Dry joints	Outward horizontal
(Alforno et al. 2020)	1:6	Segmental	62.0	Wood	Mortar joints	Outward horizontal
(Masciotta et al. 2020)	Small-scale	Segmental	190.0	Brick	Mortar joints	Outward horizontal

Table 5 Experimental investigations on masonry vaults subjected to support displacements.

Reference	Scale	Geometry	Span length [m]	Block material	Joints	Type of support displacements
(Ceradini 1996)	1:1	Cross vault	736.0	Brick	Mortar joints	Outward horizontal
		Sail vault	600.0	Tuff		
(Theodossopoulos 2001; Theodossopoulos et al. 2002)	1:4	Cross vault	127.5 (x 94.5)	Wood	Mortar joints	Outward horizontal
(Quinonez et al. 2010; Zessin et al. 2010)	Small-scale	Domes	32.9/29.5	3D printed	Dry joints	Outward horizontal
(Shapiro 2012)	Small-scale	Barrel vaults	30.8/27.8	3D printed	Dry joints	Outward horizontal
		Cross vault	27.8			
(Van Mele et al. 2012)	Small-scale	Cross vault	30.0	3D printed	Dry joints	Horizontal (outward transverse and diagonal) /vertical
(Rossi et al. 2016, Milani et al. 2016)	1:5	Cross vault	62.0	3D printed	Dry joints	Horizontal (outward transverse and diagonal) /vertical
(Rossi et al. 2017)	1:10	Pavilion vault	34.3	3D printed	Dry joints	Outward horizontal
(Calvo Barentin et al. 2017)	Small-scale	Cross vault	30.0	3D printed	Dry joints	Horizontal/vertical
(Foti et al. 2018)	Small-scale	Cross vault	100.0	3D printed	Dry joints	Horizontal (outward transverse and diagonal) /vertical
(D'Altri et. 2020)	1/12	Pointed barrel vault	50.8	Wood	Mortar joints	Linear vertical along one edge
(Torres et al. 2019a)	1:1	Timbrel cross vault	360	Brick	Mortar joints	Vertical
(Torres et al. 2019b)	1:1	Timbrel cross vault	360	Brick	Mortar joints	Up-and-down cyclical

Looking at Table 4 and Table 5, it is observed that the large majority of the experimental tests were performed on small-scale models, while only a small number of works proposed full-scale models. This is not surprising, since full-scale model testing requires significant building skills and, furthermore, it is associated with high costs and long times for fabricating the mockup. Among all the tests performed on arches, only Zampieri et al. (2018a, 2018b, 2018c) analysed a full-scale arch, which was tested to collapse due to vertical and inclined support displacements (Figure 3-1a). Full-scale vaults were built only by Ceradini (1996) and Torres et al. (2019a, 2019b). In Ceradini (1996), the response of two masonry vaults (sail and cross vaults) to horizontal support displacements was investigated, whereas in Torres et al. (2019a, 2019b) a full-scale timbrel vault was tested under vertical and up-and-down cyclic displacements of one support (Figure 3-1b). On the contrary, small-scale testing is less expensive, allows to repeat several trials for the same test and can be easily used to investigate structures with different geometries. A representative

example can be found in Romano (2005) and Romano and Ochsendorf (2010), where 150 tests on small-scale circular or pointed arches with varying geometry subjected to vertical and horizontal support displacements were performed.

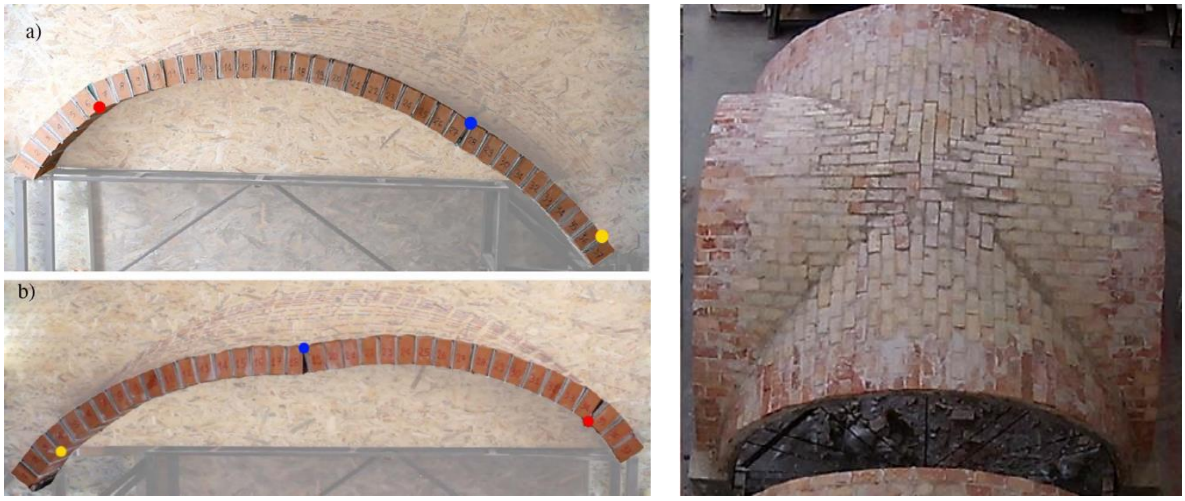

a) b)

Figure 3-1 Experimental test on full-scale models of arches and vaults on moving supports: a) segmental brick arch subjected to vertical (top) and inclined (bottom) support displacements (Zampieri et al. 2018a), b) timbrel brick cross vault subjected to vertical cyclic displacements of one support (Torres et al. 2019b).

On this subject, it is worth noting that small-scale models have been widely used to investigate the collapse state of masonry arches and vaults not only on moving supports, but also under different loading conditions, such as point loads (Pippard and Ashby 1939; Shapiro 2012) or seismic actions (Calderini et al. 2015; DeJong et al. 2008; Gaetani et al. 2017; Misseri et al. 2018). Indeed, if the stability of masonry structures is only a matter of geometry, their collapse behaviour can be considered independent on scale and, thus, it can be studied using small-scale models (Heyman 1995; Van Mele et al. 2012). The large majority of the small-scale models reported Table 4 and Table 5 were designed so as to comply as much as possible with Heyman's assumptions on the behaviour of the masonry material. In accordance with the hypothesis of no tensile strength proposed by Heyman, voussoirs were assembled with dry joints so that only compressive forces could be transmitted between them. Furthermore, special attention was paid to prevent sliding by choosing materials with high friction angles (e.g. Rossi et al. 2016) or by adopting some specific solutions for the contact surfaces. For instance, Galassi et al. 2018 glued sheets of abrasive papers on the internal faces of adjacent blocks. Nevertheless, sliding was observed in some experimental tests, especially in the case of masonry vaults (Rossi et al. 2016; Van Mele et al. 2012), whose damage mechanism often involve sliding (Van Mele et al. 2012).

The full-scale models tested were made of brick or tuff voussoirs bonded by mortar (Figure 3-1), while the majority of the small-scale models were assembled with dry joints. In the case of dry-joint arches, a number of different materials was used for the voussoirs, including cast concrete, stainless steel, PVC or autoclaved aerated concrete. In the case of the vaults, all the dry-joint specimens were made of 3D printed blocks. Three-dimensional printing is an effective method to produce voussoirs with high geometrical

accuracy, which is needed when building models with three-dimensional complex geometries, like vaults or domes. Only in the minority of cases (Alforno et al. 2020; D'Altri et al. 2020; Masciotta et al. 2020; Verstrynge et al. 2007), small-scale models were made of brick or wood voussoirs assembled with mortar joints.

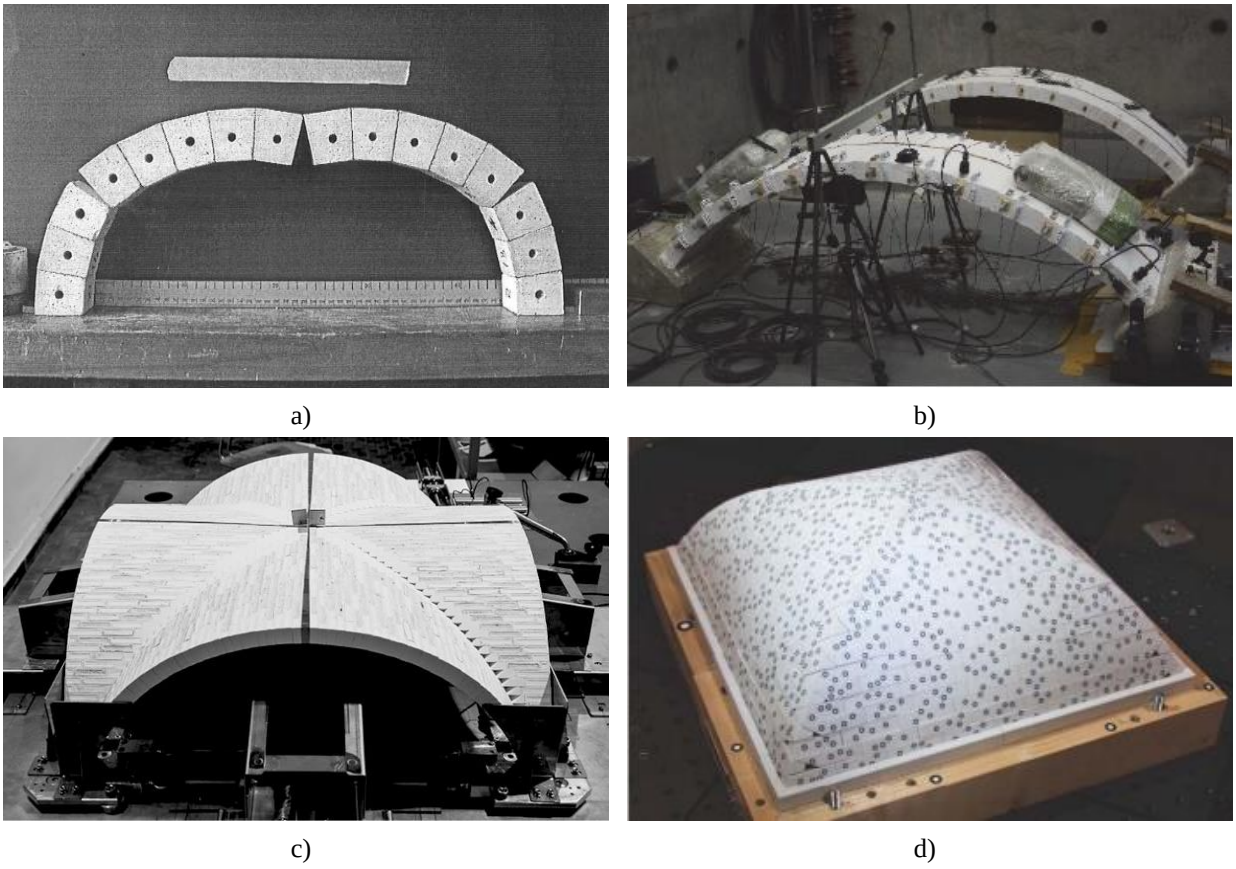

a) b) c) d)

Figure 3-2 Experimental tests on small-scale models of arches and vaults on moving supports: a) segmental dry-joint arch made of cast concrete voussoirs (Ochsendorf 2006), b) segmental arch made of brick voussoirs bonded by mortar (Masciotta 2020), c) 3D-printed cross vault (Rossi et al. 2016), d) 3D-printed pavilion vault (Rossi et al. 2017).

It is important to point out that most of the studies based on small-scale model testing did not aim to represent the unit size and arrangement that characterize real masonry structures. In the case of arches, only Alforno et al. (2020) used voussoirs whose size represented the scaled dimensions of standard bricks. As for the vaults, the same solution was adopted only in Rossi et al. (2016) and Milani et al. (2016), where the brick pattern observed in real masonry vaults was also accurately reproduced. In Rossi et al. (2017), the height-to-width ratio of the voussoirs was proportional to that of a standard brick, while in D'Altri et al. (2020) the length of the blocks represented the scaled length of the units of the original vault.

Looking at the type of imposed support displacements reported in Table 4 and Table 5, it is easy to observe that greater attention was paid to investigate the effects of horizontal support displacements compared to vertical or inclined ones. The large majority of the experimental studies (17 over 21) tested arches and vaults under horizontal support displacements, while only half of them considered vertical displacements. The response to inclined displacements, resulting from the combination of the previous two,

was investigated only by Zampieri et al. (2018a, 2018b, 2018c). In this respect, it is worth noting that imposing horizontal movements at the abutments also allows to simulate the damage mechanisms induced by seismic events, which was the goal of the works by Ceradini (1996), Rossi et al. (2016), and Milani et al. (2016).

A final comment about the geometry of the tested structures can be made. In the case of arches, the large majority of the studies investigated the response of circular or segmental arches, while less attention was paid to pointed (see Galassi et al. 2018; Romano 2005; Romano and Ochsendorf 2010; Verstrynge et al. 2007) and parabolic arches (see Verstrynge et al. 2007). In the case of the vaults, most of the experimental investigations focused on the structural behaviour of cross vaults. Conversely, Quinonez et al. (2010) and Zessin et al. (2010) tested to collapse two 3D-printed domes subjected to outward radial support displacements. Rossi et al. (2017) studied the behaviour of a 3D-printed pavilion vaults on spreading supports. D'Altri et al. (2020) investigate the effects of vertical settlement on a scaled pointed barrel vault. Ceradini (1996) tested a full-scale tuff sail vault on spreading supports.

The experimental studies provided a strong understanding of the mechanics of masonry arches and vaults on moving supports. The main outcomes are presented here for masonry arches only.

In all the tested arches, three hinges appear when supports displacements are imposed. The hinge position is strictly dependant on the type of support displacements. For horizontal spreading supports (Alforno et al. 2020; Galassi et al. 2018; Galassi et al. 2020; Masciotta et al. 2020; Ochsendorf 2002, 2006; Romano 2005; Romano and Ochsendorf 2010), the three initial hinges alternate between the intrados and the extrados in the sequence I-E-I (where I = intrados and E = extrados) (Figure 3-3). Depending on the arch shape and discretization in voussoirs, the intrados hinges occur either at the haunches (Figure 3-3a-c-d) or at the springings (Figure 3-3b). When the arch does not have a keystone, the hinge configuration is generally symmetrical (Figure 3-3a). The extrados hinge opens at mid-span, while the intrados hinges occur in a symmetrical position with respect to the vertical axis of symmetry of the arch. On the contrary, the presence of the keystone causes the extrados hinge to open at one side of the keystone only, resulting in a slightly asymmetrical hinge configuration (Figure 3-3b-c). In some cases, a slight asymmetry in the position of the intrados hinges is also obtained (Figure 3-3d). The effect of the presence of the keystone on the hinge configuration can be clearly observed in the experimental tests carried out by Romano (2005), Romano and Ochsendorf (2010), Galassi et al. (2018) and Galassi et al. (2020) on scaled circular and pointed arches on spreading supports.

For arches on closing supports (see Romano 2005; Romano and Ochsendorf 2010), the three initial hinges are again located alternately between the intrados and the intrados. However, differently from the case of spreading supports, they follow the sequence E-I-E (Figure 3-4). The intrados hinge appears at mid-span, while the two extrados hinges open at the haunches (Figure 3-4a) or at the springings (Figure 3-4b). As shown for arches on spreading supports, the hinge configuration is symmetrical when there is no keystone.

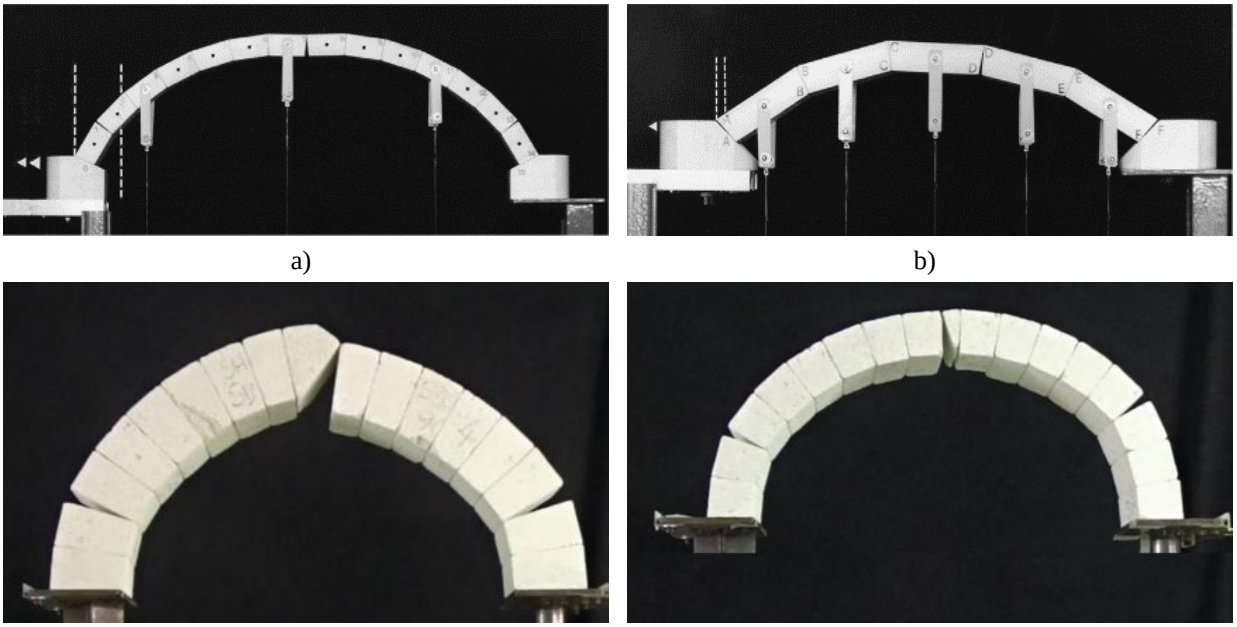

a) b)

c) d)

Figure 3-3 Position of the three initial hinges in arches on horizontal spreading supports: a) symmetrical hinge configuration for arches without keystone (Galassi et al. 2018), b-c-d) asymmetrical hinge configuration for arches with keystone (Galassi et al. 2018, 2020).

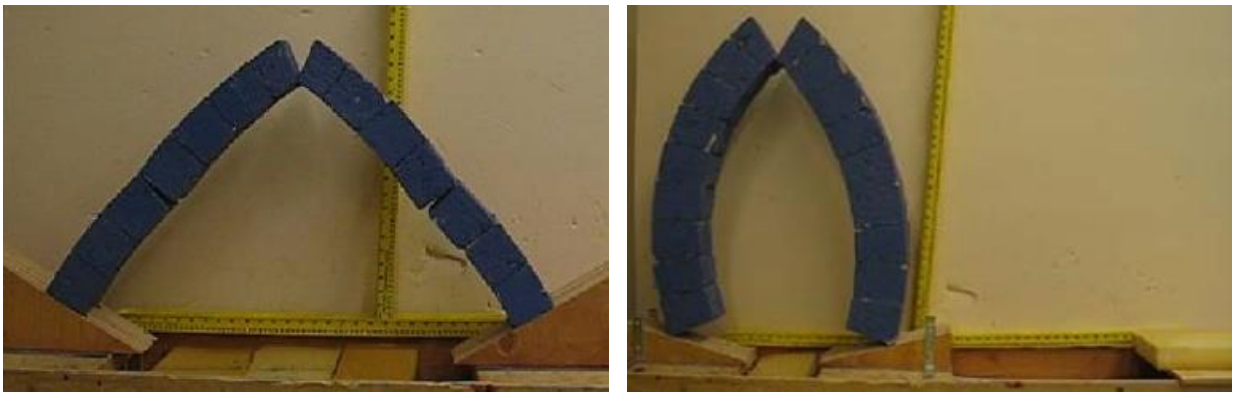

a) b)

Figure 3-4 Position of the three initial hinges in arches on horizontal closing supports: a) extrados hinges opening at the haunches, b) extrados hinges opening at the springings (Romano 2005).

When vertical downwards displacements are imposed at one support (see Galassi et al. 2018; Romano 2005; Romano and Ochsendorf 2010; Smars 2010; Zampieri et al. 2018a), in the case of circular and segmental arches, the location of the hinges follow the sequence I-E-E, beginning from the support that does not move. In the case of pointed arches, both sequences I-E-E and I-I-E can occur depending on the arch shape (see Romano 2005; Romano and Ochsendorf 2010).

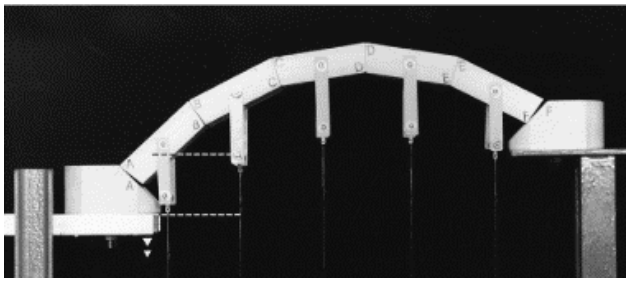

Figure 3-5 Position of the three initial hinges in arches subjected to the vertical downward displacement of one support (Galassi et al. 2018).

The only reference for inclined displacements is the test performed by Zampieri et al. (2018a, 2018b, 2018c) on a segmental arch subjected to the inclined displacement (45° with respect to the horizontal) of one support. In this case (Figure 3-1a down), the three initial hinges alternate between the intrados and extrados according to the same sequence (I-E-I) observed for horizontal spreading supports.

As clearly stated by Heyman (1995), the opening of three hinges is not a concern, but it transforms the arch in a statically determined structure able to accommodate further support displacements. As support displacements increase, the arch deforms by rigid body kinematics, experiencing significant changes in the geometry which finally cause collapse to occur (Figure 3-6). The experimental tests performed by Ochsendorf (2002, 2006), Romano (2005), Ochsendorf and Romano (2010), and Smars (2010) showed that hinges may change location with the increase of support displacements before reaching the collapse. In particular, the intrados hinges may move towards the crown as the supports spread apart (Figure 3-6b-c-d).

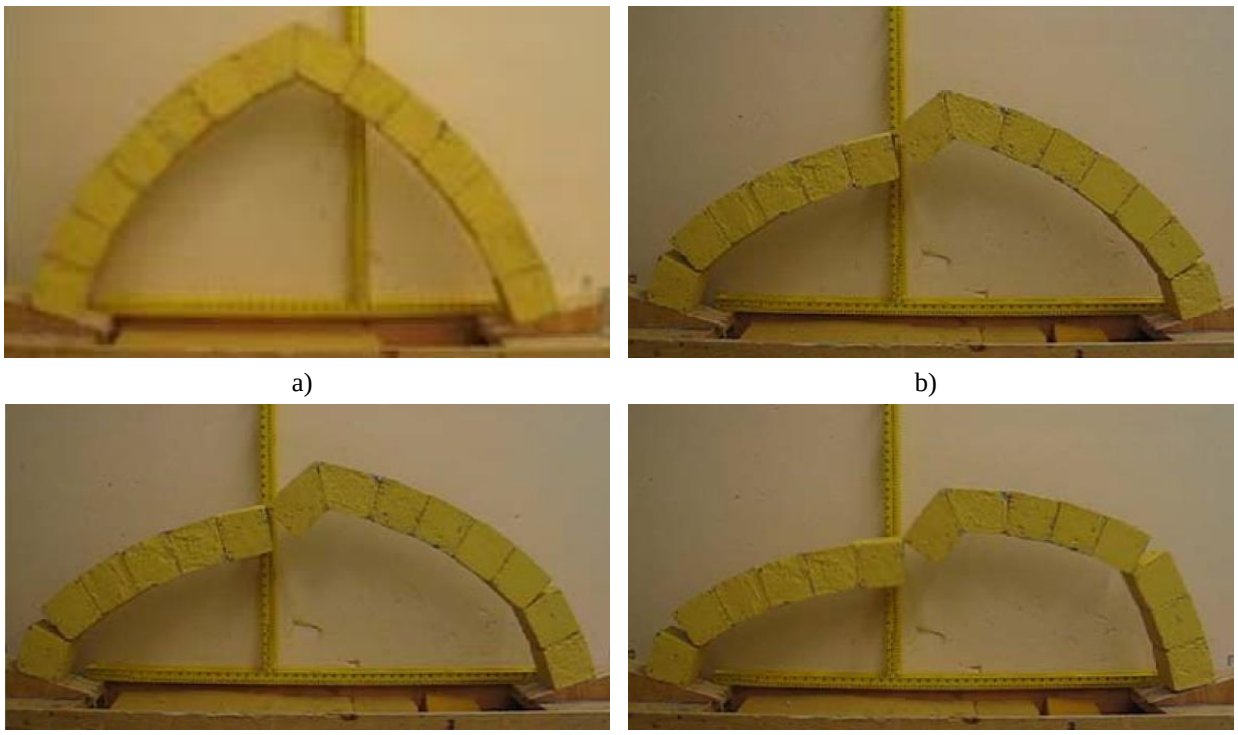

a) b)

c) d)

Figure 3-6 Evolution of the damage configuration up to collapse (the hinge movement is clearly visible in b-c-d) (Romano 2005).

According to the experimental evidence, different failure modes can occur depending on the arch shape and type of imposed support displacements. For horizontal and vertical support displacements, the arch generally collapses when a fourth hinge appears (Figure 3-7a-b-c). In the case of horizontal spreading supports, a three-hinge snap-through failure may also occur for very thick arches with small angles of embrace (Figure 3-7d). In the case of closing supports, collapse mechanisms involving sliding were also observed. For further details, the reader is referred to Romano (2005) and Romano and Ochsendorf (2010).

Figure 3-7 depicts the collapse mechanisms observed in arches with different geometry on horizontal spreading supports. In the experimental tests carried out by Ochsendorf (2002, 2006), Romano (2005), Romano and Ochsendorf (2010), and Alforno et al. (2020), collapse generally occurs by a four-hinge mechanism when a hinge appears at the extrados at one of the two supports (Figure 3-7a-b). Only for few specimens tested by Romano (2005) and Romano and Ochsendorf (2010), the occurrence of a five-hinge mechanism with hinges at both springings was reported (Figure 3-7c). In the case of the segmental and pointed arches with keystone tested by Galassi et al. (2018, 2020), the failure mode did not necessarily involve the opening of a hinge at the springing, but it was sufficient that a hinge appeared at a fourth interface. It is worth noting that the theoretical collapse mechanism for arches on spreading supports should be symmetrical and involve the opening of five hinges. However, as observed by Ochsendorf (2002, 2006), the slight asymmetry and geometrical imperfections of the physical models can result in an asymmetrical four-hinge mechanism.

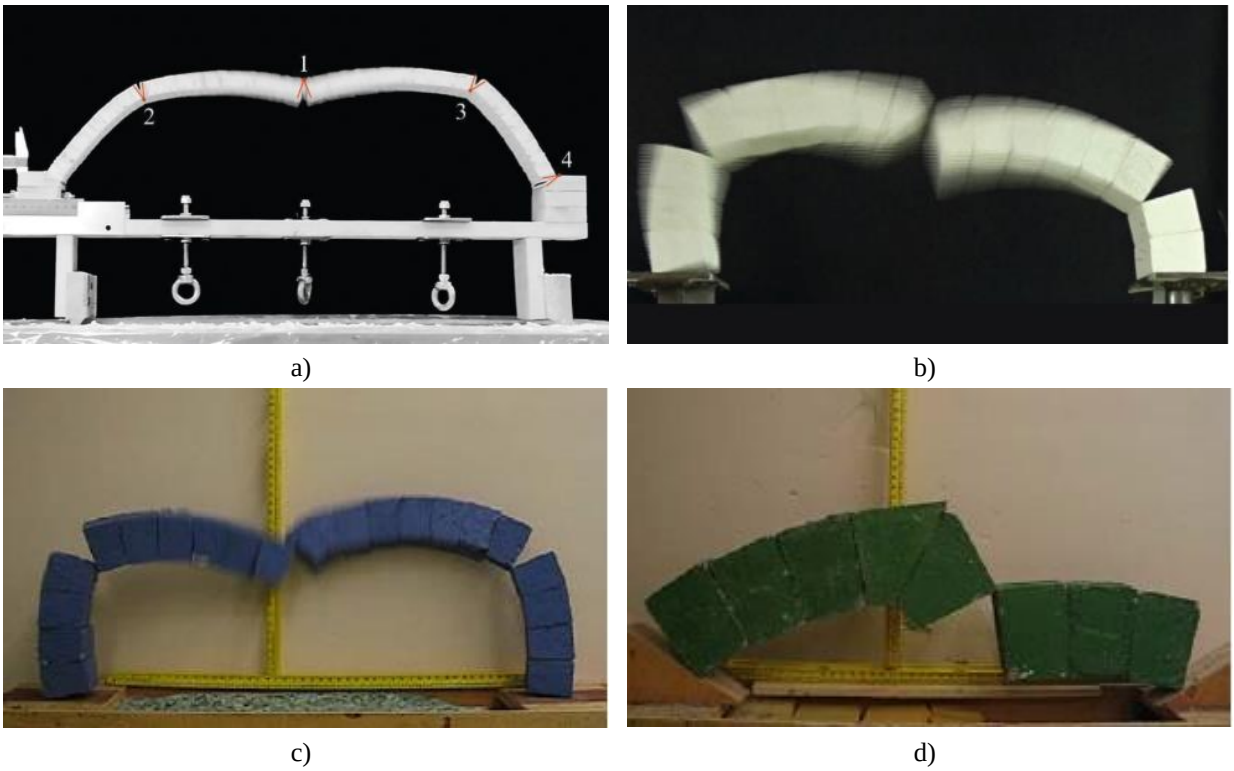

Figure 3-7 Collapse mechanism of arches on horizontal spreading supports: four-hinge mechanism in segmental (a, Alforno et al. 2020) and pointed (b, Galassi et al. 2020) arches, c) five-hinge mechanism (Romano 2005), d) snap-through failure (Romano 2005).

In the case of inclined support displacements, the only experimental test performed in the literature (Zampieri et al. 2018b, 2018c) showed a collapse mechanism due to the alignment of the three initial hinges (Figure 3-8).

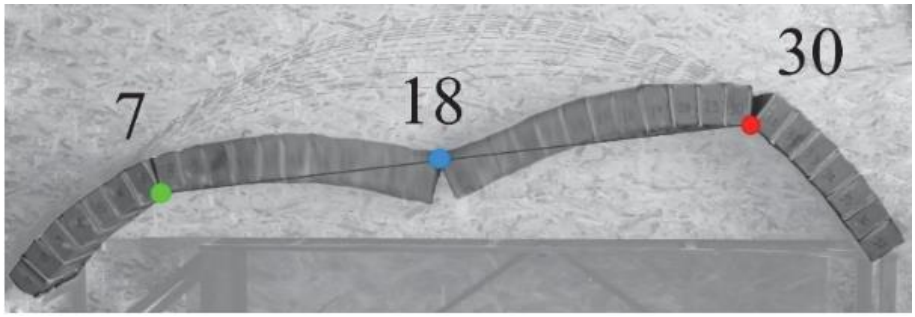

Figure 3-8 Collapse mechanism for a segmental arch subjected to an inclined (45° with respect to the horizontal) displacement of one support (Zampieri et al. 2018b).

3.3. COMPUTATIONAL METHODS

3.3.1. Analytical and computational methods based on Limit Analysis

Analytical and computational methods based on the Limit Analysis theory have been used to predict collapse due to support displacements mainly for masonry arches and bi-dimensional structures (e.g. buttressed arches), since their application to three-dimensional structures (e.g. pavilion or cross vaults) is hardly feasible. Some approaches based on Limit Analysis have been developed in the last decades to assess the stability of three-dimensional structures under gravitational or point loading, such as the funicular analysis of masonry vaults by O'Dwyer (1999) or the Thrust Network Analysis by Block (2009) and Block and Ochsendorf (2007, 2009), among others. However, these methods analyse the structure in its undeformed configuration and do not accommodate large support displacements, which, on the contrary, involve significant geometrical deformations.

It is well-known that, under the simplified assumptions on the behaviour of the masonry material introduced by Heyman, the limit theorems of plasticity can be applied to masonry structures (Heyman 1966; Roca 2010). The lower-bound and upper-bound theorems provide the basis for the so-called static and kinematic approaches, respectively (Roca 2010). According to the lower-bound (safe) theorem, a structure is safe if at least one thrust line which is in equilibrium with the external loads and falls with the boundaries of the structure can be found. The dual approach of the safe theorem is the upper-bound theorem, which states that collapse occurs if a kinetically admissible mechanism for which the work done by the external forces is positive or zero can be found. In addition to the above-mentioned theorems, the uniqueness theorem is also applicable: a limit condition (i.e. the structure is on the point to collapse) is reached if a both statically and kinematically admissible collapsing mechanism can be found. This is tantamount to state that collapse occurs when the thrust line touches the arch boundary in as many points (corresponding to hinges) as needed to activate a mechanism. Under these conditions, the mechanism is the true ultimate mechanism, and the thrust line is unique (Heyman 1966, Roca 2010).

Several studies adopted the static or kinematic approach of Limit Analysis to identify the position of the three hinges that open as soon as supports move as well as to predict the ultimate displacement capacity and collapse mechanisms for rigid no-tension arches with different geometries. As stated by Ochsendorf 2006, an initial equilibrium configuration, identified by the opening of three hinges, must be necessarily known to determine the collapse state. The first problem can be addressed by studying the arch in its undeformed configuration under the assumption of small (infinitesimal) displacements usually adopted in Limit Analysis. On the contrary, as observed in the experimental tests, the second problem involves progressive changes in the geometry and must be analysed in the framework of large displacements using iterative procedures able to follow the evolution of the arch deformed configuration with the increase of support displacements.

Within the framework of small displacements, reference should be made to the theory of the incipient settled states developed by Como (1996, 1998, 2016). In the undeformed configuration, the position of the three initial hinges that open when an infinitesimal movement of the abutments occurs can be found using the static and kinematic theorems of the minimum thrust. According to these theorems, the thrust (i.e. the horizontal reaction of the moving support) is the lowest of all the statically admissible thrusts and the highest of the kinematically admissible ones. A trust is statically admissible when the thrust line lies within the profile of the arch, while it is kinematically admissible if the internal work done for a kinematically admissible virtual mechanism is equal to zero (Coccia et al. 2015). According to the uniqueness theorem, the actual thrust is unique and is the only one being both statically and kinematically admissible.

The first examples of application of the Limit Analysis theory to rigid-block arches on moving supports in the framework of large displacements can be found in Smars (2000, 2010) and Ochsendorf (2002, 2006). Smars (2000, 2010) identified the domain of statically and kinematically admissible movements for a chosen mechanism in a circular voussoir arch. Since the arch is stable only if the thrust line is fully inside the arch boundaries, the statically admissible domain of a mechanism was defined as the subset of the kinematic domain for which this condition can be accomplished. Smars (2000, 2010) also highlighted that a transition between different mechanisms can occur as the arch deforms, since hinges can close and open at another position along the arch profile.

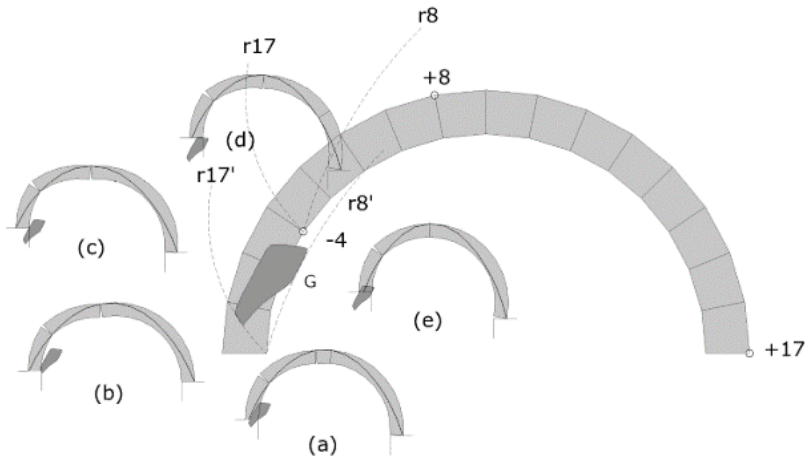

Figure 3-9 Stability domain of a circular arch subjected to large support displacements (Smars 2010).

Ochsendorf (2002, 2006) developed an iterative procedure, based on the thrust line analysis, to compute the collapse displacement and corresponding horizontal thrust for circular rigid-block arches on horizontal spreading supports. The possibility that hinges move with the increase of support displacements was also considered. The algorithm proposed by Ochsendorf, which was implemented in a MATLAB code, is presented in Figure 3-10. First, the location of the three hinges opening for a small outward movement of the abutments and the corresponding minimum thrust are determined considering the arch undeformed geometry. Once an initial equilibrium configuration is known, support displacements are gradually increased, and the equilibrium state of the structure as it deforms until collapse is followed. At each displacement increment, the geometry of the arch is updated, a new thrust line computed, and a check on possible changes in the hinge location performed.

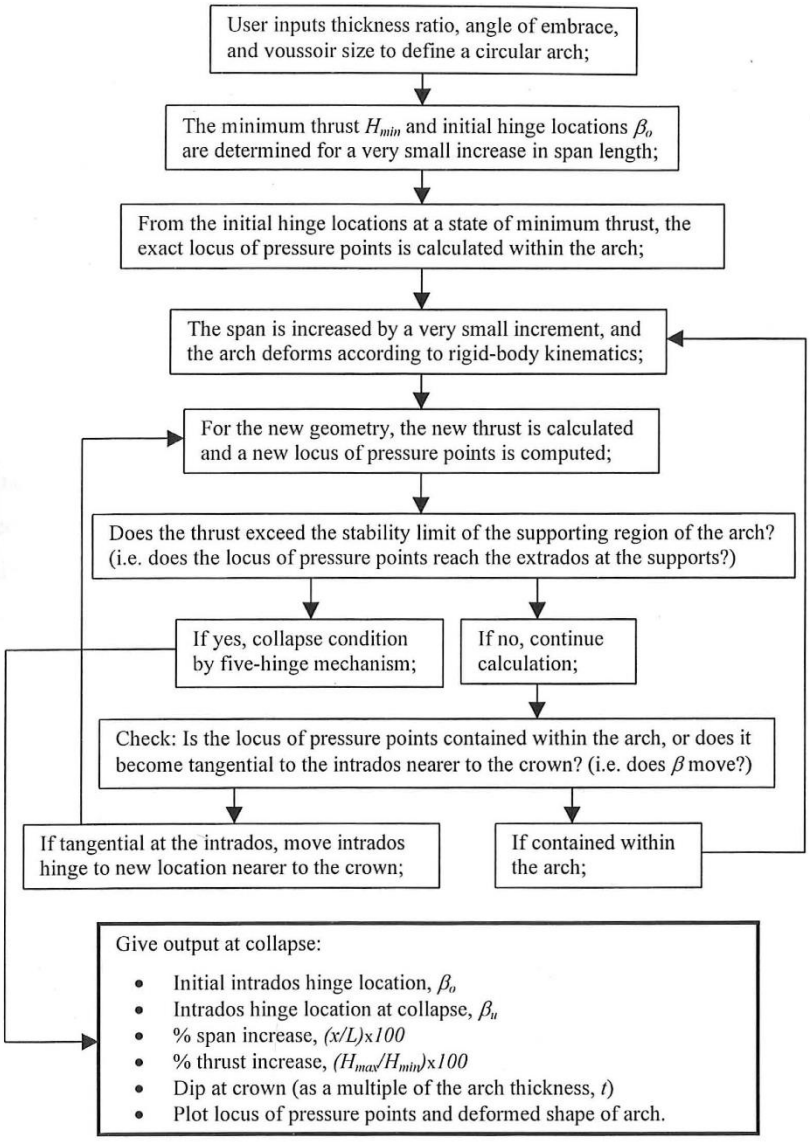

Figure 3-10 – Thrust line analysis-based iterative procedure to study the collapse state of rigid-block circular arches on horizontal spreading supports (Ochsendorf 2002, 2006).

The analytical predictions were compared to the experimental results from small-scale models testing (see Section 3.2). Although the theoretical procedure slightly overestimated the experimental displacement capacity, a good agreement was obtained in terms of both collapse mechanism and hinge position. As expected, differently from the experimental tests, where collapse involved the opening of only four hinges due to the slight asymmetry of the physical models, the predicted failure mode was a symmetrical five-hinge mechanism with hinges occurring at both supports. The difference between predicted and experimental displacement capacity was attributed to the imperfections of the experimental models.

The studies by Ochsendorf provided indications of the values of the horizontal thrust and span increase at collapse for arches with different geometries and numbers of voussoirs. Ochsendorf also demonstrated that the horizontal thrust transmitted by the arch substantially increases with the increase of support displacements due to the changes in the arch geometry as well as hinge movement.

Romano (2005) and Romano and Ochsendorf (2010) adopted the same procedure proposed in Ochsendorf (2002, 2006) to investigate the collapse of circular and pointed arches with varying geometries on horizontal spreading supports. Graphical analyses were also performed to extend the study to different configurations of support displacements, such as closing supports and vertical displacement of one support. The numerical and graphical predictions well compared with the results from small-scale model testing (see Section 3.2) in terms of collapse mechanism and hinge location. However, as already observed by Ochsendorf (2002, 2006), they generally overestimated the displacement capacity. An important result obtained from these studies is that pointed arches exhibit a significantly larger displacement capacity with respect to circular arches with the same inner span.

A further application of the thrust line analysis to study masonry arches on moving supports can be found in McInerney and DeJong (2015), where a two-dimensional analytical model based on thrust line analysis was developed to predict the ultimate displacement capacity of circular and pointed arches subjected to vertical and horizontal support displacements. After assuming an initial location of the three hinges occurring when one support moves, support displacements were gradually increased up to failure. Due to the need to consider continuous changes in the geometry, the maximum displacement prior to collapse was determined by iteratively solving the equilibrium equations in MATLAB. The analytical predictions were compared to numerical results from DE modelling (see Section 3.3.2).

An interesting analytical tool combining the use of kinematic and static analyses was proposed by Block et al. (2006) to evaluate the effect of large support displacements on the stability of vaulted masonry buildings. Several possible collapse mechanisms can be investigated in real-time thanks to the use of interactive graphic analysis, geometrically controlled loads, and animated kinematics. Different configurations of support displacements, including combinations of vertical and horizontal displacements, can also be simulated. However, an important limitation is that the possibility that hinges change location as support displacements increase is not automatically implemented. Furthermore, although conservative solutions can be provided for three-dimensional problems by using the slicing technique, the tool is mainly addressed to bi-dimensional structures.

More recently, Coccia et al. (2015) investigated the collapse of circular arches on horizontal spreading supports by using the kinematic approach of Limit Analysis. An iterative tool, similar to that proposed by Ochsendorf (2002, 2006), was developed to compute the ultimate displacement and corresponding

horizontal thrust. Simplified analytical formulations calibrated on the basis of the proposed model were also suggested. The kinematic approach was applied first in the arch undeformed configuration, calculating the position of the three initial hinges through the kinematic theorem of the minimum thrust proposed by Como (1996, 1998, 2016), and then in the deformed configuration increasing support displacements up to collapse. The possibility that hinges move as support displacements increase was also considered. The procedure proposed by Coccia et al. (2015) was validated through comparison with the results of the experimental tests performed by Ochsendorf (2002, 2006).

Di Carlo and Coccia (2020) adopted the procedure illustrated in Coccia et al. (2015) to analyse the stability of elliptical rigid-block arches on horizontal spreading supports. An innovative aspect of this work lies in the introduction of a safety check on the possible activation of sliding phenomena between blocks. For this purpose, at each displacement increment, the shear force at the joints was compared to the shear strength calculated according to a Mohr-Coulomb law with zero or finite cohesion. An interesting outcome is that neglecting sliding phenomena in elliptical arches may not lead to conservative results. Indeed, the values of displacement obtained considering the attainment of the shear strength with finite cohesion were always lower than the collapse displacements evaluated by using the kinematic approach only.

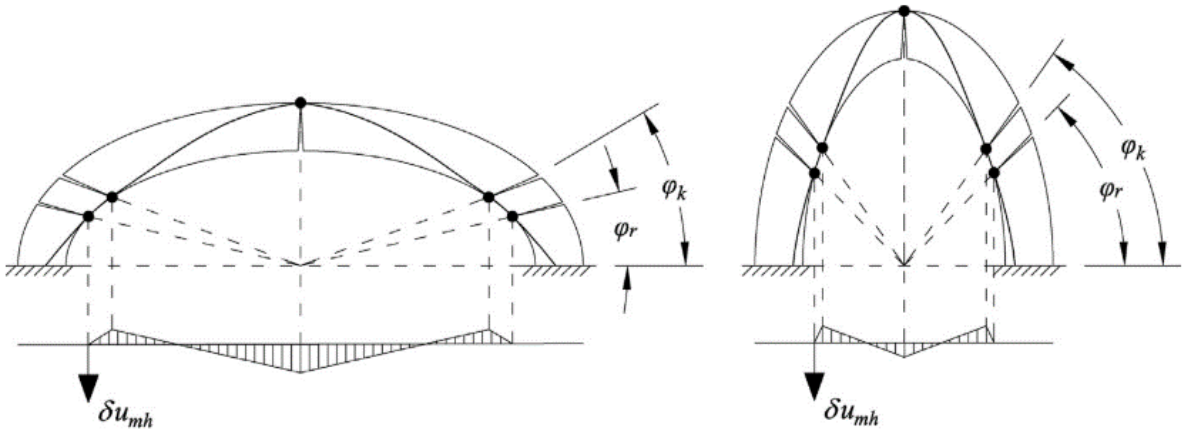

Figure 3-11 Application of the kinematic approach to study the stability of elliptical arches on horizontal spreading supports (Di Carlo and Coccia 2020).

Di Carlo et al. (2018) extended the procedure proposed in Coccia et al. (2015) to evaluate the collapse load of a circular arch undergoing a finite horizontal displacement of the springings. The approach is innovative, since the effect of large support displacements on the capacity of masonry arches to sustain point loads is still rather unexplored. An incremental vertical point load was applied at the crown of the arch as support displacements increased. The collapse load was calculated in the arch deformed configuration using the kinematic approach. The possibility of hinge movement was also taken into account.

Very recently, Zampieri et al. (2018a) developed an analytical procedure to identify the position of the three initial hinges that occur in circular continuous arches subjected to vertical, horizontal and inclined displacements of one support. To univocally determine hinge location, both the static and kinematic theorems of Limit Analysis were applied in the arch undeformed configuration. A key finding is that the initial hinge configuration varies according to the direction of the imposed support displacements. The analytical predictions were compared to the results from experimental tests and FE micro-modelling for the

case of a segmental arch subjected to vertical and inclined (45° with respect to the horizontal) displacements of one support. The proposed analytical approach was found capable to simulate the experimental response, though some differences in terms of hinge location were obtained.

The same procedure proposed in Zampieri et al. (2018a) was adopted in Zampieri et al. (2019) to analyse an arch-pillar system. In Zampieri et al. (2018b), the methodology was extended in the framework of large displacements to investigate the collapse state of masonry arches subjected to inclined support displacements. The Principle of Virtual Work, in combination with thrust line analysis, was iteratively applied to the arch deformed configuration until reaching collapse. The proposed procedure was used to simulate the experimental test carried out on a full-scale segmental arch subjected to an inclined (45° with respect to the horizontal) displacement of one support. Despite some discrepancies in terms of hinge location, the numerical procedure well captured the experimental evidence in terms of collapse mechanism. However, this procedure had an important limitation, as it assumed that collapse could occur only by the alignment of the three initial hinges.

In Zampieri et al. (2018c), an incremental procedure using both the Principle of Virtual Work and the limit equilibrium approach was proposed to investigate different configurations of support displacements in circular and segmental arches in the large displacement regime. A probabilistic approach was also introduced to consider the effects of geometrical uncertainties on the arch response. The developed methodology was applied to simulate two experimental tests on masonry arches on moving supports. The results demonstrated that including geometrical uncertainties provides a better estimate of the experimental displacement capacity, which, on the contrary, is generally overestimated when using the nominal geometry.

3.3.2. Modern computational methods

The two last decades have witnessed a continuous development of numerical methods and computational tools that assess the stability of masonry arches and vaults on moving supports going beyond the standard application of the theorems of Limit Analysis. Nevertheless, the large majority of these methods have still adopted Heyman's assumptions on the behaviour of masonry material, with the results that arches and vaults have been generally modelled as assemblages of (rigid) blocks interacting at no-tension joints.

Discrete element (DE) and finite element (FE) methods have been widely used in the framework of large displacements. Differently from the methods based on Limit Analysis, they are not limited to the study of arches and bi-dimensional structures and can also be applied to three-dimensional structures.

The DE method was first developed for rock mechanics (Cundall 1971) and subsequently applied to masonry structures (e.g., Lemos 1997, 2007). In DEM, masonry is modelled as a discontinuous material where blocks are treated as separate bodies (usually rigid or quasi-rigid) interacting by contact interfaces. Differently from FEM, DEM offers the possibility of simulating large relative movements and even full separation between the units (Lemos 2007; McInerney and DeJong 2015). For this reason, it is considered particularly suitable to investigate failure modes due to loss of stability and progressive changes in the geometry, like the ones observed in arches and vaults.

DE models can also be easily used to analyse a wide variety of geometries. An interesting example can be found in McInerney and DeJong (2015), where the response of masonry cross vaults and arches with

several different geometries was investigated under horizontal and vertical support displacements. Masonry units were assumed as rigid, while a Mohr Coulomb model was adopted for the joint contacts. In order to simulate the slow development of settlement phenomena, support displacements were applied in a quasi-static way thanks to the use of adaptive global damping. One of the main findings of the work was that both groin vaults and arches exhibited a significantly larger capacity to sustain vertical support displacements compared to horizontal displacements. Furthermore, for several of the geometries investigated, the displacement capacity of the groin vaults could be roughly estimated from the capacity of arches with similar geometries. The numerical results in terms of collapse displacement were also found to be in good agreement with the analytical predictions from a bi-dimensional model based on thrust line analysis (see Section 3.3.1). Despite these achievements, the adopted modelling approach presented some limitations: localized crushing of material at the joints was not considered and, furthermore, results were not fully repeatable when sliding between blocks was significant.

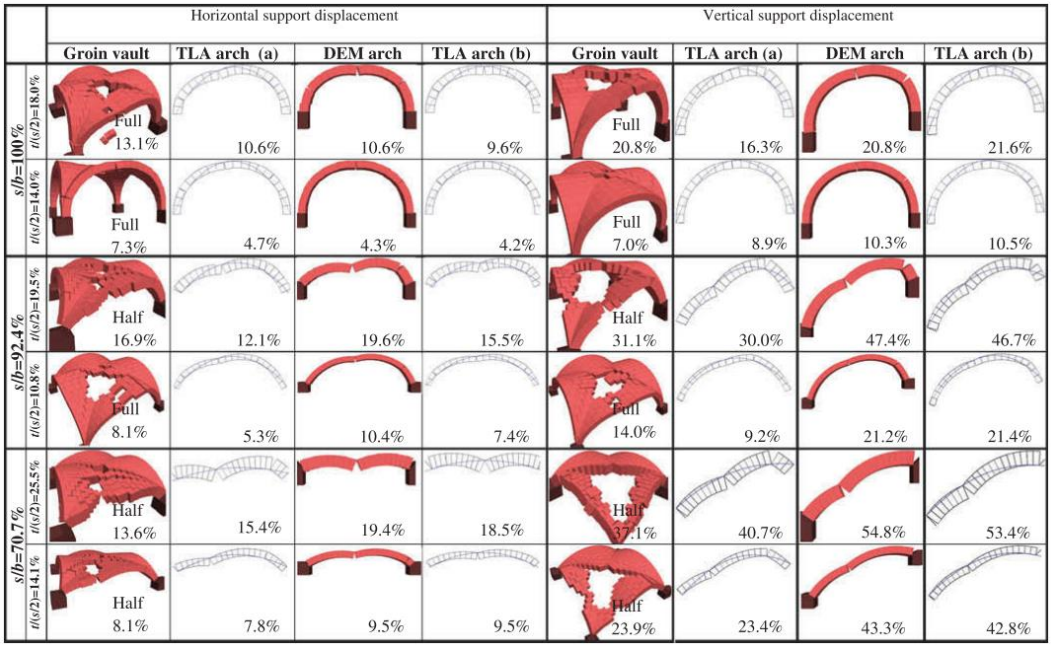

Figure 3-12 Comparison between DEM and 2D thrust line analysis to investigate the stability of groin vaults and arches with varying geometries under horizontal and vertical support displacements (McInerney and DeJong 2015).

In Lengyel (2017) and Lengyel and Bagi (2016), the response of pointed vaults was analysed using DEM. Lengyel (2017) investigated the structural behaviour of pointed barrel and cross vaults subjected to self-weight and finite horizontal support displacements. The main aim of the work was to evaluate if the pointed shape improved the performance of the vaults with respect to a circular centreline. The numerical models were created using the three-dimensional DEM software 3DEC, which is based on the compliant contact formulation of Cundall and Strack (1979). The elastic deformability of the block was also taken into consideration in the DE modelling. Lengyel and Bagi (2016) evaluated the magnitude of the horizontal thrust transmitted by pointed barrel vaults subjected to increasing outward support displacements.

Further applications of DEM to study the collapse of masonry cross vaults under large support displacements can be found in Foti et al. (2018) and Van Mele et al. (2012). In both studies, the cross vaults

were modelled as assemblages of rigid blocks using 3DEC. Horizontal (transverse and diagonal) and vertical displacements were applied at one support of the vault in a quasi-static way to simulate the evolution of the settlement process as well as to enable the structure to recover the static equilibrium after each displacement increment. In Foti et al. (2018), the effect of different block arrangements on the vault performance was also evaluated, demonstrating that the masonry pattern can affect both collapse mechanism and ultimate displacement capacity. In both the above-mentioned studies, the numerical predictions were compared to the results from experimental tests on 3D-printed small-scale models. This comparison showed that the imperfections of the physical models could significantly affect the response in term of displacement capacity and collapse mechanism. Although for some directions of imposed displacements the DE models were able to well capture the experimental failure mode (Figure 3-13a), in other cases the predicted mechanism was different from the one observed in the physical model (Figure 3-13b). Furthermore, the numerical simulations generally significantly overpredicted the displacements capacities obtained in the experimental tests.

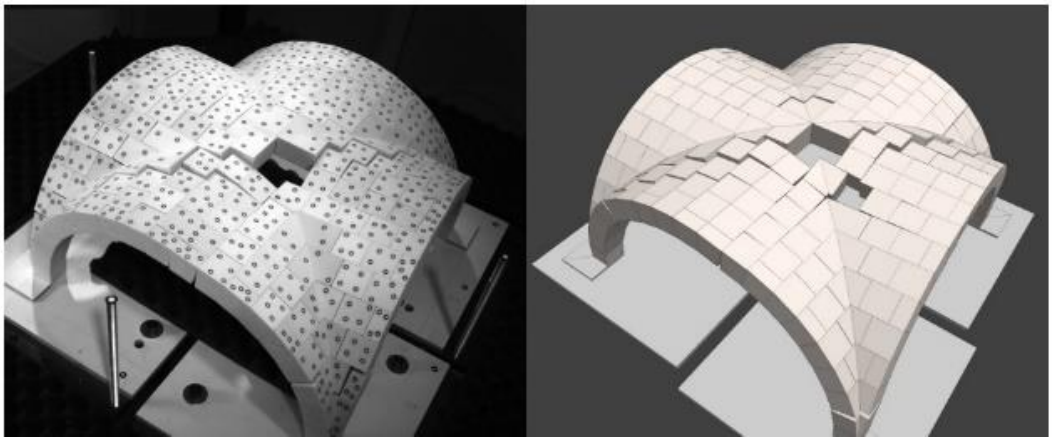

a)

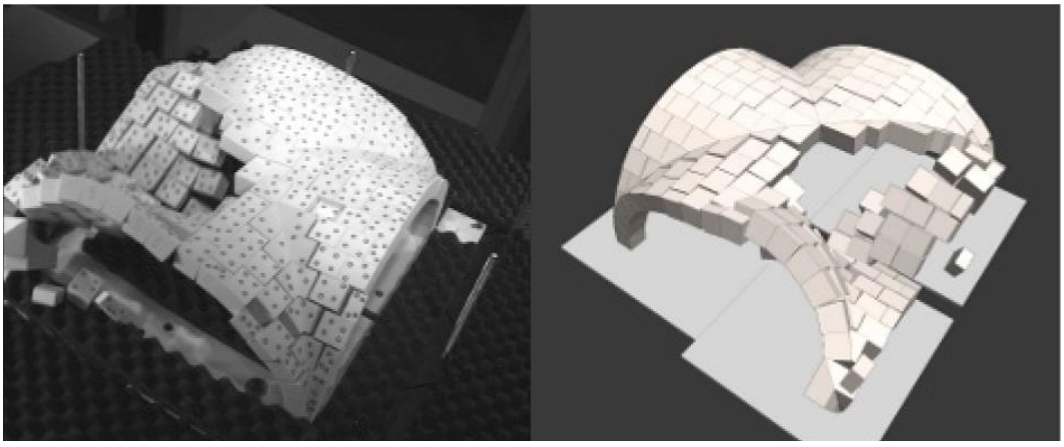

b)

Figure 3-13 Comparison of collapse mechanisms obtained from experimental tests (left) and DEM (right) for a masonry cross vault subjected to the diagonal (a) and transverse (b) displacement of one support (Van Mele et al. 2012) .

Very recently, Dell'Endice et al. (2021) proposed a new method to simulate imperfections within the DEM framework. In particular, the effect of the mechanical and geometrical imperfections on the structural behaviour of a pavilion vault on horizontal spreading supports was investigated. The results from DE analyses, performed first considering a perfect digital model geometry and then including imperfections, were compared to the results from small-scale model testing. Material and geometric imperfections were found to affect both the load path within the vault and the displacement capacity. A parametric analysis demonstrated that the collapse mechanism did not change for a small amount of imperfections, even though the internal flow path was significantly different. On the contrary, for increasing amount of imperfections, the maximum allowable displacement and the collapse mechanism could drastically change, leading to a different structural behaviour of the masonry vault. The simulation of mechanical imperfections allowed to better capture the crack pattern observed in the experimental tests.

FE methods can also be used to investigate the stability of masonry arches and vaults on moving supports. Nevertheless, geometrical nonlinearities must be properly modelled to consider the significant changes in the geometry. Furthermore, FE models have the drawback of becoming computationally demanding and very time consuming, especially when including interface or contact elements and dealing with large complicated structures. For these reasons, the use of FEM to study the collapse of masonry arches and vaults on moving supports is still very limited.

Most of the applications of FEM to masonry arches are based on a micro-modelling approach. Ayensa et al. (2015) proposed a discontinuous FE model to evaluate the effect of soil settlement on the stability of a portal frame (i.e. an arch supported on two piers) of an historic Romanesque church. Zampieri et al. (2018a) studied the response of a segmental arch to vertical and inclined support displacements by using a FE micro-model, in which the arch was built as a set of linear elastic blocks connected by non-linear 1D point-contact elements. The results were compared with experimental and analytical predictions, showing good agreement.

Very recently, Alforno et al. (2020) proposed a simplified FE micro-modelling approach, implemented in the commercial FEM software Abaqus, to study the static behaviour of masonry arches and vaults subjected to external forces and large support displacements. The numerical models were built as assemblages of linear elastic voussoirs interacting at nonlinear interfaces with zero tensile strength. The interfaces were assumed to be almost rigid in compression, with the result that all the elastic deformability of the assemblage was concentrated in the blocks. For this reason, the Young's modulus adopted for the voussoirs was not taken equal to the Young's modulus of the blocks, but it was defined considering the contribution of both blocks and interfaces. The proposed approach can be used for structures with both dry joints and mortar joints with low cohesion. In this latter case, the geometry of the voussoirs is enlarged by the half of the thickness of the mortar joint, and the deformability of the mortar is taken into account through the Young's modulus of the expanded block. The numerical modelling strategy was validated through comparison with experimental tests on small-scale models of a circular arch, made of wooden voussoirs bonded by mortar, on spreading supports and a 3D-printed dry-joint cross vault subjected to different configurations of horizontal support displacements.

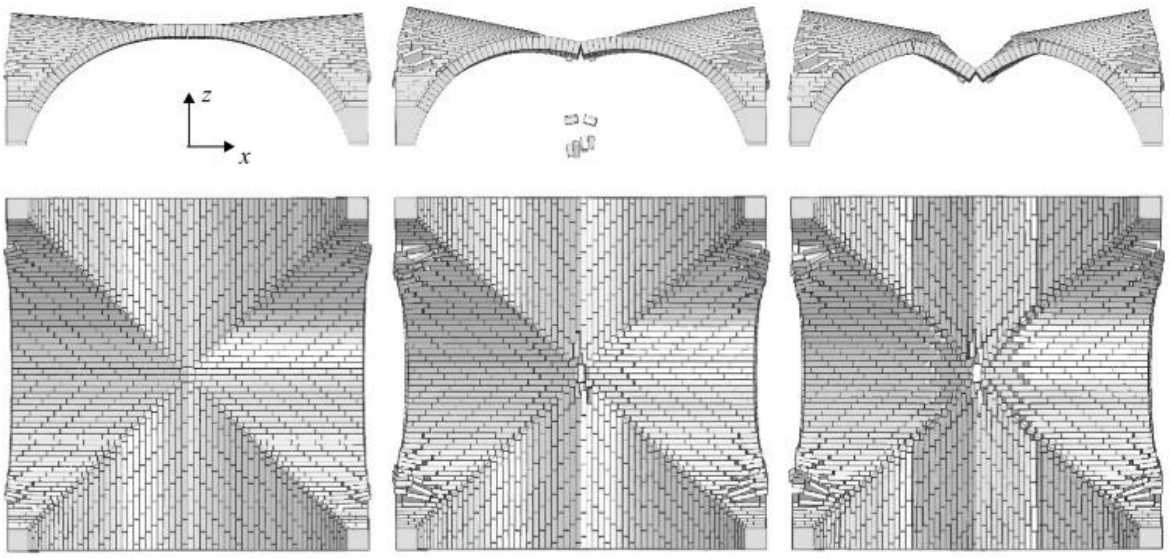

u_x = 17.2 mm u_x = 35.0 mm u_x = 36.3 mm

Figure 3-14 FE micro-modelling of a dry-joint masonry cross vault subjected to an increasing horizontal support displacement u_x: evolution of the damage configuration (Alforno et al. 2020).

Differently from the micro-modelling approaches described above, Masciotta et al. (2020) investigated the dynamic behaviour of a segmental masonry arch subjected to increasing horizontal support displacements using a non-commercial FE code which modelled masonry as a nonlinear elastic isotropic material with zero or weak tensile strength and infinite or bounded compressive strength.

Few examples of application of FE methods to masonry vaults subjected to large support displacements can be found in the literature. Theodossopoulos (2001) and Theodossopoulos et al. (2002) used FE macro- and micro-models (created in Abaqus) to better understand the results of the experimental tests carried out on a small-scale cross vault subjected to horizontal support displacements. Both material and geometrical nonlinearities were considered in the FE simulations. In Torres et al. (2019a, 2019b), 3D elastic finite element models, created in the commercial software Abaqus and Lusas, were used for the preliminary assessment of a timbrel cross vault subjected to vertical support displacements. The results of the FE simulations helped in properly designing the experimental tests on the full-scale masonry vault. D'Altri et al. (2020) developed a 3D non-standard contact-based distinct blocks model, implemented in Abaqus, to simulate the experimental tests carried out on a small-scale pointed barrel vault subjected to a non-uniform vertical displacement along one edge. The presence of mortar joints in the small-scale model was taken into consideration in the numerical model by means of expanded blocks, which were assembled by zero-thickness contact-based interfaces. The comparison between numerical and experimental results showed a good agreement in terms of crack pattern and deformation profiles. The numerical model was then used to simulate different configurations of uniform and non-uniform support displacements.

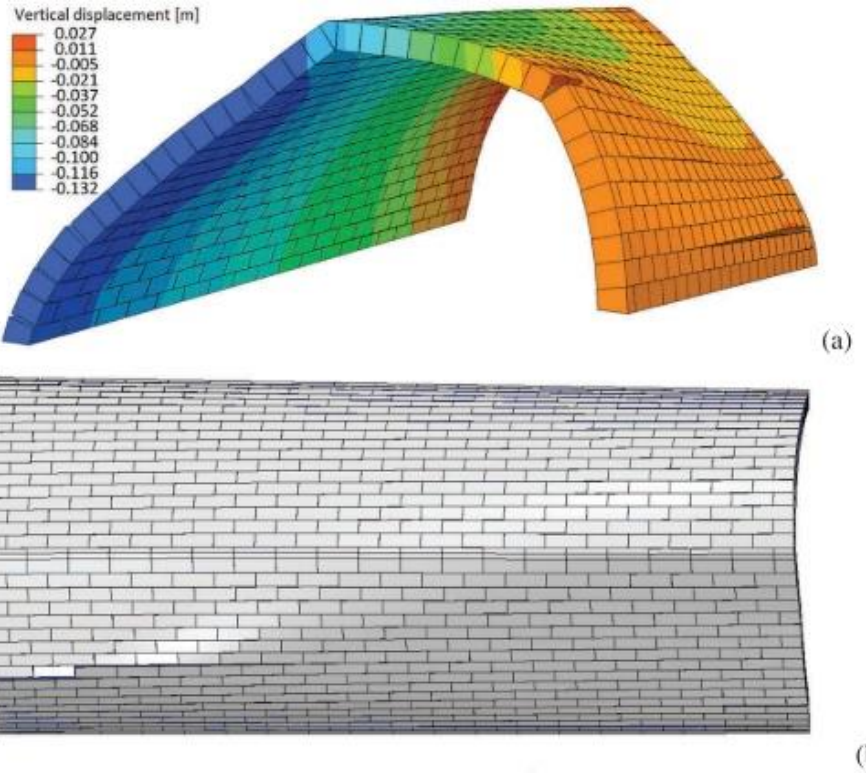

Figure 3-15 Application of a 3D non-standard contact-based distinct blocks model to study the response of a pointed barrel vault to vertical displacements along one edge (D'Altri et al. 2020).

Beyond the use of FEM and DEM, some authors recently proposed novel procedures to analyse bi-dimensional structures subjected to large support displacements under Heyman's assumptions on the behaviour of the masonry material.

Galassi et al. (2018, 2020) developed a novel numerical procedure based on rigid block modelling to analyse the response of arches of any geometric shape to different configurations of support displacements (vertical, horizontal, inclined, and rotational). The arches are modelled as systems of rigid blocks interacting at rigid-cracking interfaces (represented by links). Without using the optimization techniques that are generally employed in Limit Analysis, the proposed procedure first identifies the position of the three initial hinges that occur due to an infinitesimal support displacement by exploiting the laws of combinatorial analysis in combination with static and kinematic analyses. The ultimate displacement at collapse is then determined in the framework of large displacements by means of an iterative procedure, based on static analysis, that tracks the changing equilibrium conditions as finite support displacements increase. The possibility of hinge movement is also taken into consideration.

The proposed numerical procedure was applied to simulate the experimental tests carried out on circular and segmental arches subjected to horizontal and vertical support displacements (Galassi et al. 2018) as well as on pointed arches on horizontal spreading supports (Galassi et al. 2020). In both the studies, the numerical results were in good agreement with the experimental evidence in terms of collapse mechanism and hinge position (Figure 3-16). Nevertheless, the values of ultimate displacement predicted numerically were generally larger than the experimental ones. In Galassi et al. 2020, the numerical procedure was also used to study the response of circular arches with the same span, thickness and angle of embrace of the

pointed arches investigated both numerically and experimentally. As already observed by Romano (2005) and Romano and Ochsendorf (2010), pointed arches generally exhibited a larger displacement capacity to sustain horizontal support displacement compared to the circular ones. Interesting results on the effect of the keystone on the behaviour of circular arches were also provided. As shown in Figure 3-17, the numerical procedure was able to predict a perfectly symmetrical five-hinge collapse mechanism only for arches without keystone, while an asymmetrical hinge configuration was obtained in arches with keystone. The authors also observed that the presence of the keystone generally increased the arch displacement capacity.

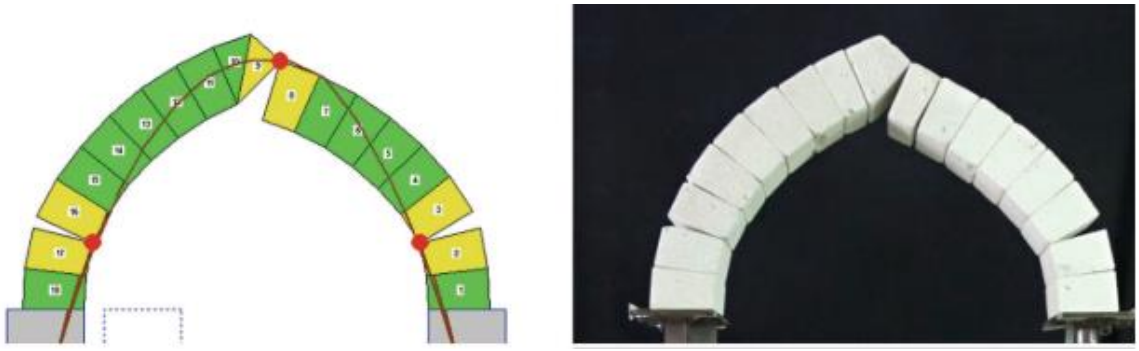

a) b)

Figure 3-16 Damage mechanism for pointed arches on horizontal spreading supports: a) numerical prediction, b) experimental evidence (Galassi et al. 2020).

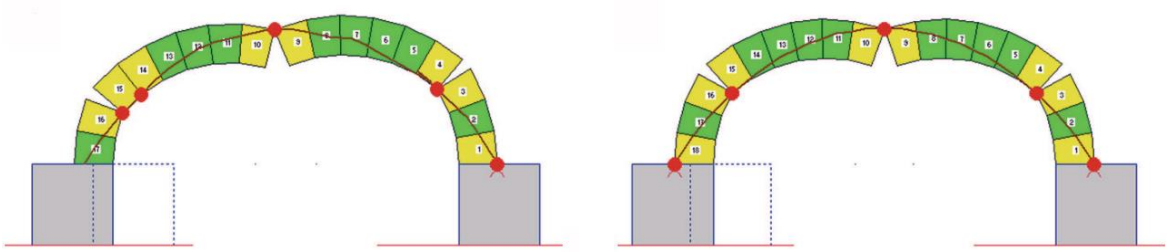

a) b)

Figure 3-17 Effect of the presence of the keystone on the collapse mechanism of circular arches subjected to horizontal support displacements: a) four-hinge asymmetrical mechanism for arches with keystone, b) five-hinge symmetrical mechanism for arches without keystone (Galassi et al. 2020).

Portioli et al. 2017 proposed a rigid block model for the large displacement analysis of two-dimensional dry-joint masonry structures subjected to support displacements. The numerical formulation was developed in the framework of incremental limit equilibrium analysis and the associated contact problem was solved through linear programming. An application for arches was presented for the specific case of a circular arch on horizontal spreading support. The arch was modelled as an assemblage of rigid blocks interacting at no-tension frictional contact interfaces with infinite compressive strength. Large displacements were taken into account implementing an incremental solution procedure divided into displacement increments. At each displacement increment, a force-based optimization problem and its dual displacement-based problem, analogous to the classic lower and upper bound problems of Limit Analysis, were solved.

In Tralli et al. 2020, an approach which deviates from the classic Limit Analysis was used to evaluate the effect of foundation settlements in masonry structures. Two variational formulations traditionally

adopted to solve the kinematic and equilibrium problems for masonry structures, namely the minimum of the total potential energy and a complementary boundary formulation, were extended to the case of contact between multiple no-tension rigid bodies satisfying Heyman's material assumptions. An application of this approach was presented to assess the effect of large support displacements on the load bearing capacity of a circular arch subjected to variable point loads.

Very recently, Iannuzzo et al. (2021) extended the Piecewise Rigid Displacement (PRD) method (Iannuzzo et al. 2020) to investigate the response of a generic bi-dimensional masonry structure to large support displacements. The PRD method is a numerical displacement-based approach to solve the boundary value problem for a continuum composed of the so-called normal, rigid, no-tension (NRNT) material (Angelillo 1993). This approach, initially derived for infinitesimal boundary displacements, was extended to large displacement fields through a proper sequence of linear programming problems, where the geometry is updated, and the NRNT material restrictions are written on the deformed configuration using proper gap functions. New hinges can also open while others close, allowing to track the changes in the mechanism occurring when the imposed displacements increase. The proposed extension of the PRD method was validated through comparison with experimental results (Romano 2005) and DE predictions (3DEC) for the case of a pointed arch on horizontal spreading supports. The PRD method well captured the collapse mechanism and hinge position shown in the experimental test. However, as already observed for the large majority of the computational methods here described, it overestimated the ultimate displacement capacity.

3.4. SUMMARY

This chapter collected an exhaustive review of the existing literature for masonry arches and vaults on moving supports. Both the experimental investigations and the computational studies carried out so far were reviewed, with a special attention to those focusing on masonry arches.

The experimental tests allowed to gain insight on the damage and collapse mechanisms induced by large support displacements in arches and vaults, showing that these structures can accommodate very large displacements and deformations before reaching the collapse. Key features of the response of masonry arches to large support displacements are the progressive changes in the geometry and the hinge movement that occur as support displacements increase.

Regarding the structural analysis, in the last two decades a large number of analytical procedures as well as numerical rigid block modelling-based procedures were developed to investigate the stability of bi-dimensional structures, mainly arches, under large support displacements. To simulate the experimental evidence, most of these studies proposed iterative procedures that followed the changes in the deformed configuration as support displacements increased. The possibility of hinge movement was also taken into consideration. Since these procedures could be hardly applicable to three-dimensional problems, DE and FE modelling approaches were used for the study of masonry vaults undergoing large support displacements.

In order to verify the ability of computational methods to predict the experimental results, the analytical and numerical predictions were usually compared to the results of experimental tests performed on full-

scale or small-scaled models of arches and vaults on moving supports. Although most of the computational tools and numerical models were able to well capture the experimental response in terms of collapse mechanisms, they generally overpredicted the displacement capacity. This difference was attributed to the imperfections of the manually assembled geometries, which may affect the stability of the physical models and cause them to collapse for a smaller support displacement than the one sustained by perfect numerical models. On the contrary, Zampieri et al. 2018c demonstrated that a better estimate of the displacement capacity can be obtained by including the geometrical imperfections in the computational models.

Despite the increasing attention paid in the recent years to masonry arches and vaults on moving supports, there are still some features of their structural behaviour that have not been thoroughly investigated. In particular, most of the research carried out so far dealt with vertical and horizontal support displacements, whereas little attention was paid to their combination, especially in the framework of large displacements. Only one work addressing the stability of masonry arches subjected to inclined support displacements was found in the literature. Further investigation on the effects of inclined displacements is thus needed, also considering the severe and extensive damage caused by slow-moving landslides, which produce a combination of vertical and horizontal support displacements, to arches and vaults of historic masonry churches (see Chapter 2). This thesis aims at addressing this gap by performing experimental tests and numerical analyses on small-scale masonry arches subjected to inclined support displacements.

REFERENCES

Acikgoz, S., K. Soga, and J. Woodhams. 2017. Evaluation of the response of a vaulted masonry structure to differential settlements using point cloud data and limit analyses. *Construction and Building Materials* 150: 916–31. http://dx.doi.org/10.1016/j.conbuildmat.2017.05.075.

Alforno, M., F. Venuti, and C. Calderini. 2020. Validation of Simplified Micro-Models for the Static Analysis of Masonry Arches and Vaults. *International Journal of Architectural Heritage*. https://doi.org/10.1080/15583058.2020.1808911.

Angelillo, M. 1993. Constitutive relations for no-tension materials. *Meccanica* 28(3): 195-202.

Ayensa, A., B. Beltran, E. Ibarz, and L. Gracia. 2015. Application of a new methodology based on Eurocodes and finite element simulation to the assessment of a Romanesque church. *Construction and Building Materials* 101(1): 287–97. https://doi:10.1016/j.conbuildmat.2015.10.115.

Block, P. 2009. Thrust Network Analysis: exploring three-dimensional equilibrium. PhD diss., Massachusetts Institute of Technology.

Block, P., and J. A. Ochsendorf. 2007. Thrust network analysis: a new methodology for three-dimensional equilibrium. *Journal of the International Association for Shell and Spatial Structures* 48(155): 167-173.

Block, P., T. Ciblac, and J. A. Ochsendorf. 2006. Real-time limit analysis of vaulted masonry buildings. *Computers and Structures* 84(29-30): 1841–52. https://doi.org/10.1016/j.compstruc.2006.08.002.

Calderini, C., S. Lagomarsino, M. Rossi, G. De Canio, M. L. Mongelli, and I. Roselli. 2015. Shaking table tests of an arch-pillars system and design of strengthening by the use of tie-rods. *Bulletin of Earthquake Engineering* 13(1): 279–97.

Ceradini, V. 1996. Modelli sperimentali di volte in tufo e mattoni. In: *Atti del Convegno Nazionale La meccanica delle murature tra teoria e progetto,* 157–66. Messina (In Italian).

Coccia, S., F. Di Carlo, and Z. Rinaldi. 2015. Collapse displacements for a mechanism of spreading-induced supports in a masonry arch. *International Journal of Advanced Structural Engineering* 7(3): 307–20.

Como, M. 1996. On the role played by settlements in the statics of masonry structures. In: *The conference on geotechnical engineering for the preservation of monuments and historic sites*. Rotterdam: Balkema.

Como, M. 1998. Minimum and maximum thrust states in Statics of ancient masonry buildings. In: *Proceedings of the 2nd international arch bridge conference*, ed. A. Sinopoli. Rotterdam: Balkema.

Como, M. 2016. *Statics of historic masonry constructions*. 2nd ed. Springer.

Cundall P.A. 1971. A computer model for simulating progressive large-scale movements in blocky rock systems. In: *Proceedings of the symposium of the international society of rock mechanics*, Nancy, France.

Cundall, P.A., and O.D.L. Strack. 1979. A discrete numerical model for granular assemblies. *Géotechnique* 29(1): 47–65.

D'Altri, A.M., S. De Miranda, G. Castellazzi, V. Sarhosis, J. Hudson, and D. Theodossopoulos. 2020. Historic barrel vaults undergoing differential settlements. *International Journal of Architectural Heritage* 14(8): 1196-1209. https://doi.org/10.1080/15583058.2019.1596332.

DeJong, M. J. 2016. Settlement effects on masonry structures. In *SAHC2016: Proceedings of 10th International Conference on Structural Analysis of Historical Constructions*, ed. K. Van Balen and E. Verstrynge. Leiden, The Netherlands: CRC Press.

DeJong, M. J., L. De Lorenzis, S, Adams, and J.A. Ochsendorf. 2008. Rocking Stability of Masonry Arches in Seismic Regions. *Earthquake Spectra* 24(4): 847-65.

Dell'Endice, A., A. Iannuzzo, M. J. DeJong, T. Van Mele, and P. Block. 2021. Modelling imperfections in unreinforced masonry structures: discrete element simulations and scale model experiments of a pavilion vault. *Engineering Structures* 228. https://doi.org/10.1016/j.engstruct.2020.111499.

Di Carlo, F., and S. Coccia. 2020. Collapse state of elliptical masonry arches after finite displacements of the supports. *Engineering Failure Analysis* 114. https://doi.org/10.1016/j.engfailanal.2020.104593.

Di Carlo, F., S. Coccia, and Z. Rinaldi. 2018. Collapse Load of a Masonry Arch after Actual Displacements of the Supports. *Archive of Applied Mechanics* 88(9): 1545–58. https://doi.org/10.1007/s00419-018-1386-6.

Foti, D., V. Vacca, and I. Facchini. 2018. DEM modeling and experimental analysis of the static behavior of a dry-joints masonry cross vaults. *Construction and Building Materials* 170: 111–20. https://doi.org/10.1016/j.conbuildmat.2018.02.202.

Gaetani, A., M. Moroni, P. B. Lourenço, and G. Monti. 2017. Dry-joint arch undergoing windowed sine pulses. *Bulletin of Earthquake Engineering*. 15:4939-61.

Galassi, S., G. Misseri, L. Rovero, and G. Tempesta. 2018. Failure modes prediction of masonry voussoir arches on moving supports. *Engineering Structures* 173: 706–17. https://doi:10.1016/j.engstruct.2018.07.015.

Galassi, S., G. Misseri, L. Rovero, and G. Tempesta. 2020. Analysis of masonry pointed arches on moving supports: a numeric predictive model and experimental evaluations. In *AIMETA 2019: Proceedings of XXIV AIMETA Conference 2019*, ed. A. Carcaterra, A. Paolone and G. Graziani, 1-21. Springer.

Heyman, J. 1966. The Stone Skeleton. *International Journal of Solids and Structures* 2(2): 249–79.

Heyman, J. 1995. *The stone skeleton. Structural engineering of masonry architecture*, Cambridge: Cambridge University Press.

Iannuzzo, A., A. Dell'Endice, T. Van Mele, and P. Block. 2021. Numerical limit analysis-based modelling of masonry structures subjected to large displacements. *Computers and Structures* 242. https://doi.org/10.1016/j.compstruc.2020.106372.

Iannuzzo, A., T. Van Mele, and P. Block. 2020. Piecewise rigid displacement (PRD) method: a limit analysis-based approach to detect mechanisms and internal forces through two dual energy criteria. *Mechanics Research Communications* 107.

Lemos, J. V. 1997. Discrete element modelling of the seismic behavior of stone masonry arches. In: *Proceedings of the 4th International Symposium Computer Methods in Structural Masonry*, ed. J. Middleton and G. Pande. Swansea, UK: Books & Journals International.

Lemos, J. V. 2007. Discrete element modeling of masonry structures. *International Journal of Architectural Heritage* 1(2): 190-213.

Lengyel, G. 2017. Discrete element analysis of gothic masonry vaults for self-weight and horizontal support displacement. *Engineering Structures* 148:195–209. http://dx.doi.org/10.1016/j.engstruct.2017.06.014.

Lengyel, G. and K. Bagi. 2016. Horizontal reaction components of pointed vaults. *International Journal of Masonry Research and Innovation* 1(4): 398–420.

Masciotta, M. G., D. Pellegrini, M. Girardi, C, Padovani, A. Barontini, P.B. Lourenço, D. Brigante, and G. Fabbrocino. 2020. Dynamic characterization of progressively damaged segmental masonry arches with one settled support: experimental and numerical analyses. *Frattura ed Integrità Strutturale* 51: 423-41.

McInerney, J., and M. J. DeJong. 2015. Discrete element modeling of groin vault displacement capacity. *International Journal of Architectural Heritage* 9(8): 1037-49. http://dx.doi.org/10.1080/15583058.2014.923953

Milani, G., M. Rossi, C. Calderini, and S. Lagomarsino. 2016. Tilting plane tests on a small-scale masonry cross vault: experimental results and numerical simulations through a heterogeneous approach. *Engineering Structures* 123: 300-312. http://dx.doi.org/10.1016/j.engstruct.2016.05.017.

Misseri, G., M. J. DeJong, and L. Rovero. 2018. Experimental and numerical investigation of the collapse of pointed masonry arches under quasi-static horizontal loading. *Engineering Structures* 173: 180-90. https://doi.org/10.1016/j.engstruct.2018.06.009.

O'Dwyer, D. 1999. Funicular analysis of masonry vaults. *Computers and Structures* 73: 187–97.

Ochsendorf, J. A. 2002. Collapse of masonry structures. PhD diss., University of Cambridge.

Ochsendorf, J. A. 2006. The masonry arch on spreading supports. Structural Engineer 84(2): 29–35.

Pippard A.J.S. and R. Ashby. 1939. An experimental study of the voussoir arch. *Journal of the Institution of Civil Engineers* 10(3): 383-404.

Portioli, F., and L. Cascini. 2017. Large displacement analysis of dry-jointed masonry structures subjected to settlements using rigid block modelling. *Engineering Structures* 148: 485–96.

Quinonez, A., J. Zessin, A. Nutzel, and J. A. Ochsendorf. 2010. Small-scale models for testing masonry structures. *Advanced Materials Research* 133-134: 497–502.

Roca, P., M. Cervera, G. Gariup, and L. Pelà. 2010. Structural analysis of masonry historical constructions. classical and advanced approaches. *Archives of Computational Methods in Engineering* 17(3): 299–325.

Romano, A. 2005. Modelling, analysis and testing of masonry structures. PhD diss., University of Naples Federico II.

Romano, A., and J. A.Ochsendorf. 2010. The mechanics of gothic masonry arches. *International Journal of Architectural Heritage* 4(1): 59–82. http://dx.doi.org/10.1080/15583050902914660

Rossi, M., C. Calderini, and S. Lagomarsino. 2016. Experimental testing of the seismic in-plane displacement capacity of masonry cross vaults through a scale model. *Bulletin of Earthquake Engineering* 14(1): 261–81.

Rossi, M., C. Calvo Barentin, T. Van Mele, and P. Block. 2017. Experimental study on the behaviour of masonry pavilion vaults on spreading supports. *Structures* 11: 110-20. http://dx.doi.org/10.1016/j.istruc.2017.04.008.

Shapiro, E.E. 2012. Collapse mechanisms of small-scale unreinforced masonry vaults. Master thesis, Massachusetts Institute of Technology.

Smars, P. 2000. Sur La Stabilité Des arcs et voutes. PhD diss., Catholic University of Leuven.

Smars, P. 2010. Kinematic stability of masonry arches. *Advanced Materials Research* 133–134: 429-34.

Theodossopoulos D. 2001. Structural behaviour of historic masonry cross vaults. PhD diss., University of Edinburgh.

Theodossopoulos, D., B. P. Sinha, A. S. Usmani, and A. J. Macdonald. 2002. Assessment of the structural response of masonry cross vaults. *Strain* 38(3): 119–27.

Torres, B., E. Bertolesi, P. A. Calderón, J. J. Moragues, and J. M. Adam. 2019a. Experimental investigation of a full-scale timbrel masonry cross vault subjected to vertical settlement. *Construction and Building Materials* 221: 421–32. https://doi.org/10.1016/j.conbuildmat.2019.06.015.

Torres, B., E. Bertolesi, P. A. Calderón, J. J. Moragues, and J. M. Adam. 2019b. A full-scale timbrel cross vault subjected to vertical cyclical displacements in one of its supports. *Engineering Structures* 183: 791-804. https://doi.org/10.1016/j.engstruct.2019.01.054.

Tralli, A., A. Chiozzi, N. Grillanda, and G. Milani. 2020. Masonry structures in the presence of foundation settlements and unilateral contact problems. *International Journal of Solids and Structures* 191-192: 187–201.

Van Mele, T., J. McInerney, M. J. DeJong, and P. Block. 2012. Physical and computational discrete modelling of masonry vault collapse. In *SAHC2012: Proceedings of 8th International Conference on Structural Analysis of Historical Constructions*, ed. J. Jasienko, 2552–2560. Dolnośląskie Wydawnictwo Edukacyjne.

Verstrynge, E, L. Schueremans, P. Smars, and D. Van Gemert. 2007. Design and testing of masonry arches: a project of bachelor students in civil engineering. In *ARCH'07: Proceedings of the International Conference on Arch Bridges 351-358,* ed. P. B. Lourenço, D. V. Oliveira and A. Portela. Guimarães: University of Minho, Department of Civil Engineering.

Zampieri, P., F. Faleschini, M. A. Zanini, and N. Simoncello. 2018a. Collapse mechanisms of masonry arches with settled springing. *Engineering Structures* 156: 363–74. doi:10.1016/j. engstruct.2017.11.048.

Zampieri, P., M. Amoroso, and C. Pellegrino. 2019. The masonry buttressed arch on spreading support. *Structures* 20: 226–36. https://doi.org/10.1016/j.istruc.2019.03.008.

Zampieri, P., N. Cavalagli, V. Gusella, and C. Pellegrino. 2018c. Collapse displacements of masonry arch with geometrical uncertainties on spreading supports. *Computers and Structures* 208: 118–29. https://doi.org/10.1016/j.compstruc.2018.07.001.

Zampieri, P., N. Simoncello, and C. Pellegrino. 2018b. Structural behaviour of masonry arch with no-horizontal springing settlement. *Frattura ed Integrità Strutturale* 12(43): 182–90.

Zessin, J., W. Lau, and J. A. Ochsendorf. 2010. Equilibrium of Cracked Masonry Domes. *Proceedings of the Institution of Civil Engineers: Engineering and Computational Mechanics* 163(EM3): 135–45.

CHAPTER 4

NUMERICAL PREDICTIONS FOR A RIGID-NO TENSION ARCH

4.1. INTRODUCTION

As explained in Chapter 1, the methodology proposed in the research to investigate the response of masonry arches to inclined support displacements included both experimental and numerical analyses on a segmental small-scale dry-joint masonry arch. Prior to performing the experimental tests, some numerical simulations were carried out for the preliminary assessment of the arch behaviour when subjected to different combinations of horizontal and vertical support displacements. Since the response of masonry arches to inclined support displacements has never been systematically investigated in the literature (see Chapter 3), these analyses were aimed at identifying the expected collapse mechanisms and determining the corresponding ultimate displacement capacity. These information were essential for the design of the experimental set-up.

The arch behaviour was analysed in the framework of large displacements using, to improve the robustness of the results, two different numerical approaches, namely finite element (FE) modelling and rigid block (RB) modelling (Section 4.2). Both approaches were based on a micro-modelling strategy, in which the arch was discretized as an assemblage of voussoirs, very stiff and infinitely resistant in compression in the FEM and rigid in the RBM, interacting at no-tension friction interfaces. The choice to adopt this modelling strategy was based on two main reasons: on one hand, it complied with Heymans' assumptions on the behaviour of the masonry material, and on other hand it was particular suitable to simulate the response of the small-scale arch tested in the experiments. Indeed, each block of the numerical models represented a voussoir of the mock-up, and the no-tension friction interfaces simulated the dry-joints.

The adopted numerical approaches were first validated against experimental results from literature (Section 4.3) and were then used to investigate the response of the segmental arch under study to different configurations of support displacements (Section 4.4). The effect of the displacement direction on the arch performance was evaluated in terms of initial hinge position, collapse mechanism, support reaction-displacements curves as well as ultimate displacement capacity and support reactions at collapse. The sensitivity of the results to the number of voussoirs was also investigated (Section 4.5).

This chapter is based on Ferrero et al. (2021b)

4.2. NUMERICAL MODELLING

This section presents the two numerical approaches, based on a micro-modelling strategy (Figure 4-1), used in this thesis to investigate the response of dry-joint masonry arches to large support movements. FE and RB models were prepared for the small-scale arches tested in the literature and used for validation (Section 4.3) as well as for the segmental arch investigated in this research (Section 4.4). In all the arches analysed, one support was fixed, while the other was subjected to an imposed displacement δ, whose direction was identified with the angle α measured from the vertical (Figure 4-1). The horizontal and vertical components of the imposed displacement δ, indicated respectively as δ_x and δ_z (Figure 4-1), were expressed in a dimensionless form as span increase δ_x/L and deflection ratio δ_z/L, where L is the span length of the arch (Figure 4-1).

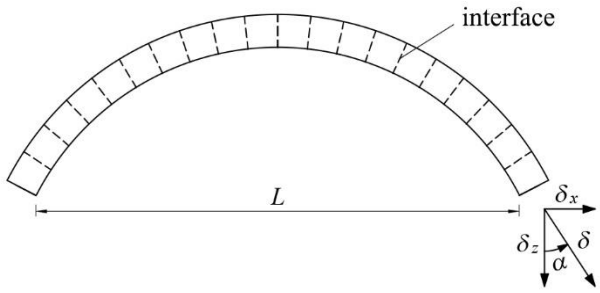

Figure 4-1 Micro-modelling strategy and application of support displacements.

4.2.1. Finite element modelling

FE analyses were performed using the commercial FEM software DIANA (DIANA FEA BV 2017). Two-dimensional FE models of the arches to be investigated were created through Midas FX+ Version 3.3.0 Customized Pre/Post-processor for DIANA software (Midas IT 2013). According to the micro-modelling approach adopted in this work, arches were discretized as assemblies of very stiff voussoirs connected by no-tension friction interfaces (Figure 4-2). Further interface elements were placed at the springing to allow for hinge opening at the supports. The outer edges of these interface elements were pinned to provide boundary conditions (Figure 4-2).

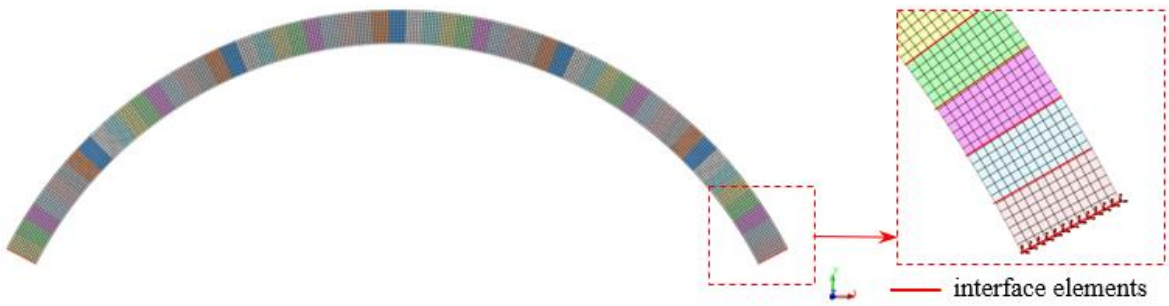

Figure 4-2 FE micro-modelling.

The voussoirs were modelled as linear elastic elements with infinite compressive strength, whereas all the nonlinearity was concentrated in the interfaces. A Coulomb friction model (Figure 4-3) with cohesion and dilatancy angle equal to zero was adopted for interface elements, even if no sliding between blocks was expected. With the aim of simulating the opening of hinges occurring in masonry arches, the friction criterion was extended with a gap criterion with zero tensile strength so that a gap opened as tensile stresses arose. For further details about the Coulomb friction model, the reader is referred to DIANA FEA BV (2017).

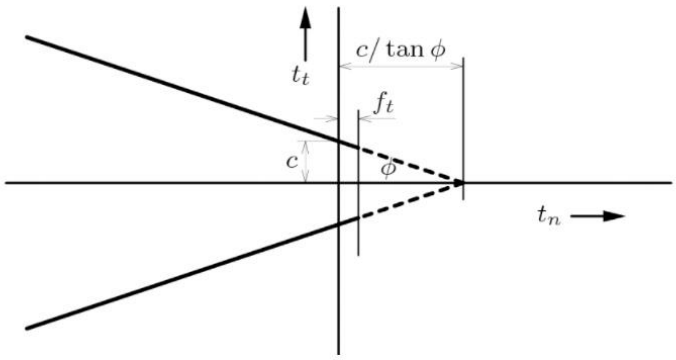

Figure 4-3 Coulomb friction criterion adopted in the FE model (DIANA FEA BV 2017).

The values of Young's modulus, Poisson's ratio and unit weight adopted for the voussoirs as well as the friction angle assumed for the interfaces were derived from literature or measured experimentally (further details are provided in Sections 4.3 and 4.4.1). The interface stiffness was determined by means of a sensitivity analysis aimed at evaluating its effect on the predicted arch response. As indeed described in Lourenço et al. (2010) and Gaetani et al. (2017), this parameter can significantly affect the results of numerical simulations when dealing with masonry arches. For the purposes of this work, it was essential to guarantee that, for the adopted values of interface stiffness, arches behaved as assemblies of rigid blocks deforming only by opening hinges.

The mesh of the FE models was generated adopting four-node quadrilateral isoparametric plane stress elements (Q8MEM, DIANA FEA BV 2017) for the voussoirs and 2D four-node line interface elements (L8IF, DIANA FEA BV 2017) for the interfaces.

The response of the arches to large support displacements was assessed by means of nonlinear static analyses. Self-weight was firstly applied, then support displacements were increased monotonically up to collapse. A regular Newton-Raphson iteration method in combination with a line search algorithm was adopted. In order to check convergence, an energy-based convergence criterion with a tolerance value of 0.001 was assumed. Since large displacements were involved, numerical analyses were performed considering geometric nonlinearities. To this end, the Total Lagrange formulation available in DIANA software (DIANA FEA BV 2017) was adopted.

4.2.2. Rigid block modelling

The adopted rigid block modelling approach relies on a formulation based on mathematical programming which was implemented in an in-house MATLAB code (Portioli and Cascini 2017). The developed model is herein extended to include the effects of inclined support movements.

The model is used for the analysis of the limit equilibrium conditions which are associated to an imposed support movement and to different geometric configurations of the structural system when large displacements are considered. With this regard, it is worth noting that the implemented modelling approach is based on a pure static formulation, i.e. the equilibrium conditions are expressed in terms of static forces, with no need to introduce inertia effects for the analysis of the failure mechanisms, as it is for most of discrete element models.

The arches are modelled as assemblages of rigid blocks *i* interacting at no-tension, frictional contact interfaces *j* (Figure 4-4). The block *i* is subjected to vertical dead loads $f_{Di} = \rho V_i$, where ρ is the unit weight and V_i the volume of the block. The blocks interact at contact points *k* which are located at the vertices of each contact surface *j* with shear and normal force components t_k and n_k (Figure 4-5a). The positions and displacements at block centroid are collected in the vectors $\boldsymbol{x_i} = [x_i \quad z_i \quad \omega_i\,]^{\mathrm{T}}$ and $\boldsymbol{\Delta x_i} = [\Delta x_i \quad \Delta z_i \quad \Delta\omega_i\,]^{\mathrm{T}}$, respectively. The displacement rates at contact points are collected in vectors $\boldsymbol{\Delta u_k} = [\Delta u_{tk} \quad \Delta u_{nk}\,]^{\mathrm{T}}$ (Figure 4-5b).

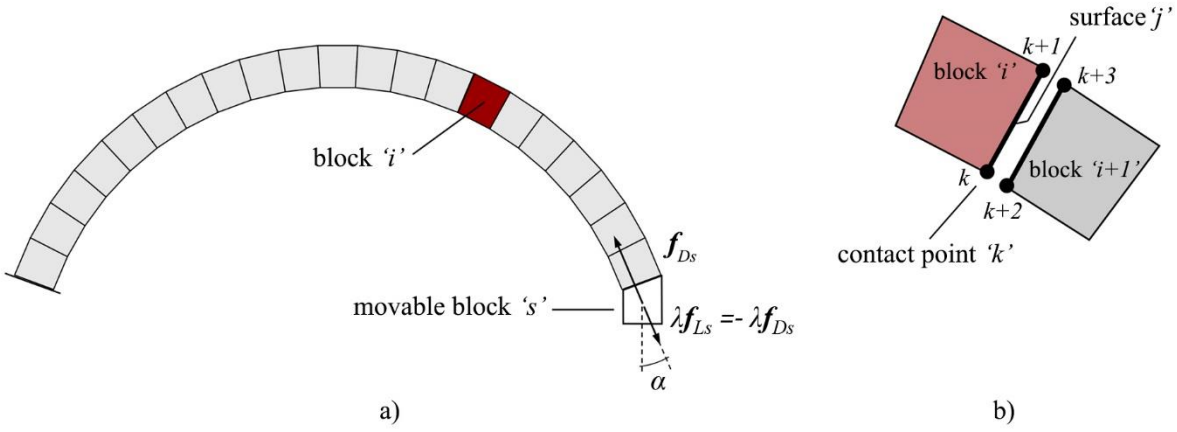

Figure 4-4 a) Rigid block model of a circular arch subjected to support displacements; b) Rigid block *i*, surface *j* and contact point *k*.

A movable block *s* is also used to model the moving support, with a single *dof* associated to the direction of the imposed displacement δ (e.g. the inclined direction with angle α in Figure 4-4a). Following classic formulations of limit equilibrium analysis, the inclined load f_s applied at this block - which is work conjugated to the imposed displacement δ - is expressed as the sum of the constant dead load f_{Ds} and the live load $\lambda f_{Ls} = -\lambda f_{Ds}$, where λ is the unknown collapse load multiplier. As such, the inclined load at the support block can be expressed as follows: $f_s = (1-\lambda) f_{Ds}$.

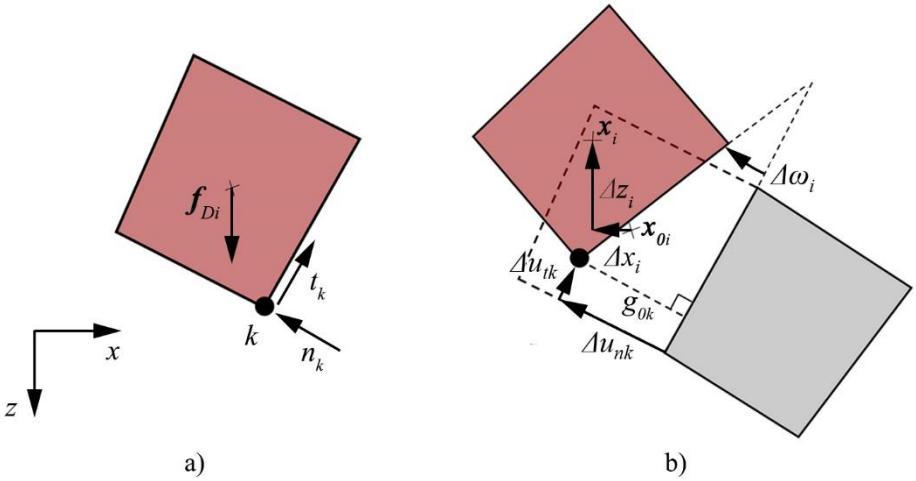

Figure 4-5 a) Dead loads and contact forces at block *i* and b) kinematic variables and normal gap g_{0k} at block centroid *i* and contact point *k*.

The arch response to support movements is analysed in the large displacement regime by using an incremental solution procedure that is divided into displacement increments.

At each displacement increment, a force-based optimization problem and its dual displacement-based problem are solved, which are analogous to the classic lower and upper bound problems of limit analysis (Ferris and Tin-Loi 2001; Portioli and Cascini 2017).

The force-based optimization problem is expressed as follows:

$$\begin{aligned} &\max \quad \lambda - \boldsymbol{g_0}^{\mathrm{T}}\boldsymbol{c} \\ &\text{s.t.} \quad \boldsymbol{A_0 c} = \boldsymbol{f_D} + \lambda \boldsymbol{f_L} \\ &\qquad \boldsymbol{Y}^{\mathrm{T}}\boldsymbol{c} \leq \boldsymbol{0} \end{aligned} \tag{1}$$

where:

$\boldsymbol{c}$ is the ($2c \times 1$) vector of the unknown internal forces at interfaces, being *c* the number of contact points, which collects subvectors $\boldsymbol{c_k} = [t_k \quad n_k]^{\mathrm{T}}$;

$\boldsymbol{g_0}$ is the ($2c \times 1$) vector collecting the gaps between contact point *k* and related surfaces in subvectors $[0 \quad g_{0k}]$;

$\boldsymbol{f_D}$ is the ($3b+1 \times 1$) vector of dead loads applied at the centroid of the blocks, being *b* the number of the blocks of the arch. $\boldsymbol{f_D}$ collects the subvectors $\boldsymbol{f_{Di}} = [0 \quad f_{Di} \quad 0]^{\mathrm{T}}$ and the dead load component at the support block, f_{Ds};

$\boldsymbol{f_L}$ is the vector of live loads, which also contains the live load component at the support block, f_{Ls};

$\boldsymbol{A_0}$ is the ($3b+1 \times 2c$) equilibrium matrix, with coefficients determined by the position of contact points and geometry of rigid blocks;

$\boldsymbol{Y}^{\mathrm{T}}$ is the ($3c \times 2c$) matrix of failure conditions corresponding to sliding and opening failure at contact points.

In Eq. (1) the first and second constraints represent the equilibrium and failure conditions governing the force-based problem, respectively.

The solution procedure is organized as follows. For a given configuration $\boldsymbol{x_0}$, with initial gaps $\boldsymbol{g_0}$, the force-based optimization problem defined in (1) is solved to obtain the contact forces $\boldsymbol{c}$ and the collapse load multiplier λ. The kinematic variables $\boldsymbol{\Delta x}$ and $\boldsymbol{\Delta u}$ are obtained from the solution of the dual displacement-based problem, which is directly derived from Lagrange multipliers associated to the solution of the force-based problem. A new optimization problem is then formulated and solved on the basis of new block positions $\boldsymbol{x} = \boldsymbol{x_0} + \boldsymbol{\Delta x}$ and contact gaps $\boldsymbol{g}$.

4.3. VALIDATION AGAINST EXPERIMENTAL TESTS

The two modelling approaches adopted in this work were validated against the experimental tests on small-scale models performed by Ochsendorf (2002, 2006). In Ochsendorf (2002, 2006), the stability of two dry-joint masonry arches (circular and segmental) on horizontal spreading supports was investigated. Both arches were made of 16 voussoirs cast as concrete blocks and measured 50 mm in radial thickness. The circular arch had a mean radius of 220 mm and a span length of 390 mm, whereas the segmental arch had a mean radius of 385 mm and a span length of 709 mm.

FE and RB models were prepared for both arches. In the FE models, a mesh with 12 elements along the radial thickness was adopted. Spreading supports were simulated by imposing an increasing outward purely horizontal displacement δ_x at the right abutment. The unit weight of the voussoirs (25.0 kN/m^3) as well as the friction coefficient of the interfaces (0.7) were taken from Ochsendorf (2002, 2006). Since the voussoirs of the experimental tests were made of concrete, the Young's modulus and Poisson's ratio of the blocks of the FE models were set equal to 30 GPa and 0.2, respectively.

The normal stiffness k_n of the interface elements used in the FE models was determined by means of a sensitivity analysis, where k_n was varied between 0.1 and 100 N/mm^3 according to the values proposed in Gaetani et al. (2017). The interface tangential stiffness k_s was set equal to $0.5k_n$ for any considered value of k_n. This choice was made only to optimize numerical convergence, as the ratio between the two stiffnesses did not affect the structural response of the considered arches.

The effect of k_n on the arch response was evaluated in terms of ultimate displacement capacity, expressed as span increase at collapse $\delta_{x,u}/L$, and collapse mechanism. Figure 4-6 shows the variation in the span increase at collapse $\delta_{x,u}/L$ with the interface normal stiffness k_n for the circular and segmental arches. The results obtained from Ochsendorf's experimental tests and RB models are also reported.

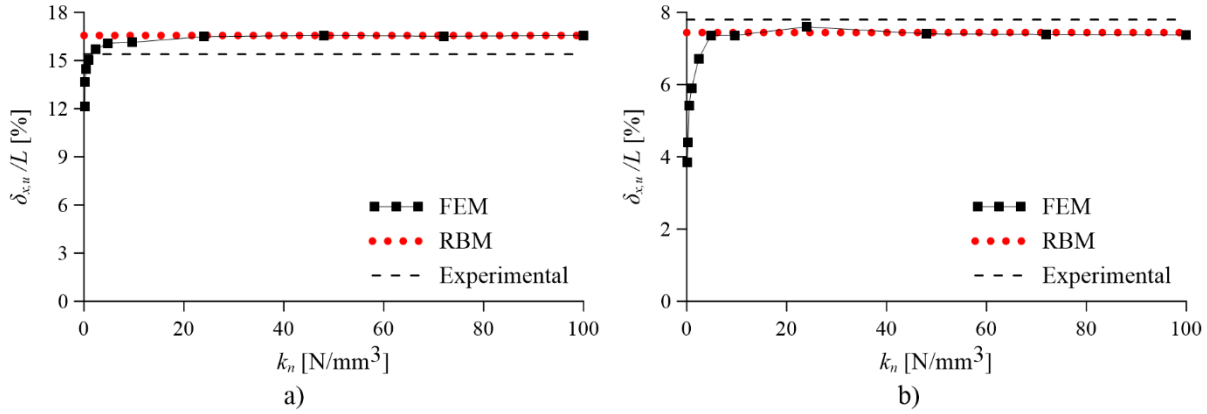

Figure 4-6 – Comparison between the experimental results by Ochsendorf (2002, 2006) and the numerical results obtained from FE analyses (presented in terms of span increase at collapse $\delta_{x,u}/L$ vs. interface normal stiffness k_n) and RB analyses: a) circular arch, b) segmental arch.

For both arches, the span increase at collapse $\delta_{x,u}/L$ increases with interface stiffness k_n until converging to a maximum constant value that is not affected by any further stiffness increase. This behaviour can be explained considering that small values of k_n result in large interpenetration between the voussoirs, as shown by compressive stresses being distributed over several FEs (Figure 4-7a). Under these conditions, as already described by Gaetani et al. (2017), hinges do not appear at the intrados or extrados of the arch but move inward, with the result that the effective thickness of the arch is reduced, and the displacement capacity is smaller. Conversely, large values of k_n significantly reduce the voussoir interpenetration and lead hinges to occur at the edge line of the arch, as shown by compressive stresses acting in only one out of the twelve FEs composing the interface (Figure 4-7b). This behaviour better simulates the response of rigid-no tension structures, as also demonstrated by the almost perfect agreement obtained between FE and RB results for large values of k_n (Figure 4-6). For these reasons, a reference value of 48 N/mm^3, falling approximately at the middle of the plateau region of the curve of the span increase at collapse $\delta_{x,u}/L$ versus interface normal stiffness k_n, was adopted for k_n in the FE simulations. The interface tangential stiffness k_s was set equal to 24 N/mm^3.

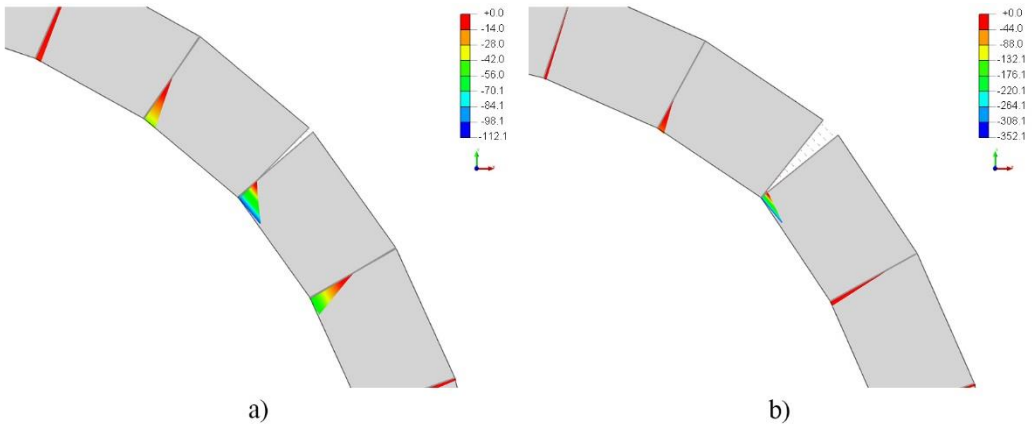

Figure 4-7 - Hinge opening in the FE model for: a) k_n = 0.1 N/mm^3 and b) k_n = 48 N/mm^3 (results shown in terms of compressive stresses in the interfaces).

The values of span increase at collapse $\delta_{x,u}/L$ obtained from the FE and RB models for both the circular and segmental arches are summarized and compared with the experimental results by Ochsendorf in Table 6. Results from the analytical and numerical formulations proposed in Ochsendorf (2002, 2006), Galassi et al. (2018) and Coccia et al. (2015) are also reported for comparison. For both the FE and RB models, the relative error between numerical and experimental results in terms of collapse displacement is lower than 8% for both the circular and segmental arches. Note that the relative error is computed as the ratio of the difference between the span increase at collapse obtained numerically and that obtained experimentally over the experimental one.

Table 6 Comparison in terms of span increase at collapse $\delta_{x,u}/L$ (in %) and relative error (in %) between the experimental results by Ochsendorf (2002, 2006) and the analytical/numerical results from FEM, RBM and by other authors (Coccia et al. 2015; Galassi et al. 2018; Ochsendorf 2002, 2006).

	Exp	Analytical/Numerical									
	$\delta_{x,u}/L^{(1)}$	$\delta_{x,u}/L$ (FEM)	Rel. Err.	$\delta_{x,u}/L$ (RBM)	Rel. Err.	$\delta_{x,u}/L^{(1)}$	Rel. Err.	$\delta_{x,u}/L^{(2)}$	Rel. Err.	$\delta_{x,u}/L^{(3)}$	Rel. Err.
Circular	15.4	16.6	7.79	16.6	7.79	16.9	9.74	16.59	7.73	16.53	7.34
Segmental	7.8	7.4	-5.13	7.4	-5.13	8.8	12.82	6.94	-11.03	-	-

(1) Ochsendorf (2002, 2006); (2) Galassi et al. (2018); (3) Coccia et al. (2015).

The collapse mechanisms obtained from the FE and RB models for the circular arch on spreading supports are presented in Figure 4-8. As observed in the experimental test (Ochsendorf 2002, 2006), as soon as the supports spread apart, three hinges (A, B and C) are formed. The initial position of these three hinges (indicated as A_0, B_0 and C_0 in Figure 4-8) is the same as that of Ochsendorf's arch: one hinge appears at mid-span at the extrados and two hinges occur at the interfaces between 3rd and 4th voussoirs at the intrados. In full accordance with the experimental tests, hinges do not move for further spreading of the supports, with the result that their position at collapse (indicated as A_u, B_u and C_u) coincides with the initial one (A_0, B_0 and C_0). In both the FE and RB models, a symmetrical five-hinge collapse mechanism is predicted to occur when two further hinges (D and E) open at the supports at the extrados (Figure 4-8). In the experimental test, the not perfect symmetry of the physical model caused the arch to collapse by a four-hinge mechanism (Ochsendorf 2002, 2006).

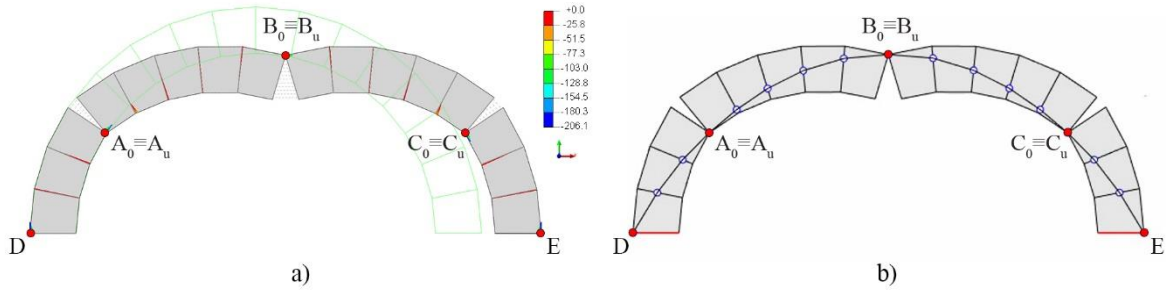

Figure 4-8 – Collapse mechanisms for Ochsendorf's circular arch: a) FE model ($\delta_{x,u}/L$ = 16.6 %) and b) RB model ($\delta_{x,u}/L$ = 16.6 %) (initial and final hinge locations of hinges A, B and C are indicated as A_0, B_0, C_0 and A_u, B_u, C_u, respectively).

The results obtained for the segmental arch in terms of collapse mechanisms and evolution of the hinge configuration with increasing support displacements are presented in Figure 4-9 for both the FE and RB models. Also in this case, the initial and final locations of the three initial hinges A, B and C are indicated as A_0, B_0 and C_0 and A_u, B_u and C_u, respectively.

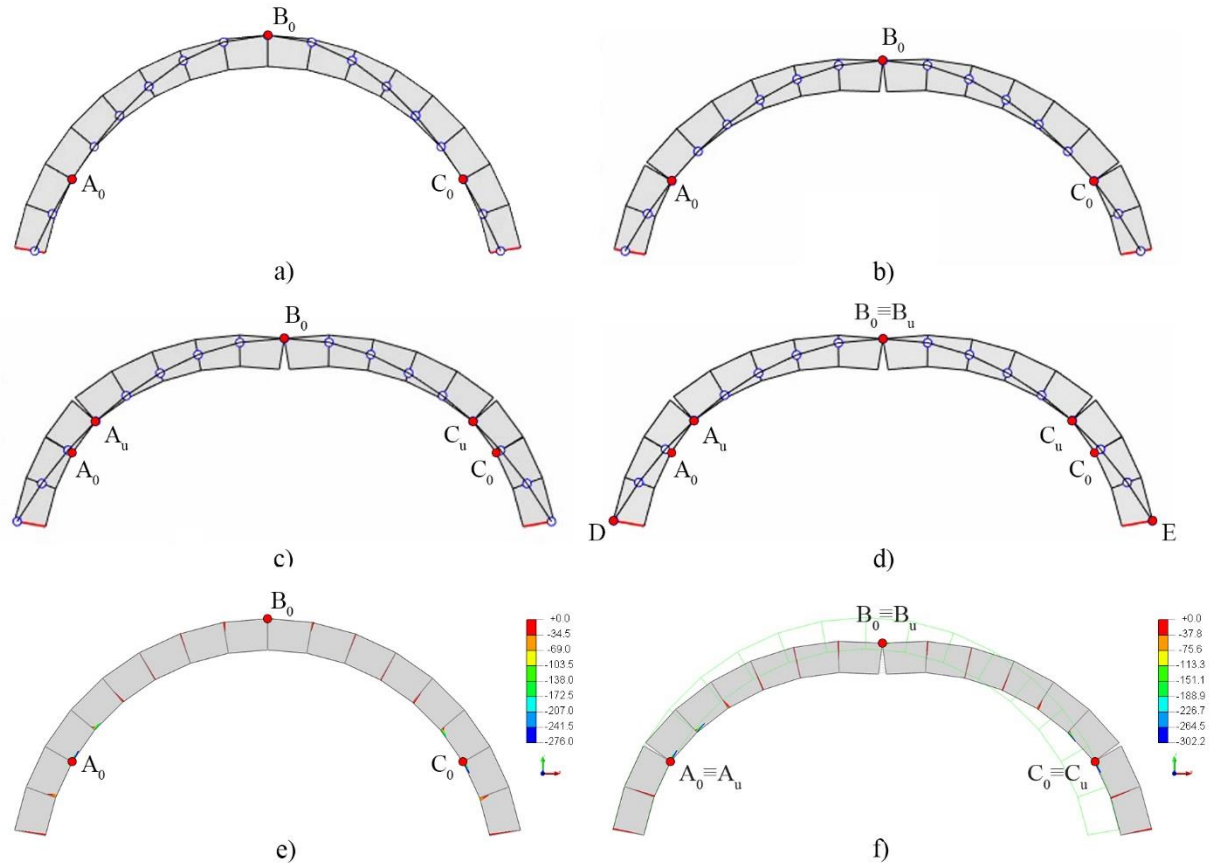

Figure 4-9 – Evolution of the hinge configuration for Ochsendorf's segmental arch. RB model: a) initial hinge configuration, b) hinge configuration before the intrados hinge movement (δ_x/L = 7.0%), c) hinge configuration after the intrados hinge movement (δ_x/L = 7.4%), d) collapse ($\delta_{x,u}/L$ = 7.4%). FE model: e) initial hinge configuration, bf) last convergent configuration (δ_x/L = 7.4 %).

The RB predictions are in very good agreement with the experimental results. As observed in Ochsendorf's physical model, as soon as the supports move apart, three hinges initially appear, hinge B being located at mid-span at the extrados, and hinges A and C occurring at the intrados between 2nd and 3rd voussoirs (Figure 4-9a). In full agreement with the experimental tests, the intrados hinges A and C move towards the crown by one voussoir before collapse is reached. Figure 4-9b and Figure 4-9c show the kinematic configuration of the arch just before and after the hinge movement, respectively. Collapse occurs by a symmetrical five-hinge mechanism when hinges D and E appear at the supports (Figure 4-9d). In the case of the experimental tests, as already described for the circular arch, failure was governed by a four-hinge collapse mechanism. It is worth noting that in the RB model both the hinge movement (Figure 7c) and collapse (Figure 7d) occur for the same span increase (δ_x/L = 7.4%), indicating that failure is triggered by the change in the position of hinges A and C.

The FE model predicts the same results as obtained from both the experimental tests and the RB model in terms of initial hinge configuration (Figure 4-9e), but not in terms of final hinge configuration, as no hinges appear at the supports at the last convergent step of the FE analysis (Figure 4-9f). Furthermore, the intrados hinges A and C do not move from their initial positions as the supports spread. Nevertheless, the ultimate span increase predicted by the FE model (Figure 4-9f) is equal to that obtained at collapse from the RB model ($\delta_{x,u}/L$ = 7.4%). Since no further span increase occurs in the RB model after the movement of the intrados hinges, it is likely that the FE analysis will stop just before hinges move and collapse occurs. In confirmation of this, it is noted that two additional hinges are developing at the interfaces between 3rd and 4th voussoir at the last convergence step of the FE analysis, as shown by compressive stresses being concentrated in one single FE (Figure 4-9f).

Figure 4-10 shows the curves of the horizontal support reaction R_x versus the span increase δ_x/L obtained from FE analyses and RB analyses for both the circular and segmental arches. The span increase at collapse $\delta_{x,u}/L$ obtained from Ochsendorf's experimental tests is also reported for comparison. The results obtained from the two models are in very good agreement. In both models, the horizontal support reaction R_x increases significantly as the right support moves due to the progressive changes in the arch geometry. The initial slight decrease in the horizontal reaction obtained from the FE analyses is due to elasticity of the FE models as well as to the gradual opening of the three initial hinges A, B and C. As soon as these hinges have fully formed (Figure 4-10a-b), the curves of the FE and RB models become superimposed for both arches. In the RB models, which are perfectly rigid, hinges appear as soon as the supports move.

In the case of the segmental arch (Figure 4-10b), in the RB model, the horizontal reaction R_x increases sharply with constant span increase just before collapse. This discontinuity in the reaction increase, already observed by Ochsendorf (2002, 2006), is due to the abrupt change in the arch geometry produced by the movement of the intrados hinges A and C. In the case of the FE model, the horizontal reaction does not exhibit any jump and reaches a maximum value approximately equal to that obtained in the RB model before the change in the location of the intrados hinges. This confirms that the FE analysis stops just before hinges A and C move triggering the collapse. For this reason, no hinges are observed at the supports in the FE model (Figure 4-9f).

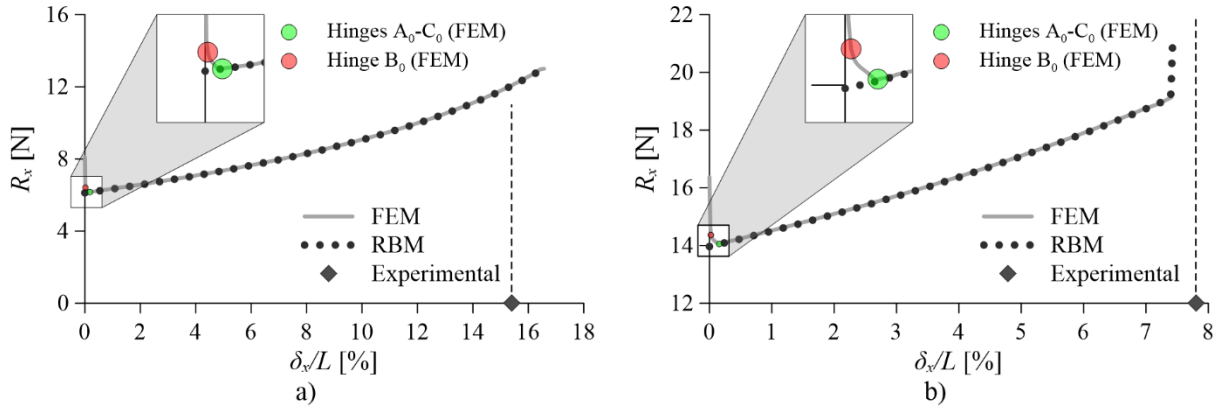

Figure 4-10 – Curves horizontal reaction R_x vs. span increase δ_x/L obtained from the FE and RB analyses for a) the circular arch and b) the segmental arch.

4.4. NUMERICAL CASE STUDY

This section focuses on the segmental dry-joint masonry arch chosen as case study in this thesis.

4.4.1. Geometry and material properties

Figure 4-11 shows the geometry of the arch under consideration, which has an angle of embrace of 125°, an internal radius of 300 mm, a span length of 533 mm and a thickness of 120 mm. The arch is composed of 55 slightly trapezoidal voussoirs with a height of 24 mm and a width of about 12 mm. Further details about the choice of the geometry and voussoirs' discretization are provided in Chapter 5.

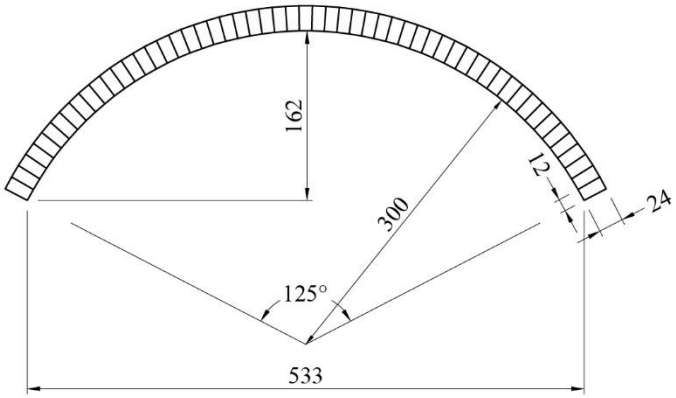

Figure 4-11 – Geometry of the considered segmental arch (dimensions in mm).

A FE model and a RB model were prepared for the considered segmental arch. The mesh discretization to be adopted in the FE model was selected based on a mesh sensitivity analysis, where the effects of the mesh size on the response of the arch to an increasing purely vertical displacement δ_z of one support were evaluated. The results of this study are presented in Table 7 in terms of deflection ratio at collapse $\delta_{z,u}/L$ and computational time. Given that almost the same displacement capacity was obtained for every mesh size considered, a mesh size of 2 mm (i.e. 12 FEs along the radial thickness) was adopted. This latter mesh was considered sufficiently fine to simulate the ideal occurrence of hinges at the edge line of the arch without, however, resulting in excessively long computational time.

Table 7 Mesh sensitivity analysis (selected mesh size highlighted in bold).

Mesh size [mm]	Nr. of elements along the radial thickness	Deflection ratio at collapse, $\delta_{z,u}/L$ [%]	CPU time*	Computational time* [min]
4	6	21.2	61.97	≈ 3
3	8	21.2	346.05	≈ 12
2	**12**	**21.1**	**1019.86**	**≈ 24**
1	24	21.1	3998.23	≈ 52

* Intel® Core™ i7-8086K (4.00 GHz), RAM 32 GB, SSD disk

In both the FE and RB models, unit weight and friction coefficient were respectively set equal to 15.4 kN/m^3 and 0.7, in accordance with the values measured experimentally for the physical models to be tested.

In the case of the FE model, a Young's modulus of 590 MPa (measured experimentally) and a Poisson's ratio of 0.2 were adopted for the voussoirs. For the interface elements, cohesion, dilatancy angle and tensile strength were set equal to zero (see Section 4.2.1 for further details about the modelling of interface elements). The interface normal stiffness k_n was determined by means of a sensitivity analysis on the response of the arch to the application of an increasing vertical displacement δ_z at the right support. As already done in the simulation of Ochsendorf's experimental tests (see Section 4.3), the interface normal stiffness k_n was varied between 0.1 and 100 N/mm^3, and the ratio between normal and tangential stiffness was set equal to 2. The results of this study are presented in Figure 4-12 in terms of deflection ratio at collapse $\delta_{z,u}/L$. As already observed in Section 4.3, the deflection ratio at collapse $\delta_{z,u}/L$ increases as the interface normal stiffness k_n increases, until converging to a maximum constant value that is not affected by further stiffness increase. On the basis of these results, the interface normal stiffness k_n was set again equal to 48 N/mm^3 (circle in Figure 4-12).

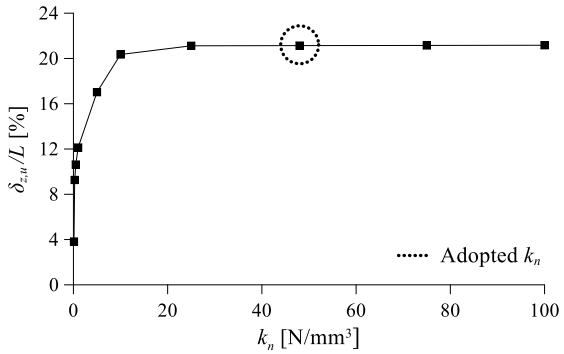

Figure 4-12 – FE model: deflection ratio $\delta_{z,u}/L$ at collapse vs. interface normal stiffness k_n.

4.4.2. Numerical analyses

With the aim of investigating the response of the arch to inclined support displacements, the angle α, which identifies the direction of the applied displacement δ (Figure 4-1) was varied between 0° and 90° at increasing steps of 5°. Note that α = 0° and α = 90° correspond to purely vertical and horizontal displacements δ_z and δ_x, respectively. In the case of FE analyses, the effect of inclined displacements was evaluated only for values of α ranging between 5° and 45°. However, as described further below, the conclusions drawn for values of α between 30° and 45° can be extended to any angle between 50° and 85°.

In the following sections, the results obtained from FE and RB analyses in terms of evolution of the hinge configuration from the opening of the three initial hinges to collapse, support reaction-displacements curves and limit displacement domain are presented.

Initial hinge configuration

For every value of α, as soon as the right support moves, three hinges (named A, B and C) open in both the FE and RB models. Their initial locations are indicated as A_0, B_0 and C_0 in Figure 4-13. The initial hinge

configuration varies with the angle α. In both models, for α between 0° and 25°, hinges A, B and C appear in the sequence I-E-E (from left to right, where E = extrados; I = intrados) (Figure 4-13a, for α equal to 0°). Hinge A is located at the intrados at the haunches, whereas the consecutive hinges B and C appear at the extrados, respectively close to the crown and at the right support. It is worth noting that the occurrence of two consecutive hinges at the extrados (or intrados) is generally observed only in arches with moving supports, since arches subjected to point or seismic loads exhibit hinges located alternately between the intrados and extrados (Galassi et al. 2018; Zampieri et al. 2018a).

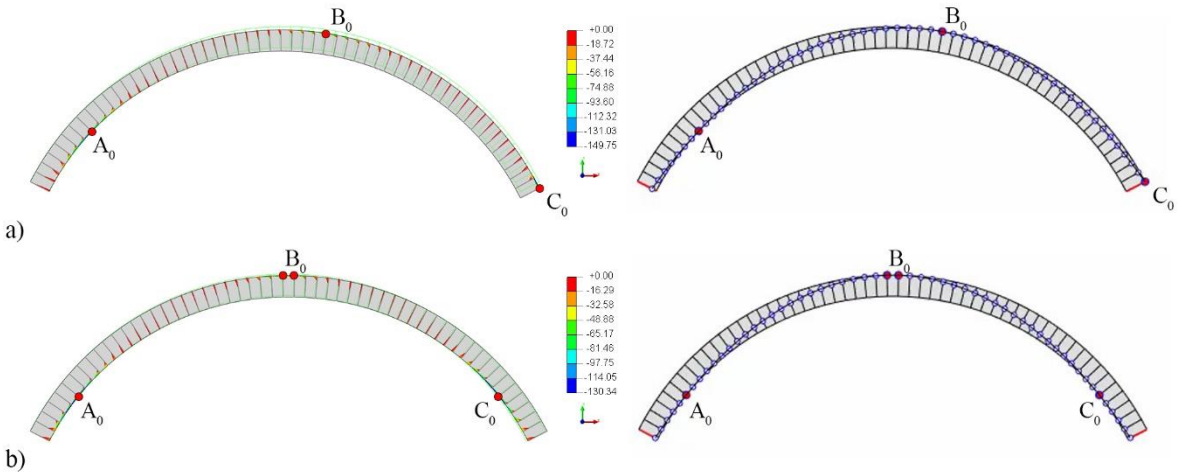

Figure 4-13 – Initial hinge configuration obtained from the FE model (left, results presented in terms of compressive stresses in the interfaces) and RB model (right): a) sequence I-E-E (α = 0°) , b) sequence I-E-I (α = 90°).

For α equal or larger than 30°, hinges A, B and C are located alternately between the intrados and extrados (sequence I-E-I) (Figure 4-13b, for α equal to 90°). Hinges A and C occur at the haunches at the intrados, while hinge B is located near the crown at the extrados. Note that the two extrados hinges opening at mid-span at the two sides of the keystone can be considered as a single hinge (hinge B), as they occur in consecutive interfaces.

Evolution of the hinge configuration and collapse mechanisms

Figure 4-14 presents the collapse mechanisms obtained from FE and RB analyses for some representative values of α. For hinges A, B and C, both the initial (A_0, B_0 and C_0) and final locations at collapse (A_u, B_u and C_u) are reported. In both FE and RB models, for α between 0° and 45°, collapse occurs by an asymmetrical four-hinge mechanism when a fourth hinge (hinge D) opens at the left support at the extrados (Figure 4-14a-b-c-d-e). In the case of α equal to 90° (Figure 4-14f), failure is governed by a five-hinge mechanism due to the symmetry in geometry and loading conditions. The collapse configuration predicted from the FE analyses is perfectly symmetrical (Figure 4-14f on the left), whereas a slight asymmetry is obtained from the RB analyses (Figure 4-14f on the right), since one of the two extrados hinges observed at mid-span in the initial hinge configuration (Figure 4-13b on the right) closes for larger support displacements.

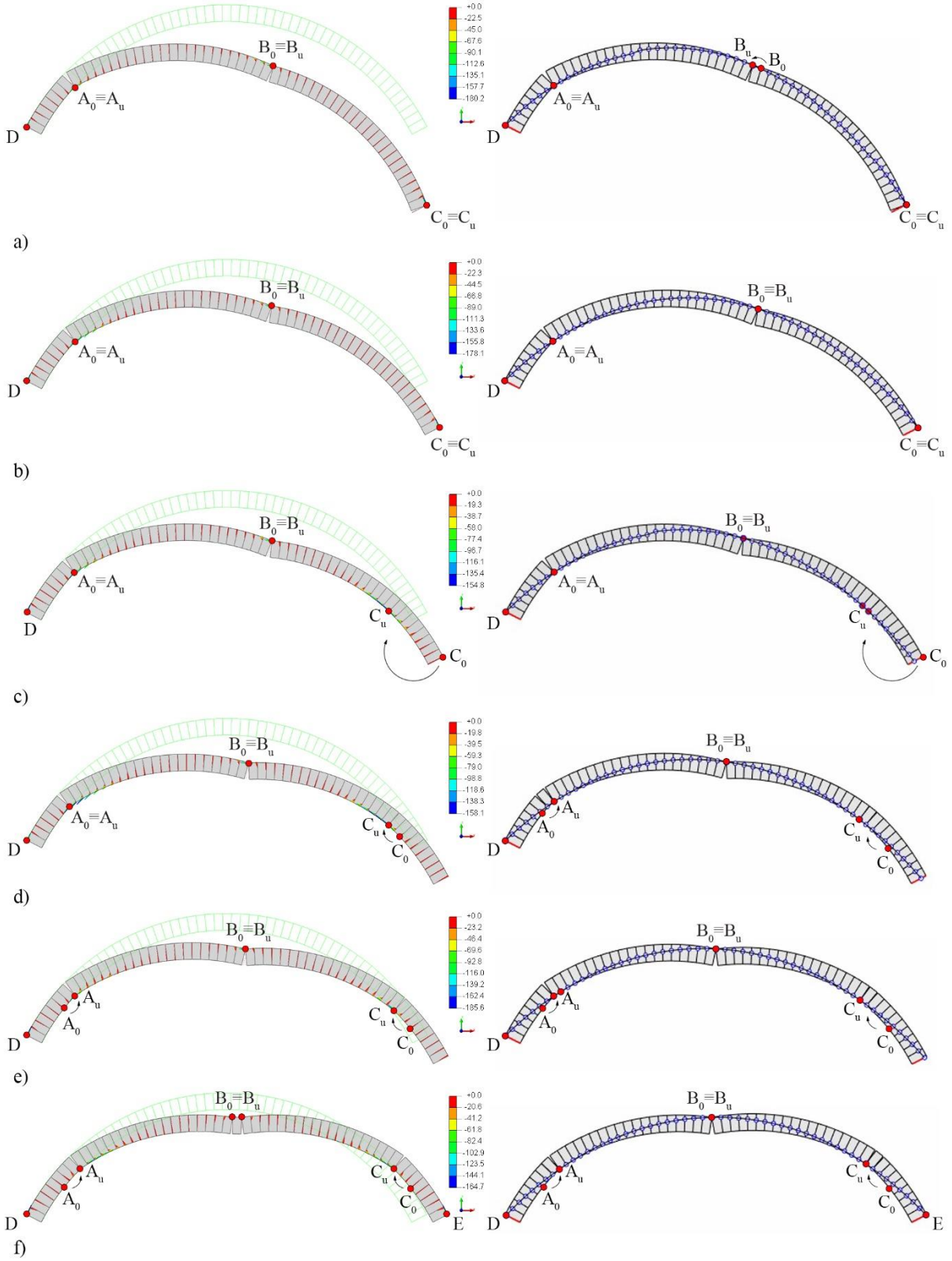

Figure 4-14 - Collapse mechanisms obtained from the FE model (left, results presented in terms of compressive stresses in the interfaces) and RB model (right): a) $\alpha = 0°$, b) $\alpha = 15°$, c) $\alpha = 20°$, d) $\alpha = 30°$, e) $\alpha = 45°$, f) $\alpha = 90°$.

As shown in Figure 4-14, hinges A, B and C may move before the final collapse state is reached, with the results that their final position at collapse may be different from the initial one. Three different *modes* of evolution of the hinge configuration from the opening of the three initial hinges to collapse (hereafter named *modes I, II* and *III*) can be identified when varying the angle α.

For α between 0° and 15° (*mode I*), in both the FE and RB models, hinges A, B and C remain fixed in their initial position (sequence I-E-E) and do not move as the support displacements increase. The only exception is hinge B moving by one voussoir at the very beginning of RB analyses for α equal to 0° (Figure 4-14b on the right). The final hinge configuration at collapse follows the sequence E-I-E-E (Figure 4-14a-b).

For α equal to 20° and 25° (*mode II*), both FE and RB analyses predict hinge C to close at the extrados (right support) and then open at the intrados (haunches) before reaching the final collapse state (Figure 4-14c). As a result, the position of hinges A, B and C changes from the initial sequence I-E-E to the final sequence I-E-I. In the case of the FE model, hinge C does not move further once it has moved from the extrados to the intrados. Conversely, in the RB model, it moves towards the crown by some voussoirs before collapse is reached. In both models, the collapse configuration is characterized by hinges located alternately between the extrados and the intrados (sequence E-I-E-I) (Figure 4-14c).

For α between 30° and 90° (*mode III*), in both models, hinges A, B and C are located alternately between the intrados and extrados (sequence I-E-I) in both the initial and final configurations (Figure 4-14d-e-f). However, as shown in Figure 4-14d-e-f, the intrados hinges A and C move towards the crown from their initial position as the support displacements increase. For values of α up to 45°, the collapse mechanism is the same as the one obtained for α equal to 20° and 25°, and the final hinge location follows the sequence E-I-E-I (Figure 4-14d-e). For α equal to 90°, the sequence obtained is E-I-E-I-E, as the arch fails by a five-hinge mechanism (Figure 4-14f).

In view of these results, the response of the arch to inclined displacements proved to be strictly related to the predominant component of the support displacements. For α between 5° and 15°, the evolution of the hinge configuration is governed by the vertical component δ_z, since the arch exhibits the same behaviour obtained for purely vertical displacements. For α between 30° and 45°, the arch response from the opening of the three initial hinges to collapse is driven by the horizontal component δ_x. For α equal to 20° and 25°, the initial and final hinge configurations are governed by δ_z and δ_x, respectively. It is interesting to note that, as α increases, the final hinge configuration at collapse (Figure 4-14) becomes more symmetrical, changing gradually from that obtained for purely vertical displacements to that obtained for purely horizontal ones.

For both FE and RB models, Figure 4-15 shows the variation in the location of hinges A, B and C as a function of the displacement applied at the right support, the latter expressed in a dimensionless way in terms of deflection ratio δ_z/L and span increase δ_x/L. The location where hinges D and E occur at collapse is also reported in Figure 4-15. The interfaces where hinges appear are numbered from left to right, being interface no. 1 the interface at the left support.

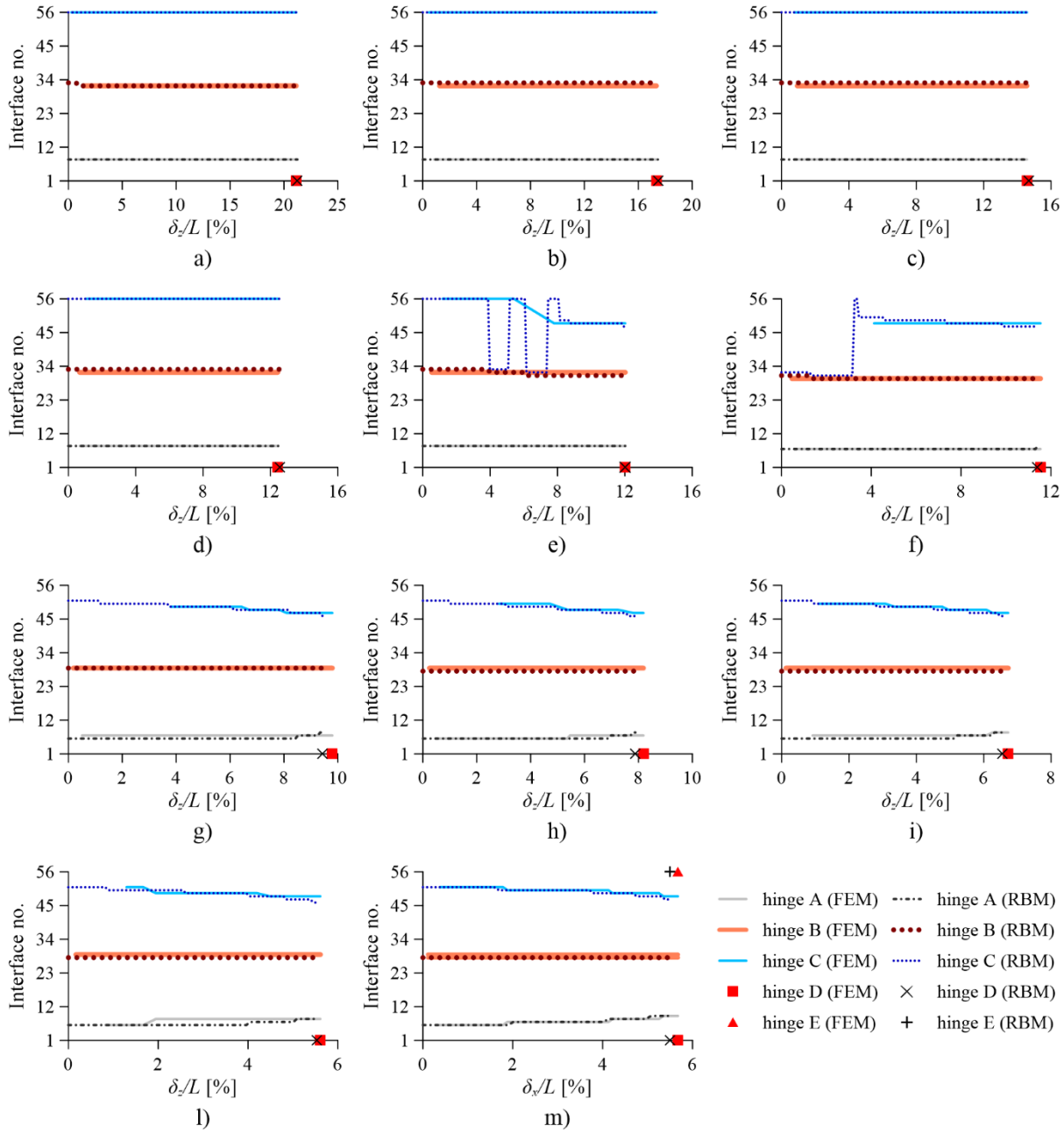

Figure 4-15 - Hinge position vs. displacement applied (expressed in terms of deflection ratio δ_z/L and span increase δ_x/L) for values of the angle α between 0° and 90° as obtained from FE and RB analyses: a) α = 0°, b) α = 5°, c) α = 10°, d) α = 15°, e) α = 20°, f) α = 25°, g) α = 30°, h) α = 35°, i) α = 40°, l) α = 45°, m) α = 90°.

Figure 4-15 confirms the results described above in terms of different evolution of the hinge configuration when varying α (*modes I, II* and *III*). For α between 0° and 15° (*mode I*), hinges A, B and C do not move as the support displacements increase (Figure 4-15a-b-c-d). For α equal to 20° and 25° (*mode II*), hinge C closes at the right support (interface n. 56) and then opens at the haunches (Figure 4-15e-f). For α between 30° and 90° (*mode III*), the intrados hinges A and C move gradually towards the crown (Figure 4-15g-h-i-l-m). It is worth noting that hinges change location for similar values of deflection ratio

and span increase in the FE and RB models. Conversely, the initial jumps in the location of hinge C obtained from RB analyses for α equal to 20° and 25° (Figure 4-15e-f) are only due to numerical instability.

For α between 25° and 45° (Figure 4-15f-g-h-i-l), the intrados hinge C seems to appear for significantly larger values of support displacement in the FE models compared to the RB models. This can be explained considering that for these values of α, in the FE models, hinge C is initially distributed among consecutive interfaces. Since the authors considered a hinge to open when compressive stresses were concentrated in a single FE of an interface only, the support displacement for which hinge A appeared was overestimated.

Support reaction-displacement curves

This section presents the results obtained from FE and RB analyses in terms of support reaction-displacement curves as well as ultimate displacement and corresponding support reactions at collapse.

For α equal to 0° and 90°, Figure 4-16 shows the support reaction-displacement curves obtained from both the FE and RB models by plotting the vertical and horizontal reactions R_z and R_x at the right (moving) support versus the deflection ratio δ_z/L and span increase δ_x/L, respectively. For both the considered values of α, the curves from the two models are almost overlapped, except for the initial decrease in the support reactions observed in the FE model (see Section 3 for further explanations). For α equal to 0° (Figure 4-16a), as the right support settles, the vertical support reaction R_z increases almost linearly, whereas the horizontal support reaction R_x has a nonlinear increase. For α equal to 90° (Figure 4-16b), the vertical support reaction R_z remains constant, whereas the horizontal support reaction R_x increases nonlinearly with the span increase δ_x/L. It is worth noting that the discontinuities in the horizontal support reaction-span increase curve of the FE model (Figure 4-16b) are caused by the movement of the intrados hinges from one voussoir to the next.

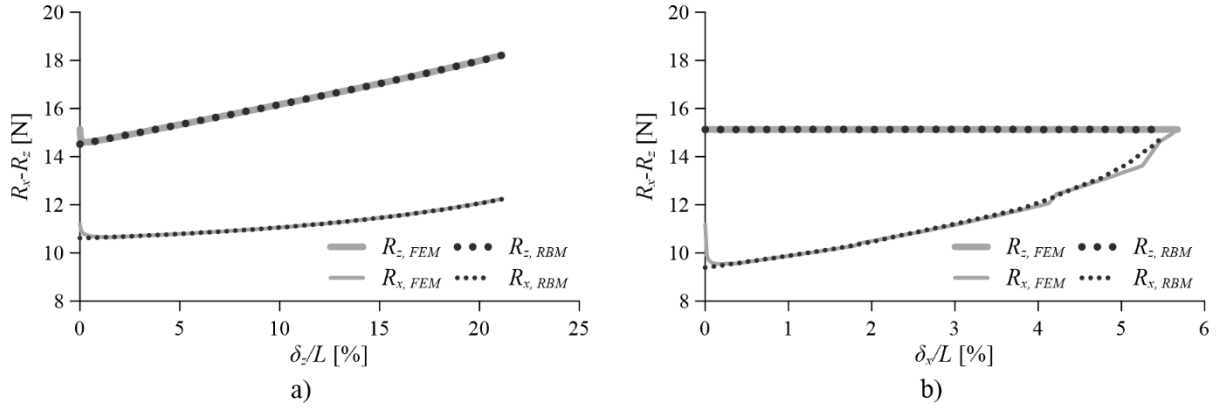

Figure 4-16 - Support reaction-displacement curves obtained from FE and RB analyses for a) α = 0° and b) α = 90°: curves vertical reaction R_z vs. deflection ratio δ_z/L, and curves horizontal reaction R_x vs. span increase δ_x/L.

The support reaction-displacement curves obtained from FE and RB analyses for α between 0° and 45° and α equal to 90° are presented in Figure 4-17. The value of the horizontal support reaction $R_{x,min}$ calculated by graphic statics (Heyman 1982; Huerta 2011) when the arch is in the state of minimum thrust due to a small outward movement of the supports is also provided for comparison. Note that, in the minimum thrust

state, hinge B opens at the extrados at mid-span, while hinges A and C are located at the intrados between 5th and 6th voussoirs.

FE and RB analyses predict the same results in terms of support reaction-displacement curves. In both models, all the curves obtained for α between 5° and 45° are included between those derived for α equal to 0° and 90°, suggesting that a similar response could be obtained for any α between 45° and 90°. Three different groups of curves, corresponding to the *modes I*, *II* and *III* described in Section 4.2.1, are obtained for α = 0°÷15°, α =20°÷25°, and α =30°÷90°. As α increases from 0° to 15°, the rate of increase decreases for the horizontal support reaction, while it increases for the vertical one. For α between 30° and 90°, the curves of the vertical reaction R_z versus deflection ratio δ_z/L as well as the curves of the horizontal reaction R_x versus the span increase δ_x/L are almost overlapped for every value of α. The curves obtained for α equal to 20° and 25° follow those derived for α between 0° and 15° until a net discontinuity in the values of the horizontal and vertical support reactions is produced by hinge C closing at the extrados and subsequently opening at the intrados (see Section 4.2.1). Then, the same trend of the curves obtained for α between 30° and 90° is followed. The initial fluctuations of the support reactions predicted by the FE and RB models for α equal to 20° and 25° are due to numerical instability.

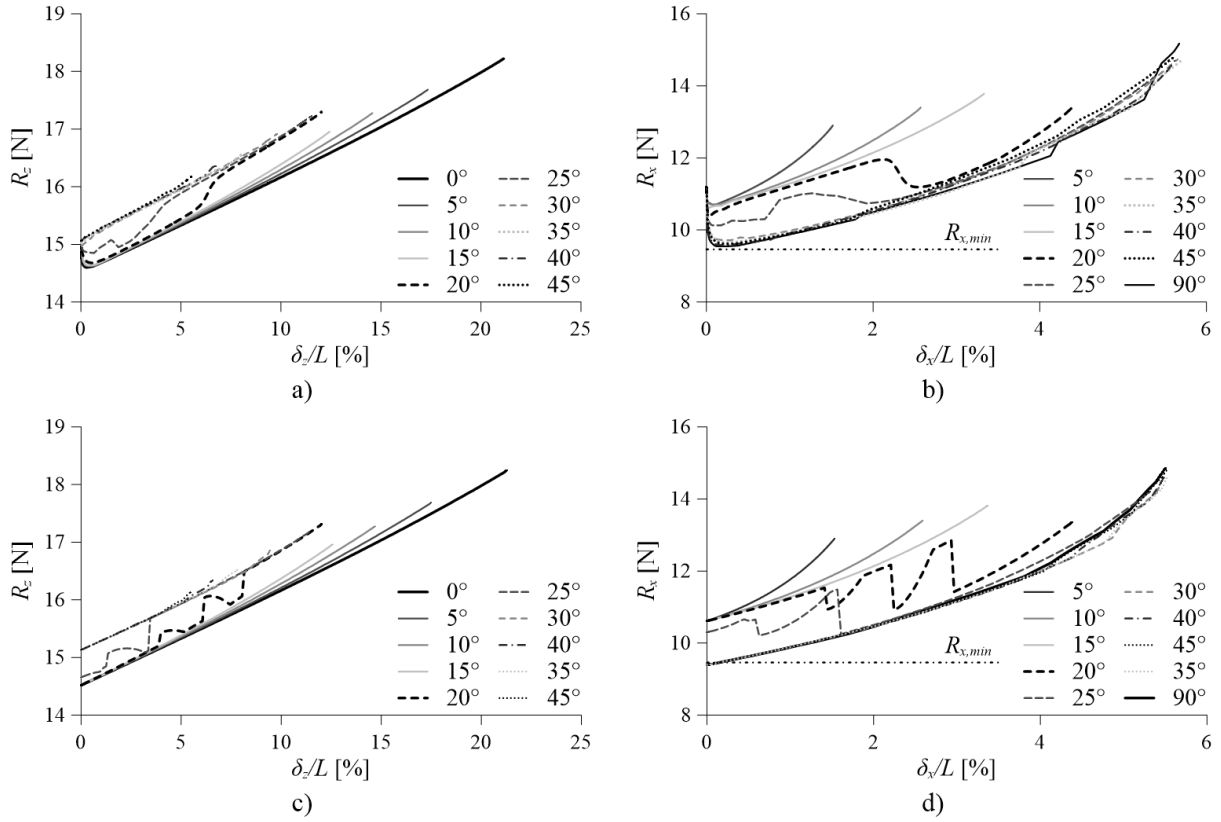

Figure 4-17 – Support reaction-displacement curves for α between 0° and 45°, and equal to 90°: curves vertical reaction R_z vs. deflection ratio δ_z/L obtained from FE analyses (a) and RB analyses (c); curves horizontal reaction R_x vs. span increase δ_x/L obtained from FE analyses (b) and RB analyses (d). Comparison with the minimum thrust calculated by graphic statics $R_{x,min}$ is provided in b) and d).

It is worth noting that for α between 30° and 90° the initial value of the horizontal support reaction R_x predicted by the RB analyses (equal to 9.4 N) is almost identical to the minimum thrust obtained from graphics statics ($R_{x,min}$ = 9.5 N) (Figure 4-17d). Also in FE analyses, the minimum value reached by R_x after its initial decrease (ranging between 9.5 N and 9.7 N depending on α) is very similar to the minimum thrust $R_{x,min}$ (Figure 4-17c). This result could be expected since the initial location of hinges A, B and C predicted by the FE and RB analyses (see Figure 4-13b) is the same as obtained in the condition of the minimum thrust. Conversely, for values of α between 0° and 15°, for which hinges A, B and C appear in the sequence I-E-E, the minimum value of the horizontal support reaction R_x is larger than $R_{x,min}$, being equal to about 10.6 N in both the FE and RB models.

Figure 4-18 reports the results obtained from FE and RB analyses in terms of support reactions, deflection ratio and span increase at collapse when varying α between 0° and 90°. The two modelling approaches predict very similar values of deflection ratio and span increase at collapse, with differences lower than 4% for every value of α considered. As the angle α increases, the deflection ratio at collapse $\delta_{z,u}/L$ decreases, dropping from about 21.2% for α equal to 0° to about 0.5% for α equal to 85° (Figure 4-18a). The rate of decrease is different in the three ranges of α corresponding to *modes I, II and III*. It is worth noting that, although the horizontal component of support displacements is smaller in the case of *mode I*, the deflection ratio at collapse $\delta_{z,u}/L$ decreases faster for α ranging between 0° and 15°.

In both models, the span increase at collapse $\delta_{x,u}/L$ increases significantly up to an angle α of 25° (*modes I and II*) (Figure 4-18b), while it remains almost constant for α between 30° and 90° (*mode III*). In this latter range, the values of span increase at collapse predicted by the FE and RB models are equal to about 5.7% and 5.5%, respectively. Comparing the deflection ratio and span increase at collapse obtained for α equal to 0° and 90°, respectively, the arch is found to exhibit a significantly larger capacity to withstand vertical support displacements compared to horizontal support displacements.

The results obtained from the FE and RB analyses are in very good agreement also in terms of support reactions at collapse, with differences lower than 3% and 1% for the horizontal and vertical reactions, respectively (Figure 4-18c-d). In both models, the vertical support reaction at collapse $R_{z,u}$ decreases with increasing α up to 15° (*mode I*), increases abruptly between 15° and 20° due to the transition from *mode I* to *mode II*, and then decreases at a lower rate up to 90° (*mode III*) (Figure 4-18c). The horizontal support reaction at collapse $R_{x,u}$ increases with increasing α except for α equal to 20°, for which it sharply drops due to the transition from *mode I* to *mode II* (Figure 4-18d). It is worth noting that the rate of increase is significantly smaller for α between 30° and 90° than for α between 0° and 15°.

As it can be observed from Figure 4-18, the results obtained from the RB analyses for angles α between 50° and 85° follow the same trend observed for α ranging between 30° and 45°. Consequently, the considerations regarding initial hinge configuration, hinge movement and collapse mechanism made so far for α between 30° and 45° can be extended to any angle between 50° and 85°.

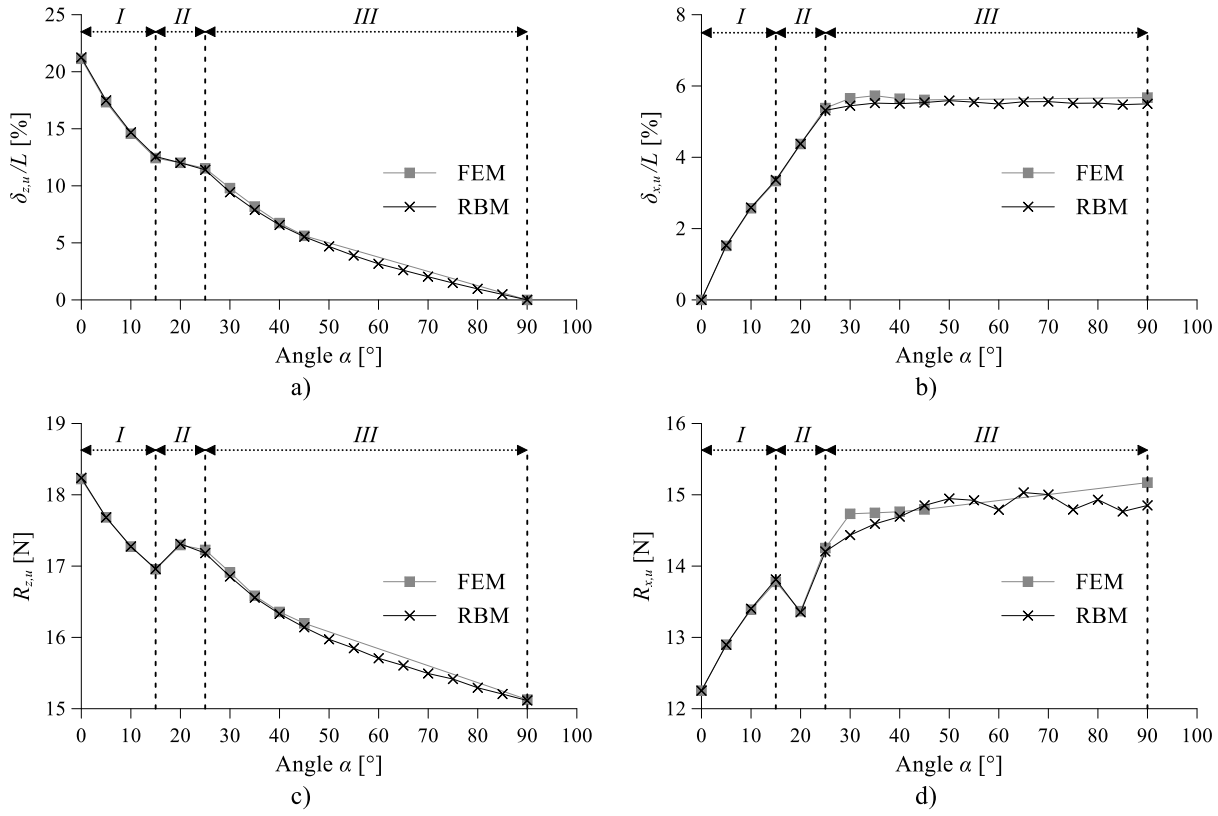

Figure 4-18 – Results obtained at collapse from the FE and RB analyses when varying the angle α between 0° and 90° (*modes I*, *II* and *III* are also indicated): a) deflection ratio at collapse $\delta_{z,u}/L$, b) span increase at collapse $\delta_{x,u}/L$, c) vertical support reaction at collapse $R_{z,u}$ and d) horizontal support reaction at collapse $R_{x,u}$.

Limit displacement domain

The RB model was used to determine the limit displacement domain of the analysed arch as a function of the angle α (Figure 4-19). The boundary of the domain consists of the pairs of deflection ratio-span increase values obtained at collapse for α ranging between 0° and 90°. The points below the boundary represent all the combinations of vertical and horizontal support displacements that the arch can sustain safely. Conversely, the pairs of deflection ratio-span increase values falling above the boundary are collapse states. The *x*-axis and the *y*-axis represent purely horizontal (α = 90°) and purely vertical (α = 0°) support displacements, respectively.

The limit displacement domain of the analysed arch exhibits three different trends, corresponding to *modes I, II* and *III*, when varying α (Figure 4-19). For α between 0° and 15° (*mode I*) and α equal to 20° and 25° (*mode II*), the deflection ratio at collapse $\delta_{z,u}/L$ decreases linearly with increasing span increase at collapse $\delta_{x,u}/L$. However, a larger rate of decrease is obtained for *mode I* with respect to *mode II*. For values of α between 30° and 90° (*mode III*), the deflection ratio at collapse $\delta_{z,u}/L$ gradually decreases with increasing α, while the span increase at collapse $\delta_{x,u}/L$ remains almost constant. It is worth noting that, although the final hinge location at collapse follows the sequence E-I-E-I for both *modes II* and *III*, the different evolution of the hinge configuration from the opening of the three initial hinges to collapse results

in significantly different values of deflection ratio and span increase at collapse for α equal to 20° and 25° and α between 30° and 90°.

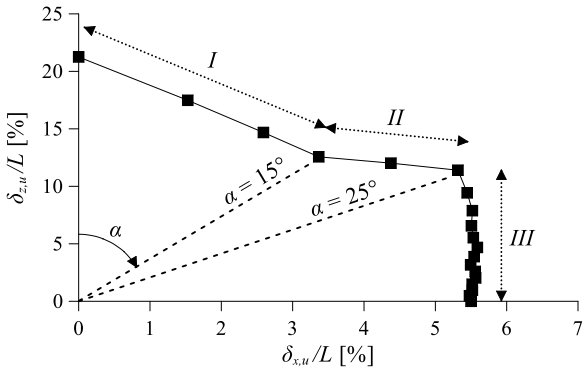

Figure 4-19 – Limit displacement domain for the segmental arch under consideration (*modes I*, *II* and *III* are also indicated).

4.5. SENSITIVITY ANALYSIS TO THE NUMBER OF VOUSSOIRS

A sensitivity analysis to the number of voussoirs was performed for the considered segmental arch using the RB model. Results from literature for arches on spreading supports (Coccia et al. 2015; Galassi et al. 2018; Ochsendorf 2002, 2006) have demonstrated that the number of voussoirs affects the arch response in terms of both hinge position and collapse displacement. In view of this, in the present work, the effect of the number of voussoirs on the deflection ratio and span increase at collapse for α equal to 0° and 90°, respectively, was investigated. Furthermore, in order to assess the sensitivity of the results to the voussoir discretization when varying the direction of the support displacements, the effect of the number of voussoirs on the limit displacement domain of the arch was evaluated.

Figure 4-20 shows the variation in the deflection ratio at collapse $\delta_{z,u}/L$ with the number of voussoirs for α equal to 0°. The value obtained for an arch made of 500 voussoirs, which is representative of a theoretical continuous arch, is also reported. It is interesting to note that the deflection ratio at collapse $\delta_{z,u}/L$ oscillates around the value obtained for the theoretical continuous arch (equal to 21.5%) with abrupt decreases for arches with very similar numbers of voussoirs. When arches are made of few blocks, large variations (up to about 16%) in the deflection ratio at collapse $\delta_{z,u}/L$ are obtained. In contrast, as the number of voussoirs increases, the arch response becomes less sensitive to the voussoir discretization, and the deflection ratio at collapse $\delta_{z,u}/L$ converges to a stable value of about 21.5%.

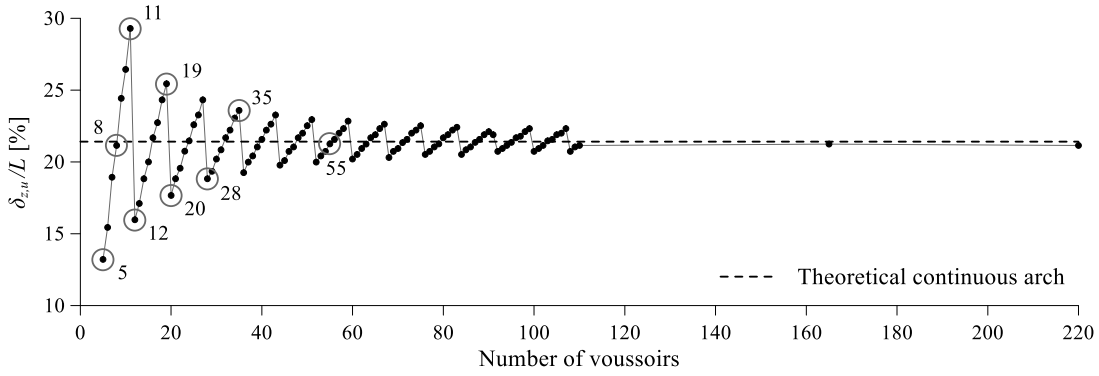

Figure 4-20 - Deflection ratio at collapse $\delta_{z,u}/L$ vs. number of voussoirs for $\alpha = 0°$.

An asymmetrical four-hinge collapse mechanism with hinges located in the sequence E-I-E-E (*mode I*) is obtained for any number of voussoirs considered. Hinges C and D always occurs at the right and left support, respectively, whereas hinges A and B change location with the number of voussoirs. For the sake of brevity, the results obtained for hinge B are not reported, as they affect the arch response only marginally. As shown in Figure 4-21, the radial position of hinge A at collapse, corresponding to the angle β shown in Figure 4-22, oscillates around the radial position obtained in the theoretical continuous arch (indicated as β_t and equal to 15.8°). Note that hinge A does not move with the increase of support displacements; thus, its final position at collapse is the same as the initial one. As the radial position of hinge A gradually decreases, the deflection ratio at collapse $\delta_{z,u}/L$ gradually increases (see the results obtained for arches with 5, 8 and 11 voussoirs, indicated with grey circles in Figure 4-20 and Figure 4-21). Furthermore, any sudden increase in the radial position of hinge A corresponds to an abrupt decrease in the deflection ratio at collapse $\delta_{z,u}/L$ (see the results obtained for 11 and 12 voussoirs in Figure 4-20 and Figure 4-21). This clearly indicates that the changes in the deflection ratio at collapse $\delta_{z,u}/L$ with the number of voussoirs are caused by the variations in the radial position of hinge A.

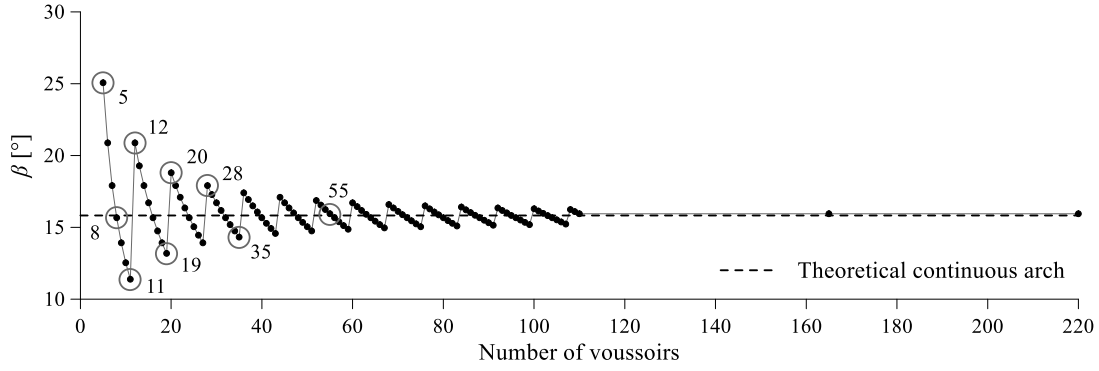

Figure 4-21 - Radial position of hinge A at collapse, β, vs. number of voussoirs for $\alpha = 0°$.

Figure 4-22 shows the collapse configuration as well as the radial position of hinge A, β, for arches made of 5, 8, 11, 12, 19 and 20 voussoirs. The radial position of hinge A for the theoretical continuous arch, β_t, is provided for comparison.

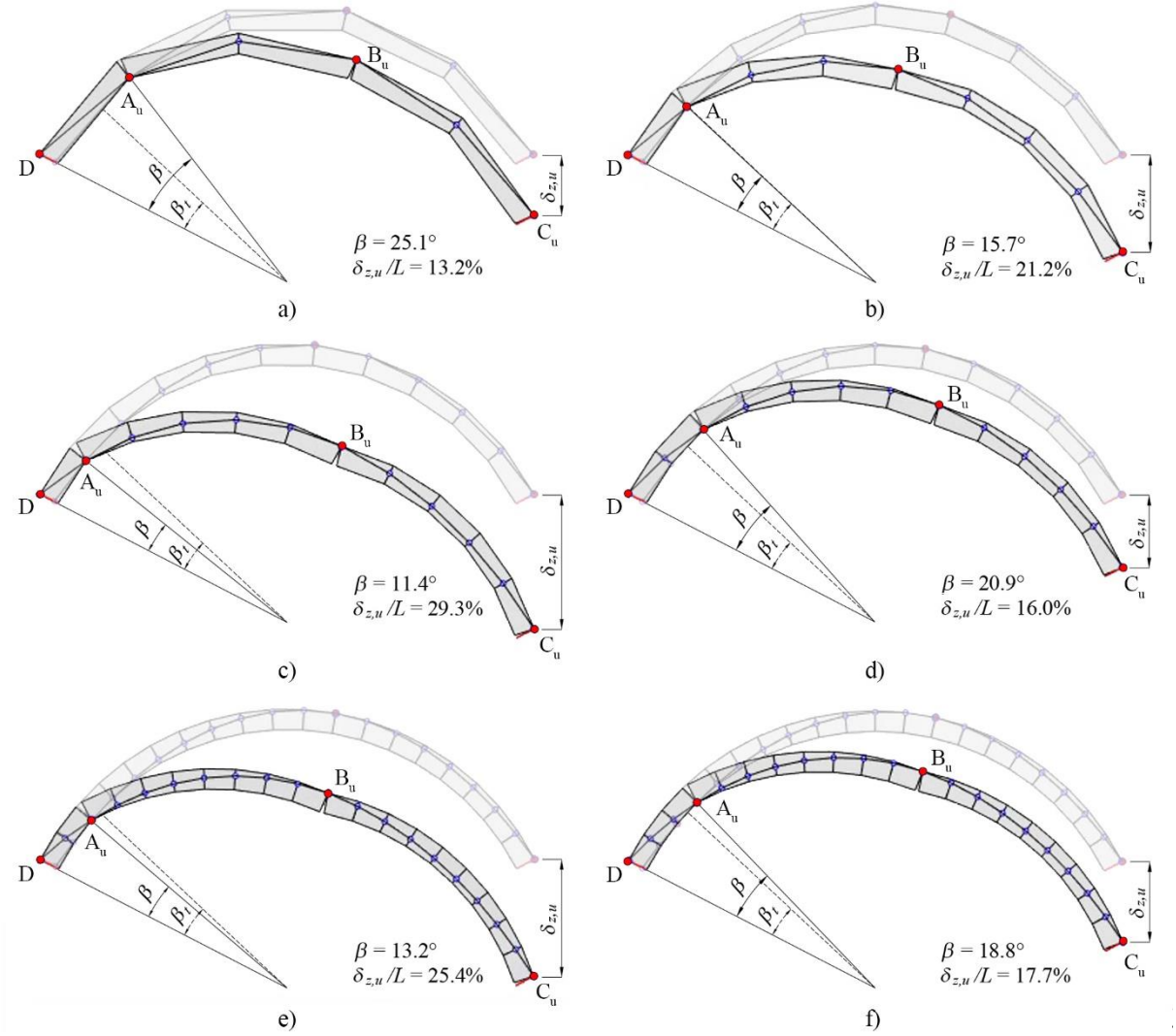

Figure 4-22 – Radial position at collapse of hinge A, β, and deflection ratio at collapse, $\delta_{z,u}/L$, for arches with a) 5, b) 8, c) 11, d) 12, e) 19 and f) 20 voussoirs (β_t indicates the radial position of hinge A in the theoretical continuous arch).

Looking at Figure 4-22, it is interesting to observe that hinge A always opens at the interface located closest to the radial position β_t, regardless of the number of voussoirs. For an arch made of 5 voussoirs, hinge A occurs between the 1st and 2nd voussoir at a radial position β equal to 25.1°. As the number of voussoirs increases from 5 to 11, the radial position β decreases, as expected since hinge A is always located between the 1st and 2nd voussoir. However, for an arch made of 12 voussoirs, hinge A opens between the 2nd and 3rd voussoir (Figure 4-22d), producing the abrupt increase in the radial position β described above. It is worth noting that every time hinge A moves by one voussoirs towards the crown (see Figure 4-22e-f as an example), the radial position β increases sharply and then decreases gradually until a further increase is obtained (Figure 4-21). As a result, large variations in the deflection ratio at collapse $\delta_{z,u}/L$ can be obtained for arches with a similar number of voussoirs, especially when few voussoirs are considered.

From the results obtained for arches made of 5, 8 and 11 voussoirs (Figure 4-22a-b-c), it is easy to observe that the more hinge A appears close to the left support, the larger is the deflection ratio at collapse

$\delta_{z,u}/L$. Furthermore, when β approaches β_t (Figure 4-22b), the deflection ratio at collapse $\delta_{z,u}/L$ approaches the value obtained for the theoretical continuous arch.

Figure 4-23 depicts the span increase at collapse $\delta_{x,u}/L$ obtained for α equal to 90° when varying the number of voussoirs. As the number of voussoirs increases, the span increase at collapse $\delta_{x,u}/L$ quickly converges to the value obtained for the theorical continuous arch (equal to 5.50%). The variation in the span increase does not exceed 2% for any number of voussoirs considered, showing that the span increase at collapse $\delta_{x,u}/L$ is less sensitive to the number of voussoirs than the deflection ratio at collapse $\delta_{z,u}/L$. The slight oscillations observed for large numbers of voussoirs are simply due to the step size adopted in the RB analyses.

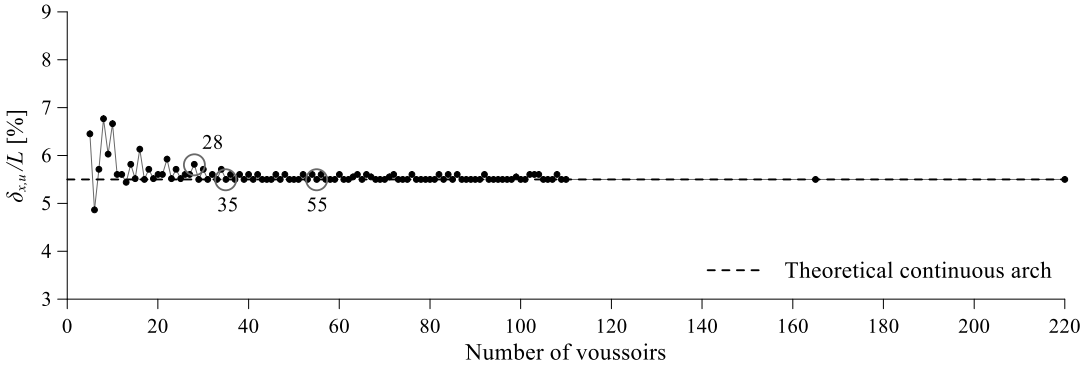

Figure 4-23 - Span increase at collapse $\delta_{x,u}/L$ vs. number of voussoirs for α = 90°.

In order to evaluate the effect of the number of voussoirs on the arch response when varying α, the limit displacement domains of the theoretical continuous arch (500 voussoirs) as well as the domains of arches with 28 and 35 voussoirs were determined and compared with the domain obtained for the arch with 55 voussoirs (Figure 4-24). Results are presented for arches with 28 (approximately equal to the half of 55) and 35 voussoirs because they respectively provide lower-bound and upper-bound estimates of the deflection ratio obtained for the theoretical continuous arch (Figure 4-20). For arches made of 28, 35 and 55 voussoirs, the deflection ratio and span increase obtained at collapse for α respectively equal to 0° and 90° are indicated with grey circles in Figure 4-20 and Figure 4-23.

As shown in Figure 4-24, the limit displacement domains of arches with 28, 35 and 500 voussoirs are very similar to the domain of the arch with 55 voussoirs, exhibiting the same three different trends for α between 0° and 15°, α equal to 20° and 25° and α between 30° and 90°. This indicates that, when a reasonable number of voussoirs is considered, the same *modes* of evolution of the hinge configuration (i.e. *modes I, II and III* described in Section 4.2.1) are obtained when varying α regardless of the adopted voussoir discretization. It should be noted that for arches with smaller number of voussoirs *mode II* may already occur for α equal to 15°.

In the case of the arch with 55 voussoirs, the limit displacement domain is almost overlapped to the domain of the theoretical continuous arch made of 500 voussoirs, as expected since approximately the same deflection ratio and span increase at collapse are obtained for both arches (see Figure 4-20 and Figure 4-23).

For arches with 28 and 35 voussoirs, the domains are slightly shifted with respect to those obtained for 55 and 500 voussoirs for α up to 25°, whereas they are almost superimposed for α equal or larger than 30°. This result confirms that the voussoir discretization has a larger influence on the arch response when the dominant component of the support displacements is vertical.

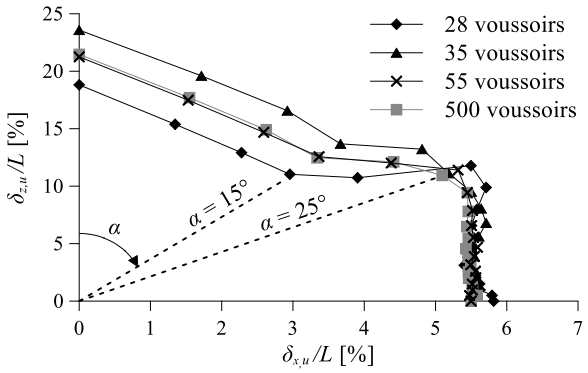

Figure 4-24 – Limit displacement domains for arches with 28, 35, 55 and 500 (theoretical continuous arch) voussoirs.

4.6. SUMMARY

In this chapter, the structural behaviour exhibited by the segmental dry-joint arch object of study when subjected to inclined support displacements was investigated using FE and RB micro-modelling. The two numerical approaches adopted were validated against experimental data derived from tests performed in the literature. A good agreement in terms of collapse mechanism and hinge configuration was obtained, indicating that both the FE and RB models can be effective in predicting the actual response of masonry arches subjected to large support displacements. The results obtained from the FE model also showed that particular attention must be paid to the evaluation of the stiffness of the interface elements when adopting a FE micro-modelling strategy.

In order to gain insight on the effects of inclined displacements, different combinations of horizontal and vertical support displacements were considered. The direction of the support displacements (indicated with the angle α) showed to significantly affect the arch response in terms of collapse mechanism, hinge position, support reaction-displacement curves as well as ultimate displacement and support reactions at collapse. Although other authors (Galassi et al. 2018; Zampieri at al. 2018a) already observed that the three initial hinges may appear in different configurations according to the direction of the support displacements (see Chapter 3), the numerical analyses here performed also allowed to identify three different *modes* of evolution of the hinge configuration with increasing support displacements when varying α. The results in terms of support reaction-displacement curves as well as ultimate displacement capacity and support reactions at collapse were found to be *mode*-specific. A limit displacement domain for the investigated arch was also computed as a function of the angle α. The very good agreement between FE and RB predictions proved the reliability and robustness of the results presented.

A sensitivity analysis to the number of voussoirs was also performed, showing that the voussoir discretization has a large influence on the hinge position as well as on the ultimate displacement capacity

when the predominant component of the support displacements is vertical. Conversely, the arch response to horizontal support displacements is less sensitive to the number of voussoirs. The results also indicate that the same *modes* of evolution of the hinge configuration occur regardless of the number of voussoirs considered.

REFERENCES

Coccia, S., F. Di Carlo, and Z. Rinaldi. 2015. Collapse displacements for a mechanism of spreading-induced supports in a masonry arch. *International Journal of Advanced Structural Engineering* 7(3): 307–20.

Ferrero C., C. Calderini, F. Portioli, and P. Roca. 2021b. Large displacement analysis of dry-joint masonry arches subject to inclined support movements. *Engineering Structures* (In press).

Ferris, M. C., and F. Tin-Loi. 2001. Limit Analysis of Frictional Block Assemblies as a Mathematical Program with Complementarity Constraints. *International Journal of Mechanical Sciences* 43(1): 209–24.

Gaetani, A., M. Moroni, P. B. Lourenço, and G. Monti. 2017. Dry-joint arch undergoing windowed sine pulses. *Bulletin of Earthquake Engineering*. 15:4939-61.

Galassi, S., G. Misseri, L. Rovero, and G. Tempesta. 2018. Failure modes prediction of masonry voussoir arches on moving supports. *Engineering Structures* 173: 706–17. doi:10.1016/j.engstruct.2018.07.015.

Heyman, J. 1982. *The Masonry Arch*. Chichester: Ellis Horwood.

Huerta, S. 2011. The analysis of masonry architecture: A historical approach. *Architectural Science Review* 51(4): 297–328.

Lourenço P. B. , T. Hunegn, P. Medeiros, and N. Peixinho. Testing and analysis of masonry arches subjected to impact loads. In *ARCH'10: Proceedings of 6th International Conference on Arch Bridges*, 11-13 October 2010, Fuzhou, China, p. 603-610.

Midas IT 2013. FX+ for DIANA. Midas FX+ for DIANA, Customized Pre/Post-processor for DIANA.

Ochsendorf, J. A. 2002. Collapse of masonry structures. PhD diss., University of Cambridge.

Ochsendorf, J. A. 2006. The masonry arch on spreading supports. Structural Engineer 84(2): 29–35.

Portioli, F., and L. Cascini. 2017. Large displacement analysis of dry-jointed masonry structures subjected to settlements using rigid block modelling. *Engineering Structures* 148: 485–96.

DIANA FEA BV. 2017. *DIANA Finite Element Analysis User's Manual Release 10.2*, Delft, The Netherlands.

Zampieri, P., F. Faleschini, M. A. Zanini, and N. Simoncello. 2018. Collapse mechanisms of masonry arches with settled springing. *Engineering Structures* 156: 363–74. doi:10.1016/j. engstruct.2017.11.048.

This page is intentionally left blank.